Molecular Investigations on the Behaviors of Surface-Active Materials

by

Komeil Jalali

A Thesis Submitted to The Faculty of Graduate Studies

in Partial Fulfillment of the Requirements for the Degree

of Master of Applied Science

Graduate Program in Mechanical Engineering

York University

Toronto, Ontario

January 2023

© Komeil Jalali, 2023

Abstract

This thesis applied molecular dynamics techniques, a powerful method based on factual observations at nanoscales, to effectively understand macroscopic and microscopic behaviors of surface-active materials in biphasic systems. First, few works have been focused on revealing the effect of naturally occurring organic materials such as naphthenic acids on the behaviors of polyaromatic compounds (known as asphaltenes that are interfacially active) during oil production. To bridge this gap, a series of MD simulations were performed to investigate the effects of molecular structures. It was revealed that naphthenic acids, depending on the solvent type, can either hinder or enhance nano-aggregation among asphaltene molecules. Furthermore, they can affect the orientations of polyaromatic molecules at the oil/water interface. The second direction of this thesis investigated biphasic systems in daily life, i.e., wastewater containing soap. The results obtained shed light on fundamental understandings and utilizations of surface-active materials during industrial applications and in our daily life.

Acknowledgement

I would like to extend my sincere gratitude to my supervisor, Prof. Cuiying Jian, for introducing me to the research field of theoretical chemistry and giving me the opportunity to work on various interesting projects. I have learned much from her profound knowledge and insightful thoughts on scientific research, and I am thankful for all her guidance, support, trust, and encouragement, without which this thesis would have been impossible. Furthermore, I am heartily thankful to my thesis committee member, Dr. Alidad Amirfazli, for his careful guidance, insightful comments, and practical questions.

My special gratitude my brother, for the love, understanding and support. I want to thank my colleagues and friends, who have made my time in lab happy and fulfilled. I am so grateful to all of you for frequent academic discussions, leisure, activities, and all kinds of help in daily life.

The financial support from Lassonde School of Engineering and the computational resources provided by the Compute Canada for computing are sincerely acknowledged. Finally, I wish to express my deepest gratitude to my parents for their constant love and support.

List of Contents

Abstract ii
Acknowledgement iii
List of Contents iv
List of Figures vi
List of Tables viii
List of Symbols and Acronyms ix
Chapter 1. Introduction 1
1.1 Crude Oil 2
1.2 Computational Methods 3
1.3 Objectives 5
Chapter 2. Methodology 7
2.1 MD Integration Algorithms 8
2.2 MD Forcefields 9
2.3 Thermostat 13
2.4 Barostat 14
2.5 Energy Minimization and Periodic Boundary Conditions 15
2.6 MD Practical Protocols 16
Chapter 3. Molecular Investigations on The Effects of Naphthenic Acids on the Aggregations and Interfacial Behaviors of Asphaltenes in Oil 19
3.1 Introduction 20
3.2 Methods 24
3.2.1 Molecular Models and Simulation Systems 24
3.2.2 Simulation Details 27
3.3 Results and Discussion 28
3.3.1 Accumulation of PA Molecules at The Heptane/Water Interface 30
3.3.2 Orientation of PA Molecules at The Heptane/Water Interface 34
3.3.3 Accumulation of PA Molecules at The Toluene/Water Interface 36
3.3.4 Orientation of PA Molecules at The Toluene/Water Interface 40
3.4 Conclusion 44
Chapter 4. Molecular Insights into Soap Functioning and Its Wastewater Treatment 47
4.1 Introduction 48

4.3 Methods 53
4.3.1 Molecular Models and Simulation Systems 53
4.3.2 Simulation Details 55
4.4 Result and Discussion 56
4.4.1 Surfactant Functioning in Aqueous Phase 56
4.4.2 Surfactant Extraction from Wastewater 59
4.5 Conclusion 64
Chapter 5. Conclusion and Future Works 66
5.1 Conclusion 67
5.1.1 Effects of Naphthenic Acids on The Aggregation and Interfacial Behaviors of Asphaltenes 67
5.1.2 Molecular Insights into Soap Functioning and Its Wastewater Treatment 69
5.2 Future Works 70
Chapter 6. Appendix 72
6.1 Input Script for NPT Run 73
6.2 Input Script for MD Run 74
6.3 Python Code for Calculating the Number of Asphaltene Molecules at Interface 75
6.4 Python Code for Determining Angle Distribution at Interface 76
6.5 VO79 Topology 77
6.6 Permission of Reusing of Published Materials 94
6.7 Measured Properties 96
Chapter 7. References 97

List of Figures

Figure 1.1 Length and time scales employed in modeling reprinted with permission **4**

Figure 2.1 Bonded and non-bonded interactions used to describe interactions between atoms in a forcefield. Each of these interactions is described in the main texts. **10**

Figure 2.2 Flowchart for MD simulations **18**

Figure 3.1 Molecular structure of PA and NA molecules, in the left from top to bottom, NA-1, NA-2, NA-3, NA-4, the right-side PA molecules (VO79), the red atom represents oxygen, the white atom represents hydrogen, and grey atom represents carbon **25**

Figure 3.2 Schematic of constructing initial configurations **27**

Figure 3.3 Snapshot of the Hep and Tol systems at the final configuration, a) Hep system and b) Tol system **29**

Figure 3.4 Orientation of the PA molecules in the systems without any NA in different solvents in a) heptane b) toluene **30**

Figure 3.5 Snapshot and density profile of a) Hep b) NA-1-Hep c) NA-2-Hep d) NA-3-Hep e) NA-4-Hep systems, the main interface has been specified by yellow line **32**

Figure 3.6 Radial Distribution Function between PA cores in heptane/water system **33**

Figure 3.7 PA molecules orientation at the heptane/water interface in the systems with and without NA molecules **34**

Figure 3.8 Snapshots and density profiles of a) Tol b) NA-1-Tol c) NA-2-Tol d) NA-3-Tol e) NA-4-Tol systems. The main interface, where PAs were initially packed, has been specified by yellow line **38**

Figure 3.9 Monomers and nanoaggregates and the number of the PA molecules at the left interface: a) NA-1-Tol, 28 b) NA-2-Tol,16 c) NA-3-Tol, 25 d) NA-4-Tol, 28, and e) Tol, 18 systems **39**

Figure 3.10 PA molecules orientation at the heptane/water interface in the systems with and without NA molecules **41**

Figure 3.11 Normalized density profile of different NA molecules **44**

Figure 4.1 Molecular structure of a) Lauryl Glucoside b) nonadecane c) chlorobenzene **54**

Figure 4.2 Initial (left) and final (right) configurations for a) system WO_S and b) system. W_S. In both a) and b), water is red dotted, Lauryl Glucoside is in green, and nondecane is in ochre. **57**

Figure 4.3 Radial Distribution Function of the center of mass of nonpolar components **58**

Figure 4.4 The initial (a) and final (b) configurations of system W_S_CH. In both figures, water is red dotted, Lauryl Glucoside is in green, nondecane is in ochre, and chlorobenzene is blue dotted, the dimmers and trimmers are highlighted by the red circles. **61**

Figure 4.5 Density profile of the final configuration **62**

Figure 4.6 Radial Distribution Function between the center of the mass of surfactants **62**

List of Tables

Table 3.1 Systems constructed for our simulations **27**

Table 3.2 Number of H-bonds between NA/PA molecules (a), and NA/Water molecules (b) **36**

Table 3.3 Number of H-bonds between a) PA and NA molecules b) NA molecules c) NA and water molecules **43**

Table 4.1 System compositions **54**

Table 4.2 Energies calculated for systems WO_S and W_S **59**

List of Symbols and Acronyms

k_e	Kinetic Energy
AA	All-atom
AMBER	Assisted Model Building with Energy Refinement
CHARM	Chemistry at Harvard Macromolecular Mechanics
DO	Dislocation Dynamics
FEM	Finite Element Method
GROMOS	GROningen Molecular Simulation
LJ	Lennard-Jones interaction
MD	Molecular Dynamics
MM	Mesoscale Methodology
N	Avogadro constant
NA	Naphthenic Acid
OPLS	Optimized Potentials for Liquid Simulation
PA	Polyaromatics
GM	Quantum Mechanics
r	Position of the particles
T	Temperature
UA	United-Atom
v	Velocity of the particles
V	Potential Energy

vdW	Van der Waals interaction
a_i	Acceleration
F_i	Force
m_i	Mass
ϕ_{bend}	Bond stretching energy
$\Phi(r_{ij})$	Bond angle among three atoms i,j
k_{ij}	Bond force constant
r_0	Equilibrium bond length
θ_0	Equilibrium angle between two position vectors
θ_{ijk}	Angle between the three adjacent atoms
k_{jlk}	Angle force constant
$k_{torsion}$	Spring constant
$\phi_{torsion}$	Interaction among four-body bonded atoms
ε_1	Effective dielectric constant
q_i	Partial charge

Chapter 1. Introduction

1.1 Surface-Active Materials in Crude Oil

Crude oil is a naturally occurring fossil fuel - meaning it comes from the remains of dead organisms. Crude oil is made up of a mixture of hydrocarbons, and often interchangeably referred to as petroleum. This is because petroleum includes both the unrefined crude oil as well as refined petroleum products. Crude oil has been an undeniable part of human civilization in many ways, e.g., energy generation, and byproducts produced in refineries. Thus, it is of great interest to optimize the efficiency of crude oil extraction and transportation.

Canada is the world's fifth largest oil producer and has the world's third largest proven oil reserves.[1] Canadian oil belongs to the category of heavy oil. Heavy oil is a highly viscous crude oil, which is highly resistant to flow and has a higher density and specific gravity than light oil. They have been defined as crude oils with an API gravity less than 20.[2] Heavy oil components, e.g., asphaltenes and naphthenic acids, have been known to be responsible for this heavy nature.

Asphaltenes are defined as insoluble complex aromatics in alkanes (n-pentane, n-heptane) but soluble in aromatics (like toluene). They are large molecules composed of polyaromatic cores with side branching, and no single chemical formula can represent the complex structures of asphaltenes.[3] Naphthenic acids are a mixture of carboxylic acids and carbon backbones mostly containing aliphatic chains.[4] They are represented by a general formula $C_nH_{2n-z}O_2$, where n indicates the carbon number and z specifies a homologous series. The z is equal to 0 for saturated, acyclic acids, and increases to 2 in monocyclic naphthenic acids, to 4 in bicyclic naphthenic acids, to 6 in tricyclic acids, and

to 8 in tetracyclic acids.

The existence of asphaltene and naphthenic acids in crude oil has drastic impacts on crude oil production. To list a few, they cause decrease in reservoir permeability, increase in energy consumption and maintenance cost, and decrease in oil production and even complete loss of production.[5] This is due to the fact that the equilibrium state of asphaltene is very fragile and can be easily disrupted by change in crude oil compositions and environmental variables. The disturbed asphaltenes can accumulate and deposit along the production lines, leading to the various problems mentioned before. Naphthenic acids are among one of the components that can have deleterious effects on the oil production either by effecting the asphaltene behavior or directly causing the corrosion of production line.[6]

In this thesis, we first aim to investigate the synergistic effects of naphthenic acids and asphaltenes in biphasic oil/water systems. Detailed reviews on up-to-date works in the literature will be presented in Chapters 3. Following this, we turned into investigating biphasic systems in our daily life (soap/water systems), and Chapter 4 provides a detailed review of similar works in the literature.

1.2 Computational Methods

To fundamentally reveal molecular mechanisms for biphasic systems, it is important to understand detailed intra/inter-molecular interactions. In this regard, computational approaches are of particular advantages to provide detailed characterizations on the systems studied. Figure 1.1 shows computational methods across different domains.

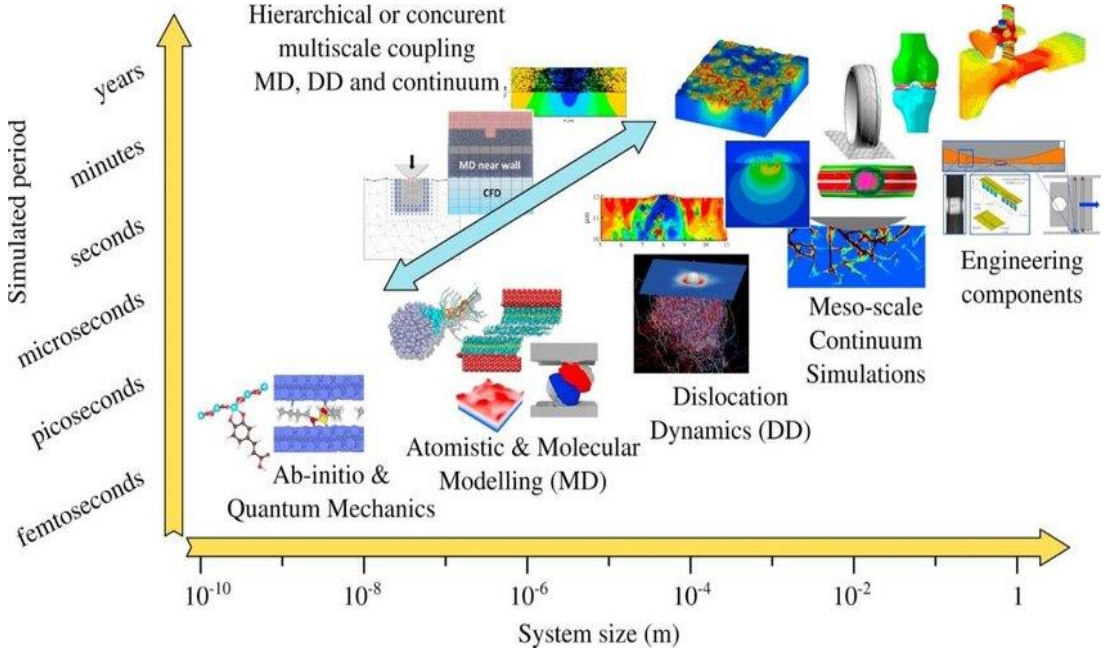

Figure 1.1 Length and time scales employed in modeling, reprinted with permission[7]

As can be seen from Figure 1.1, computational tools cover a spectrum of time and size scales. Quantum mechanics (QM) covers the smallest range sizes (femtosecond and angstrom) and can thus provide subatomic information for physical properties.[8] QM differs from classical physics, and the objects have the characteristic of both articles and waves. Molecular dynamics (MD) is a powerful method in modern computational physics, based on predefined intra-atomic potentials or molecular mechanics forcefields. It is typically utilized for analyzing motions of atoms and molecules. Dislocation dynamics (DD) is a modeling approach that aims simulating the motions and interactions of dislocation lines to gain insights into the mechanical properties of the materials on a finite length. Mesoscale methodology (MM) is commonly used in numerical weather prediction models, by discretizing the fluid domain and then solving primitive equations to probe flows, concrete analysis like chemical degradation, study of mechanical concept of alkali-silica

reaction.[9] To investigate engineering components at a millimeter or even meter scale, finite element method (FEM) is typically adopted and has been used in varies fields of study such as structure analysis and heat transfer. FEM subdivides the large system of interest into smaller, simpler parts called finite elements, and then solves partial differential equations on these finite elements. Assembling elements into a system of equations leads to modeling the original objects.

What distinguishes MD technique from other modelling approaches is that it can cover larger systems compared to QM calculations,[10] and meanwhile it can provide us with important molecular-level information compared to experimental techniques. Once the forces acting on every individual atom is obtained, classical Newton's law of motion is used to calculate acceleration. The three-dimensional trajectory of the initial configuration is then generated by updating velocities and positions of all atoms in the system studied, and physical properties of the system are obtained from the subsequent statical analysis. MD provides the convenience of performing tests under unusual circumstances (high or low pressure and temperature), and allows to study rare, novel materials for which little information is available. With the development of more realistic and accurate interaction potentials, the reliability and feasibility of MD increases. The application area for MD is broad, covering biochemistry, biophysics, material science, petroleum engineering, etc. Details of MD will be presented in Chapter 2.

1.3 Objectives

Using MD, this thesis aims to fundamentally elucidate the role of surface-active agents at the oil/water interface for industrial and daily applications. From industrial perspectives,

we focused on the ones that are the most important factors in crude oil industry, i.e., the most surface-active material, asphaltenes and NAs. These two are of the most concerns in oil/gas industry, causing severe problems like, blocking the pipelines, making the oil/water emulsion more stable, increasing costs in oil/water separation cost, and leading to corrosions in pipelines, refinery and other downstream and upstream facilities. From daily-application perspectives, the surface-active materials we focused on is soap. Although using soap has its own undeniable perks, it contaminates the wastewater and high concentration of soap surfactant can lead to serious problems, e.g., increasing the cancer rate, and toxicity of aquatic life. These two materials are inevitably existing, and there is a lack of knowledge on the molecular-level interactions and the effects of molecular structures on their behaviors (details available in Chapters 3 and 4)[11].

The rest of the thesis is organized as follows. In Chapter 2, we introduced the methodology adopted in this thesis. Chapter 3 investigated the effects of naphthenic acids on asphaltene behaviors in the oil/water biphasic system. In total, we designed 10 different systems with and without presence of naphthenic acids of different structures. In Chapter 4, we investigated how soap acts as a cleaner at intra and inter-molecular levels, and then focused on designing an efficient and reliable strategy in oily water treatment. Conclusions, as well as future directions, are discussed in Chapter 5.

Chapter 2. Methodology

Molecular dynamics (MD) is predominantly used in this thesis, as it can cover a much larger system compared to quantum calculations and meanwhile accurately capture collective behaviors at the atomistic level. This chapter presents details of MD techniques.

2.1 MD Integration Algorithms

The MD approach employs computational resources to carry out virtual simulation on the initial configuration of an interested system. During each run, forces on each atom are determined by predefined potential functions, and once forces are obtained, classical newton's law of motion is used to calculate acceleration:

$$\mathrm{F_i} = -\nabla_i \mathrm{V(r)} \qquad (2.1)$$

$$\mathrm{a_i} = \frac{\mathrm{F_i}}{\mathrm{m_i}} \qquad (2.2)$$

Here, $\mathrm{m_i}$ is the mass, $\mathrm{V_i}$ is the potential of the $\mathrm{i^{th}}$ atom. With acceleration obtained, the most widely used mathematic method to update velocity and position in MD is the Velocity-Verlet algorithm,[11,12] which acts over a single timestep from t to $\mathrm{t} + \Delta\mathrm{t}$ as follows:

$$\mathrm{v}\left(\mathrm{t} + \frac{1}{2}\Delta\mathrm{t}\right) = \mathrm{v(t)} + \frac{1}{2}\Delta\mathrm{t}\,\mathrm{a(t)} \qquad (2.3)$$

$$\mathrm{r(t + \Delta t)} = \mathrm{r(t)} + \Delta\mathrm{t}\,\mathrm{v}\left(\mathrm{t} + \frac{1}{2}\Delta\mathrm{t}\right) \qquad (2.4)$$

$$\mathrm{v(t + \Delta t)} = \mathrm{v}\left(\mathrm{t} + \frac{1}{2}\Delta\mathrm{t}\right) + \frac{1}{2}\Delta\mathrm{t}\,\mathrm{a(t + \Delta t)} \qquad (2.5)$$

Here, Δt is on the order of femtoseconds. v is the velocity of the particle, and r is the position of the particle. This method is reversible and has been proven to have excellent energy-conserving properties.[13,14]

2.2 MD Forcefields

As mentioned above, MD calculates forces on each atom based on pre-defined interaction functions. They are a set of equations, and typically referred to as forcefields or potentials in MD. A potential or forcefield describes the interaction among various atoms using analytical expressions. There are many flavors of available forcefields, and the most commonly used ones are Chemistry at Harvard Macromolecular Mechanics (CHARM),[13] Assisted Model Building with Energy Refinement (AMBER),[14] GROningen Molecular Simulation (GROMOS),[15] and Optimized Potentials for Liquid Simulations (OPLS).[16] In these force fields, each atom is represented by a sphere of mass 'm' and a partial charge 'q'. The sum over all the bonded and non-bonded interactions of all the atoms in the system constitutes the potential energy (V) of the system:[17]

$$V_{system} = V_{bond} + V_{angle} + V_{torsion} + V_{coulomb} + V_{vdw} \qquad (2.6)$$

The parameters in equation 2.1 are shown in Figure 2.1 and presented in detail below.

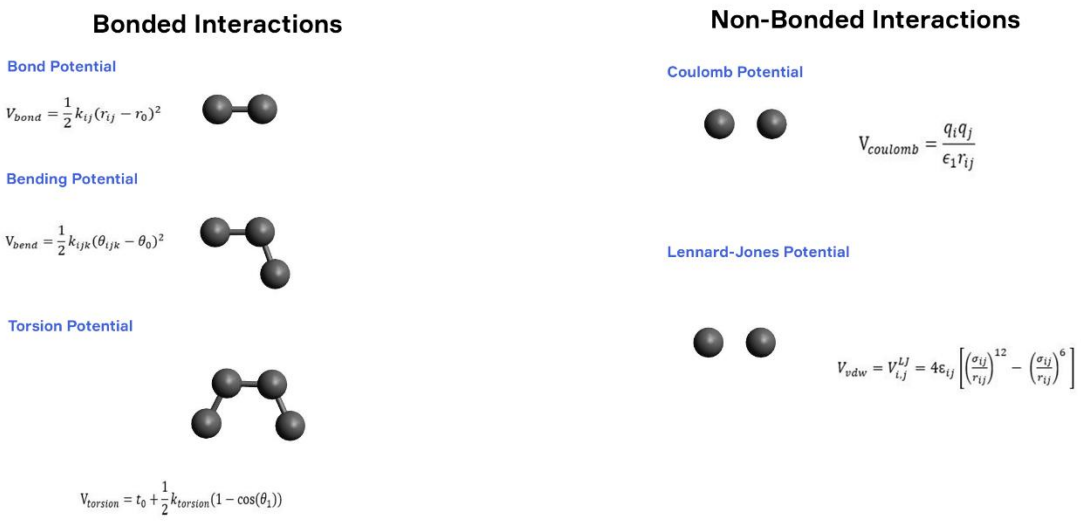

Figure 2.1 Bonded and non-bonded interactions used to describe interactions between atoms in a forcefield. Each of these interactions is described in the main text.

Bond stretching energy can be expressed by:[18]

$$\emptyset(\mathrm{r_{ij}}) = \frac{1}{2}\mathrm{k_{ij}}(\mathrm{r_{ij}} - \mathrm{r_0})^2 \qquad (2.7)$$

Similarly, the bond bending (angle) among three atoms i, j, k can be put as:

$$\emptyset_{\mathrm{bend}} = \frac{1}{2}\mathrm{k_{ijk}}(\theta_{\mathrm{ijk}} - \theta_0)^2 \qquad (2.8)$$

Here, $\mathrm{k_{ij}}$ is the bond force constant, $\mathrm{r_{ij}}$ is the distance between atom i and j, $\mathrm{r_0}$ is the equilibrium bond length, θ_0 is the equilibrium angle between two position vectors of $\mathrm{r_{ij}}$ and $\mathrm{r_{jk}}$, θ_{ijk} is the angle between the three adjacent atoms i, j, and k, and $\mathrm{k_{ijk}}$ is the angle force constant. Following this, the interaction among four-body bonded atoms (i, j, k, l) can be expressed as:[18]

$$\emptyset_{\text{torsion}} = t_0 + \frac{1}{2} k_{\text{torsion}}(1 - \cos(\theta_1)) \qquad (2.9)$$

Here, t_0 is a constant, θ_1 is the torsional angle, and k_{torsion} is the spring constant describing the resistance to torsional deformation of a group of atoms. Based on these definitions, the total bond, angle, and torsion energy of the system can be described as the summation of the contributions from all pairs of atoms (bond stretching), all triple of atoms (bond bending), and all quadruples of atoms (bond rotation), respectively:

$$V_{\text{bond}} = \sum_{\text{pairs}} \emptyset_{\text{bond}} \qquad (2.10)$$

$$V_{\text{bend}} = \sum_{\text{triples}} \emptyset_{\text{bend}} \qquad (2.11)$$

$$V_{\text{torsion}} = \sum_{\text{qualruples}} \emptyset_{\text{torsion}} \qquad (2.12)$$

The Lennard-Jones potential (LJ) is a simple pair potential that can accurately model weak van der Waals interactions, and has the following form:

$$V_{\text{vdw}} = V_{i,j}^{LJ} = 4\varepsilon_{ij}\left[\left(\frac{\sigma_{ij}}{r_{ij}}\right)^{12} - \left(\frac{\sigma_{ij}}{r_{ij}}\right)^{6}\right] \qquad (2.13)$$

Here, r_{ij} is the distance between any two atoms, and ε_{ij} and σ_{ij} are parameters determined by fitting to known properties and correspond to non-bonded energy and non-bonded length, respectively. The attractive interactions are due to temporary dipoles created by fluctuations of the electron clouds, and the repulsive interactions are due to overlap of the electron clouds (Pauli exclusion principle) which forces electrons into higher energy states.[22] In the case of electrostatic interactions, charges on atoms interact according to Coulomb's law:

$$V_{coulomb} = \frac{q_i q_j}{\epsilon_1 r_{ij}} \qquad (2.14)$$

Here, q_i and q_j are the partial charges of atoms, respectively, i and j, r_{ij} is the distance between two charged atoms, and ϵ_1 is the effective dielectric constant. [18]

Among all available force fields, OPLS is widely used for biomolecules. Several sets of OPLS parameters have been published. The original OPLS potential functions used a partially united-atom model (OPLS-UA), which integrates parameters for hydrogen atoms into the parameters for carbon atoms that the hydrogen atoms are bonded with. Thus, the only hydrogens that are implicit are attached to aliphatic carbons. Sites for nonbonded interactions are placed on all non-hydrogen atoms and on hydrogens attached to heteroatoms or carbons in aromatic rings.[19–21] This strategy can save simulation time. Actually, the computational time is roughly proportional to the total number of interaction sites squared, making the OPLS-UA computationally attractive. Another OPLS force field developed to study organic materials and proteins is OPLS-AA (all-atoms), which includes every atom explicitly. The OPLS-AA force field has been proven to be one of the most accurate force fields by testing thermodynamics properties, e.g., enthalpy and density.[22–24] Therefore, in this thesis, we have chosen OPLS-AA force field to study our systems.

To further validate OPLS-AA[25] force fields, we also compared it with other force fields. Compared to GROMOS96[15] force field, OPLS-AA gave us more accurate results in terms of physical properties, e.g., density, interfacial tension, and compressibility (see Appendix 6.7 Solvent Properties), while it didn't give us an accurate result for diffusion coefficient. In the literature, it has been reported that one of the disadvantages of using OPLS-AA is its lack of accuracy to calculate diffusion coefficient.[26] Because of this fact, we have designed our initial configuration in a way that we could diminish this factor in our simulation, meaning initially placing asphaltene molecules at the oil/water interface (details in Chapters 3 and 4).

2.3 Thermostat

In MD, the temperature of a system is calculated from its kinetic energy, shown as follows:

$$K_e = {}^{3}/_{2}\, N K_B T \qquad (2.15)$$

Here, K_e is kinetic energy of molecules, N is Avogadro constant, T temperature, and K_B is Boltzmann constant. The instantaneous temperature can then be translated through the instantaneous kinetic energy:

$$T(t) = \frac{1}{3k_B N}\sum_{i=1}^{N} m_i v_i^2(t) \qquad (2.16)$$

Thus, by scaling velocities, we can control the temperature in an MD system. Several formulations are available, including Andersen,[27] Nose-Hoover,[28] etc.

In the Andersen thermostat, the system is coupled to a heat bath that can transfer the system from one energy state to another.[27] This is achieved by stochastic collision that acts occasionally on random selected particles. Through exchanging energy with the heat bath, the system temperature is maintained. A disadvantage of the Anderson thermostat is that since the algorithm randomly decorrelates velocities, the dynamics of the system is not physical. Thus, the Anderson thermostat is inefficient when working with dynamical properties. An alternative and more accurate approach compared to the Anderson thermostat, is the Nose-Hoover thermostat, which employs an extended ensemble approach.[28] Specifically, the system is extended by introducing not only a heat reservoir but also a friction term in the equation of motion. This friction term, which is a fictitious dynamical variable, slows down or accelerates particles until the temperature measured through kinetic energy is equal to the desired value. Then, through integrating the Newtonian's law for both the bath and the system, instead of using stochastic collision on the system, dynamics of the system can be physically modelled. This thesis adopts the Nose-Hoover thermostat[28] to control temperatures.

2.4 Barostat

In MD, it is typically desirable to control the pressure of the system studied, which requires the usage of barostat. Practically, barostat functions by scaling the system volume and/or coordinates of each atom since instantaneous pressure is related to the system volume and positions of each particle.[29]

Berendsen developed a protocol to change the volume of the system to regulate the pressure.[30] This method is very efficient in equilibrating the system, but pressure

fluctuations with this barostat can be significant. In addition, the algorithm induces artifacts when simulating in-homogenous systems. More accurate methods are developed using an extended ensemble approach, similar to the algorithm adopted in the Nose-Hoover thermostat. The Anderson barostat is the pioneer approach in this category.[27] This approach couples the system to a pressure bath and adds a new degree of freedom corresponding to the volume of a simulation domain to the total energy of the system. Furthermore, scaling is performed on both the system volume and positions of atoms. An extensions of Andersen method is adopted in this thesis (Parrinello-Rahman barostat),[31] which also allows the changes in the shape of the simulation box.

2.5 Energy Minimization and Periodic Boundary Conditions

Before running an actual MD simulation, energy minimization is essential to optimize the molecular arrangements in the system, since the initial chemical structures may not be energetically favorable. Energy minimization is a static process, during which forces among different atoms (thus potential energy) are minimized through adjusting atom positions (geometries). Another technique used by MD is periodic boundary conditions (PBCs), in order to preserve mass in the system studied and further approximate a large system by using a small unit domain (cell). Using PBCs, atoms or molecules that go outside of the simulation box (system) during integrating equations of motion will re-enter the box from the opposite side of the box. By doing so, it ensures the constant number of particles throughout the simulation. [29]

2.6 MD Practical Protocols

Practically, to run a MD simulation, several files are needed. Using GROMACS (a widely used MD package) as an example, these files are listed below.

1) Molecular topology file (.top): The molecular topology file contains a complete description of all the interactions in the simulation system.

2) Molecular Structure file (.gro): The .gro file contains all geometry information for the system studied.

3) Run Parameter file (.mdp): This file specifies parameters required to perform a simulation, e.g., thermostat, barostat, timestep, and number of steps. Figure 2.2 shows an overview of a typical MD run.

To ensure accuracies during MD simulations (equilibrations and productions), we need to determine a series of parameters in .mdp files. The first parameter is defining optimum time step, since small timesteps limit the length of MD trajectories and increase the simulation run time, and large timesteps can cause a MD simulation to become unstable with energy increasing rapidly with time. The next step was to identify a suitable constraint algorithm and its related parameters. After careful considerations and based on literature works, we chose LINCS[32] algorithm. For searching the neighboring grid cells, we chose a cut-off method. After sensistiveis studies with different cut-off values, we found that the optimum cut-off value for short-range electrostatic and van der Waals is 1.4 nm. To calculate long-range electrostatics, we used particle-mesh Ewald method, for which the grid spacing was 0.16 and 0.12 for NPT and MD respectively. Regaridng thermostat, the Nose-Hoover thermostat is widely used and was adopted in this thesis.[28] For barostats, [32]we first used Berendsen[33] for equilibrating the system and then used utilized Parrinello-

Rahman for the main production simulations. The parameters used in this thesis were validated using simulations performed on pure solvents (see Appendix 6.7 Solvent Properties).

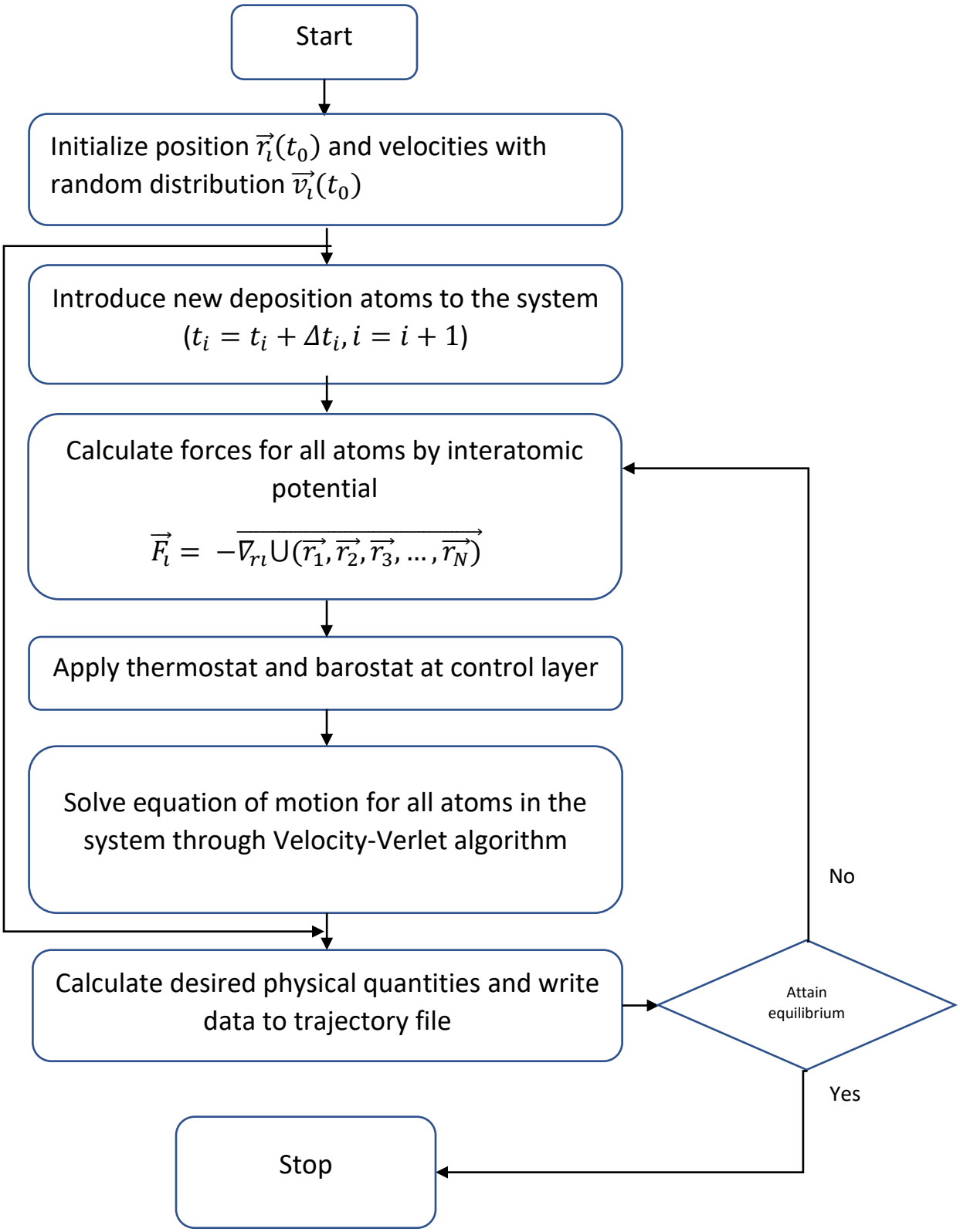

Figure 2.2 Flowchart for MD simulations [34,35]

Chapter 3. Molecular Investigations on The Effects of Naphthenic Acids on the Aggregations and Interfacial Behaviors of Asphaltenes in Oil

3.1 Introduction

Understanding the behaviors of polyaromatic (PA) molecules in organic solvents and at oil/water interfaces is of great interest for crude oil industrial processes. In particular, the heaviest fractions in crude oil, known as asphaltenes, belong to the family of PA molecules, and they have imposed great challenges for oil transportation in pipelines and water/oil separations.[36] For instance, nanoaggregates formed by asphaltenes can easily grow into larger aggregates of various sizes and eventually lead to coagulation and precipitation, thus blocking transport, preventing water/oil separations, and deactivating catalysts.[37]

Quite a lot of studies based on molecular dynamics (MD) have been performed to uncover the nature of asphaltene behaviors (i.e., PA molecules behaviors) in biphasic systems. In the study done by Jian et al.,[38] they investigated the effects of solvents on the aggregation of neutral PA molecules and showed that insoluble solvents (n-heptane) enhanced the π-π stacking of PA molecules compared to soluble solvents (toluene). It has been revealed that asphaltene molecules preferably interact within themselves, forming dimer, trimer, tetramer, and stackings containing up to 6 sheets.[39–41] Pacheco-Sánchez et al. [42] focused on the effect of temperatures on the asphaltene aggregation, and claimed that the number of PA aggregates decreases with increment in temperatures. They also showed the distance observed in different asphaltene stackings is due to the different geometric structures, which lead to a different type of interactions between asphaltenes.

Zhang and Greenfield[43] found that the inter-molecular orientation is closely related to the molecular structure and the system temperature, in a way that low-aromatic PA

molecules with long-range alkane branches tend to form parallel stacking at high temperatures and perpendicular stacking at low temperatures.[43] They observed opposite behaviors for highly aromatic PA molecules. Especially, at low temperatures, highly aromatic molecules tend to stay parallel to each other and form π-π stacking, while at the higher temperatures they rather form T-shape stacking.[43] Regarding aggregation driving forces, Sedghi et al. [44] confirmed that the interaction between the polyaromatic cores of asphaltene molecules plays dominant role, and meanwhile, the presence of the heteroatoms in the aromatic core enhances this stacking behavior.

With the presence of interfaces, Gao et al.[45] showed that the presence of anionic terminals on the aliphatic chains can strongly influence the behavior both in bulk and at the interface. In detail, a neutral asphaltene tends to form face-to-face (π-π) stacking among PA cores at the interface, and asphaltenes with the anionic terminals tend to have both face-to-face(π-π) and T-shape stacking at the interface. Teklebrhan et al.[46] investigated the orientation of PA molecules at the oil/water interface and they postulated that the predominant orientation of PA molecules is perpendicular to the interface, due to π-π stacking between the polyaromatic rings and the hydrogen bonds (H-bond) between water molecules and the carboxylic groups presented in the asphaltene structure. In a study done by Jian et al.,[47] they also showed asphaltene molecules at the toluene/water interface to be perpendicular to the interface. Mikami et al.[48] studied oil/asphaltene/water interface systems and found that asphaltenes in heptane tend to go to the interface and form stable parallel structures to the interface.

In another study done by Yaseen & Mansoori,[49] one other factor helping the stacking is the H-bond between asphaltene and asphaltene and between asphaltene and water.

To emphasize the importance of H-bond in the interfacial behavior of asphaltenes, Singh et al. [50] investigated different molecular structures of asphaltene and showed that the presence of asphaltene at the oil/water interface is due to the H-bond between water molecules and heteroatoms, which is strongly dependent to the asphaltene molecular structure and the presence of different heteroatoms. In our previous study,[51] we investigated the effects of different solvents on the synergistic behaviors of asphaltene aggregations and adsorptions, and it was found that asphaltene aggregations can modulate the adsorption amounts of asphaltenes. Beyond external conditions and asphaltene molecular structures, the presence of other oil components can also affect the asphaltene aggregation and interfacial behaviors. One close example is Naphthenic Acids (NAs) which are naturally present in crude oil. NAs are mixture of saturated aliphatic and alicyclic carboxylic acids, accountable for crude oil acidity. NAs are toxic and it has been shown that their existence in crude oil has led to corrosion problems and mystified asphaltene aggregation and adsorption.[52–54]

Östlund et al.[55] conducted their study based on Nuclear Magnetic Resonance (NMR) and observed, the interaction between NAs and PAs is strongly dependent on the PA type. Heaps et al. [56] studied the effect of NAs on PA precipitations and depositions with the help of Dynamic light scattering (DLS) and NMR supported by MD. They found that the experimental sample containing 5β-cholanic acid-3-one has the least effect on the PA aggregation, although it has the highest dipole momentum among the molecules. It was postulated that the reason is the self-aggregation of the aforementioned NA molecule. Teklebrhan et al.[57] investigated the configuration of PA aggregation in presence of NAs in toluene and found that by forming H-bond between NAs and PAs, NAs can reduce the

number of PA-PA H-bond and enhance the π-π stacking between PAs.

In a later study, Kiran et al.[58] investigated the effect of NAs-PAs on oil/water separations. In their study, heptol (mixtures of heptane and toluene) was used as the solvent for bitumen, and it was found that the presence of NAs in heptol-bitumen-water systems promotes the oil/water separation due to the segregation of asphaltene at the oil/water interface. However, there is no information/discussion on how PA-NA interacts with one another. As such, the mechanisms responsible for the effects observed were unclear. Mokhtari et al.[59] experimentally investigated the effects of the presence of NAs on asphaltene stabilization, and in their study, NAs did not show any effect in low salinity, while in brines they show the tendency to stabilize asphaltenes. Teklebrhan et al. [60] studied the adsorption of PA molecules at the oil/water interface with different NA/PA concentrations and different NA molecular structures. They observed that at low NA concentrations, PA adsorption at the interface is dependent on the NA molecular structure. Specifically, small NAs almost didn't have any effect on the PA adsorption and large NAs tend to enhance the PA migration to the interface. On the other hand, in the system with a high NA concentration, the presence of small NAs tends to hinder the PA migration gravely. In this work, while the size effects of NAs were discussed, information was not available on other structural factors (e.g., linear chains vs. cyclic rings).

As can be seen from the above, the roles played by the molecular structures of NAs have not been thoroughly investigated in the literature. To bridge this gap, a series of MD simulations were performed in this chapter to provide informative atomistic insights. In total, 4 NAs of different molecular structures were adopted, and their effects on PA behaviors at the oil/water interface and in bulk phases were reported along with

interaction mechanisms. It is expected the results obtained can help to understand the synergistic behaviors of NAs and PAs, and further shed lights on how to remove them using mechanical or chemical methods.

3.2 Methods

3.2.1 Molecular Models and Simulation Systems

The NA models studied are named as NA-1, NA-2, NA-3, NA-4, which have the same polar head, but different aliphatic/alicyclic side chains (Figure 3.1a). These models are either mostly used in the literature or originated from the most abundant NAs in crude oil.[61] The oil phase was represented using toluene or heptane, and violenthrone-79 (VO79) was adopted as the uncharged PA molecule (Figure 3.1b). VO79 has a chemical formula of $C_{50}H_{48}O_4$ with a molecular weight of 712.9 g/mol. It is critical to note that VO79 is similar to the island-type asphaltenes, and its oxygen content (9%) is relatively close to that of the asphaltene fractions adsorbed onto the oil/water interfaces.[62,63] In total, 10 different systems have been built to investigate the effects of NAs on the PA behavior in bulk and at the interface in different solvents (toluene vs. heptane). Details for these systems are listed in Table 3.1.

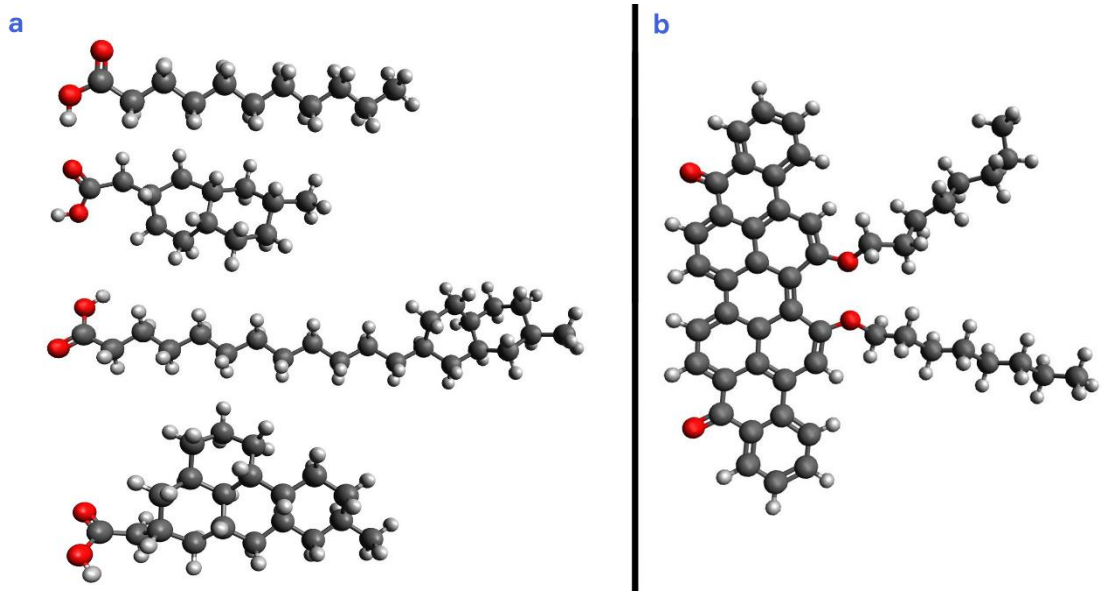

Figure 3.1 Molecular structure of PA and NA molecules, in the left from top to bottom, NA-1, NA-2, NA-3, NA-4, the right-side PA molecules (VO79), the red atom represents oxygen, the white atom represents hydrogen, and grey atom represents carbon

In the first 5 systems of Table 3.1, we introduced heptane as solvent, and the system without NA was named as system Hep. In the other systems, we introduced different NAs. These systems were named using the NA molecules they contained. For instance, the system containing PA, NA-1, heptane, and water was referred to as NA-1-Hep. In the next 5 systems, toluene was adopted as the solvent. Each of the 10 systems contains the same number of PA molecules (180) and NA molecules (180).

Table 3.1 systems constructed for our simulations

	System	No. Solvent	No. Water	No. NA	No. PA
1	Hep	3585	15624	0	180
2	NA-1-Hep	3070	16690	180	180
3	NA-2-Hep	3085	16437	180	180
4	NA-3-Hep	2675	17463	180	180
5	NA-4-Hep	2845	17304	180	180
6	Tol	5120	14509	0	180
7	NA-1-Tol	4409	15823	180	180
8	NA-2-Tol	4403	16046	180	180
9	NA-3-Tol	3815	17100	180	180
10	NA-4-Tol	4268	15466	180	180

The initial structure of organic solvents, VO79, and NAs were built using Avogadro molecule editor,[64,65] and then equilibrated in Gaussian.[65] During the construction of the initial configuration for Hep/Tol, a box of 11.3*11.3*4 nm^3 was first filled with two rows of asphaltene, each row containing 90 VO79 molecules with their polyaromatic cores parallel with one another and the z-direction but perpendicular to the x-y plane. Then, the dimension of this box was expanded in the negative z-direction, and the new box has a

dimension of 11.3*11.3*11.3 nm, followed by that solvent (toluene or heptane) molecules were randomly introduced. The box was then expanded in the positive z-direction to a length of 22.6 nm and water molecules were introduced to the empty part. For the systems with NAs, the procedure is the same except that 180 corresponding NAs were randomly added to the organic solvents (toluene or heptane). A schematic of the aforementioned procedure is shown in Figure 3.2.

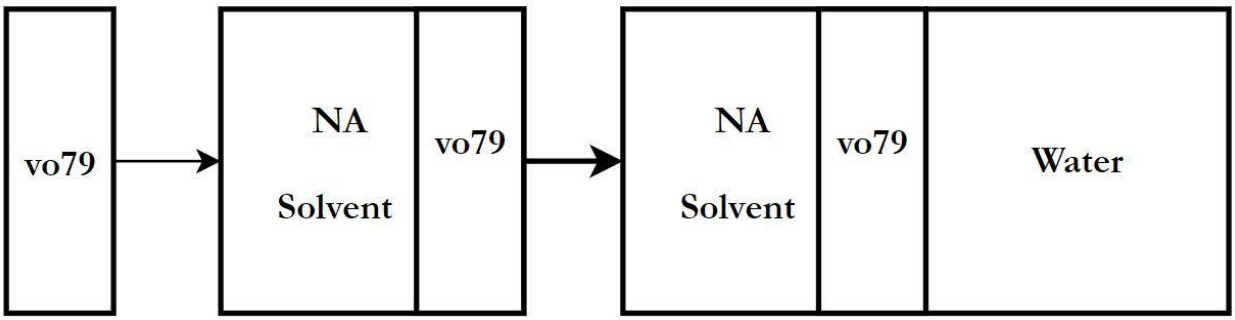

Figure 3.2 Schematic of constructing initial configurations.

3.2.2 Simulation Details

The force field adopted in this work was all-atom Optimized Potentials for Liquid Simulations (OPLSAA) force field,[25] which has shown to be a suitable force field to study biphasic systems containing organic liquids.[25,66,67] The topologies for VO79, NAs, and solvents were built using MKTOP algorithm,[68] by supplying the coordinates of the molecule to the MKTOP algorithm. The default topology obtained from MKTOP was then manually modified by adopting the partial charges obtained from Gaussian geometry optimization to be compatible with the OPLSAA force field. A simple-point-charge (SPC/E) model was used for water,[33] as it has been proven to provide reliable results for

oil/water interface investigation.[33,69]

All simulations were performed using the MD package GROMACS.[70] After constructing the initial configuration, we first performed static structure optimization to ensure the maximum force is less than 100 KJ/(mol*nm). In this study, we used steep descent algorithm , a robust algorithm to find the local energy minimum.[71] Full dynamics simulations were conducted in two stages. The first stage was performed in the NPT ensemble using Berendsen barostat[30] for 100ns, and the second stage was performed in the $NP_{normal}AT$ ensemble using Parrinello-Rahman barostat[31] for 200ns simulation. All dynamics simulations adopted periodic boundary conditions, constrained all bonds with the LINCS algorithm,[32] used a cutoff distance of 1.4 nm for van der Waals and short range electrostatic, treated the full electrostatics with the particle-mesh Ewald method,[72] and defined a 2fs time step. In addition, for all dynamics simulations, temperature was maintained at 300k using a Nose-Hoover thermostat.[28]

3.3 Results and Discussion

Figure 3.3 shows the final snapshots in systems without NAs. Comparing heptane systems with toluene systems, PA molecules tend to stay at the heptane/water interface due to the immiscible nature of PA cores in heptane, while in toluene, PA molecules tend to migrate to the bulk phase. This observation aligns with the definition of asphaltene molecules, which is defined as the fraction of the crude oil soluble in aromatics (toluene) and insoluble in alkanes (n-heptane). Based on Figure 3.3, in heptane phase, we have more PA molecules at the interface, and this adsorption of PA molecules at the interface is responsible for the enhanced stability of the emulsion in heptane. To probe the effect

of solvents on orientations of PA molecules with respect to the oil/water interface, we calculate the angle distributions for systems Hep and Tol. For this calculation, PA molecules were determined to be at the interface, if the centers of geometry of PA molecules were within 1nm from the oil/water interface. For PA molecules located at the interface, we then calculated the cos(θ) of each PA molecule with respect to the oil/water interface. The criterion for the interfacial width is 1nm, given that the maximum length of the polyaromatic core is less than 2nm. For the cos(θ), we refer to the orientation as parallel to the interface when $\theta < 25^{\circ}$, the orientation as perpendicular to the interface when $\theta > 60^{\circ}$, and the orientation as cross (oblique) to the interface when $25^{\circ} < \theta < 60^{\circ}$.

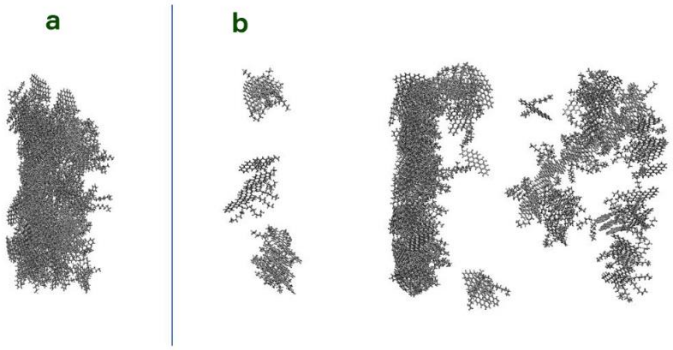

Figure 3.3 Snapshot of the Hep and Tol systems at the final configuration, a) Hep system and b) Tol system

Figure 3.4 shows the angle distributions in systems Hep and Tol. It can be seen that in Hep system, PA molecules prefer to be oblique with respect to the heptane/water interface, and in Tol, both oblique and perpendicular orientations are preferred. That is due to the fact that PA molecules are less crowded compared to Hep system, corresponding to that PAs prefer to go to the interface and stabilize emulsion in heptane. This is consistent with the fact that compared to oxygen atoms on the side chains, the

oxygen atoms connected to the PA core are more likely to interact with water molecules by forming H-bonds. This strong tendency of PA cores to form non-parallel orientation has also been discussed in the literature.[46,47] The difference between Tol and Hep may be attributed to that PA molecules are less crowded in the toluene phase compared to those in the heptane phase, so that they can oscillate between different orientations.

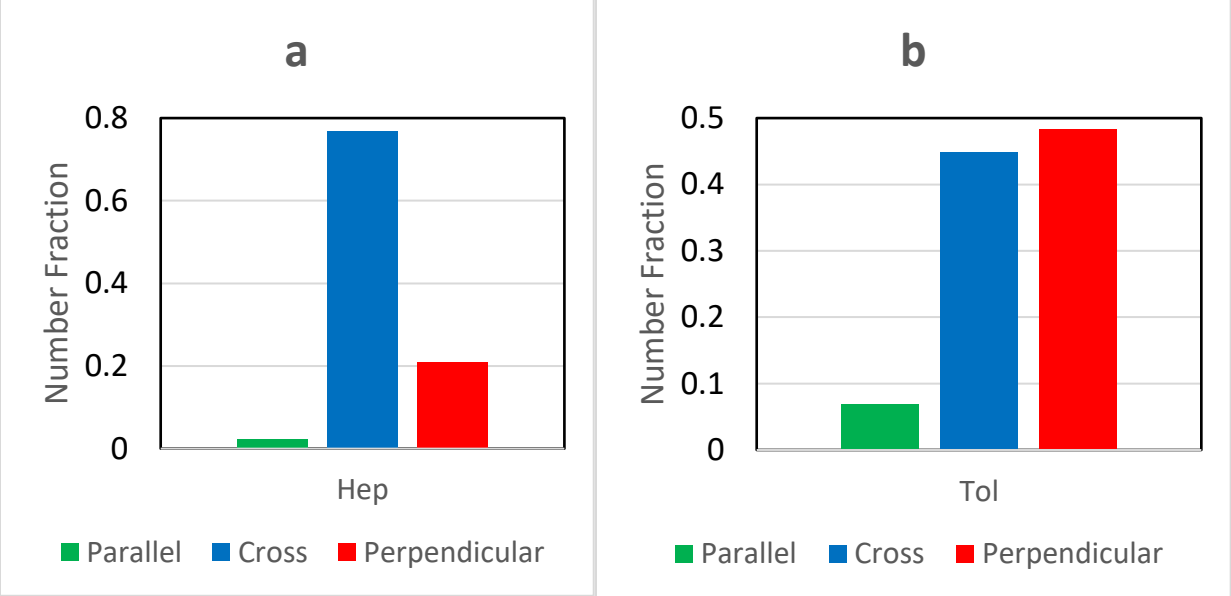

Figure 3.4 Orientation of the PA molecules in the systems without any NA in different solvents in a) heptane b) toluene

3.3.1 Accumulation of PA Molecules at The Heptane/Water Interface

Figure 3.5 shows the density profiles for systems using heptane to represent the oil phase. As can be seen, in all the heptane simulations, PA molecules are at the oil/water interface and heptane and water are immiscible. Initially, there is no NA molecule at the interface. But throughout the simulation phase, due to the interaction between NA and water, NA tends to go to the heptane/water interface and lead to interfacial tension reduction at the interface, as observed in the literature.[59] Detailed examinations show that

the numbers of PAs at the heptane/water interface for NA-1-Hep, NA-2-Hep, NA-3-Hep, NA-4-Hep, and Hep systems are 118, 140, 127, 128, and 134, respectively. Compared to Hep which has no NA molecules, in the system containing NA-1 (i.e., system NA-1-Hep in Table 3.1), PAs tend to migrate to the bulk from the interface, the number of PA molecules at the heptane/water interface is lowest (118)Contrarily, in system NA-2-Hep, it seems that PAs are more crowded at the interface, which is evidenced by that in Figure 3.5c, the shoulder originally observed in system Hep (Figure 3.5a) has disappeared. However, it doesn't mean that PAs in system NA-2-Hep is less favorable to stacking, evident by the number of PAs at the interface to be highest for NA-2-Hep system (140). Interestingly, Figure 3.5d shows that PA molecules are more organized in the system containing NA-3 (i.e., system NA-3-Hep), and correspondingly, a sharper shoulder appears in the density profile of the PA molecules, and the thickness of the PA molecules is the same with that of system Hep. In system containing NA-4 (i.e., system NA-4-Hep), PAs are still more or less at the interface, and insignificant changes are observed in the shape of the asphaltene density profile (Figure 3.5e). Also, it seems NA-4 mainly migrates to the interface where PAs are absent.

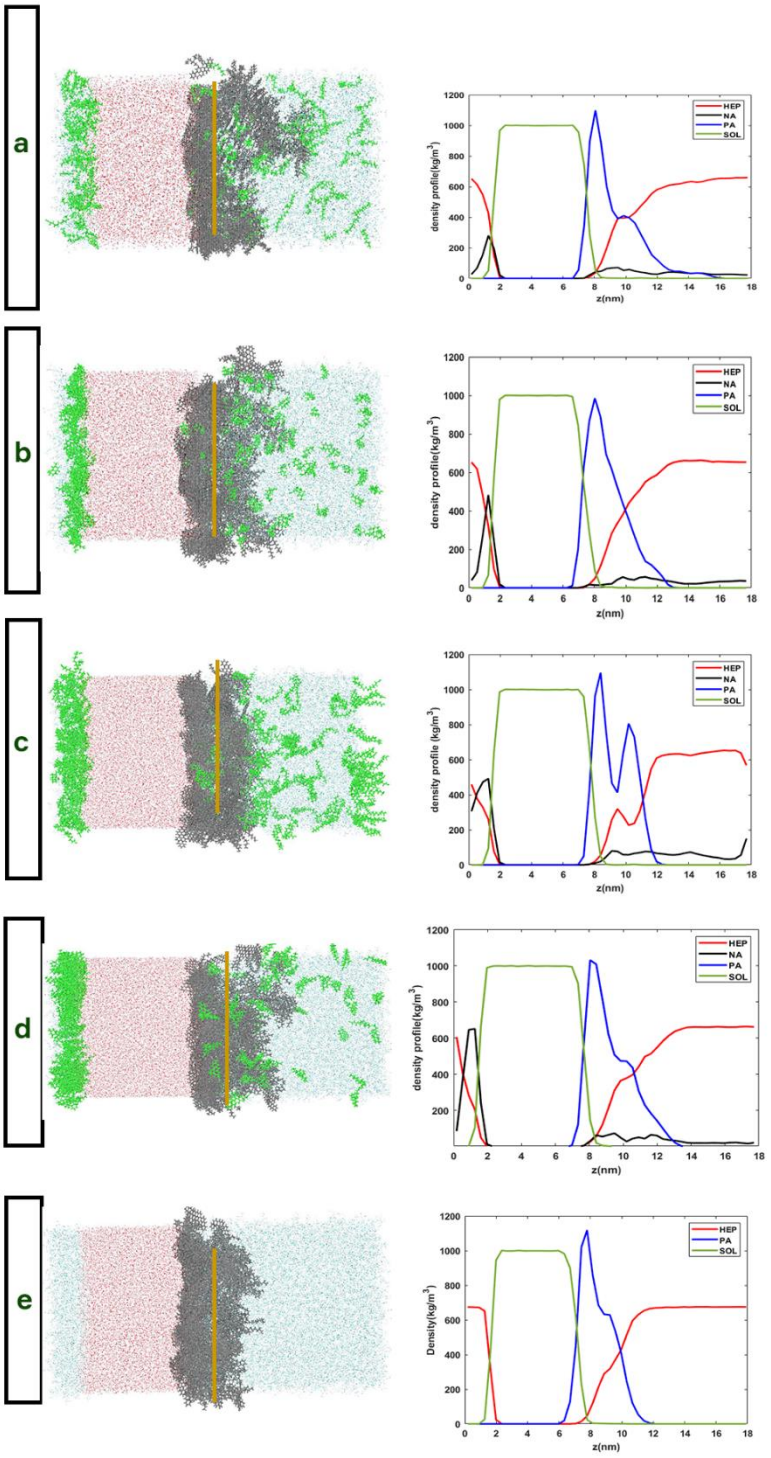

Figure 3.5 Snapshot and density profile of system a) Hep, b) NA-1-Hep, c) NA-2-Hep, d) NA-3-Hep, and e) NA-4-Hep. The main interface is highlighted using a yellow line.

We further investigated the effects of NAs on the $\pi - \pi$ stacking of PA molecules. Figure 3.6 plots the radial distribution function $g(r)$ between PA cores. As can be seen, the presence of NA molecules promotes and enhances the π-π stacking between PA molecules. Among the NAs studied, NA-3 tends to enhance the π-π stacking more compared to the other NAs. NA-2 shows slightly less prominent effects compared to NA-3. For NA-1 and NA-4, it seems they have almost the same and least effect on the PA stacking. These observations are directly correlating with the accumulation of PAs at the interface, where PAs are more ordered in system NA-3-Hep, and the corresponding density profile shows a prominent shoulder.

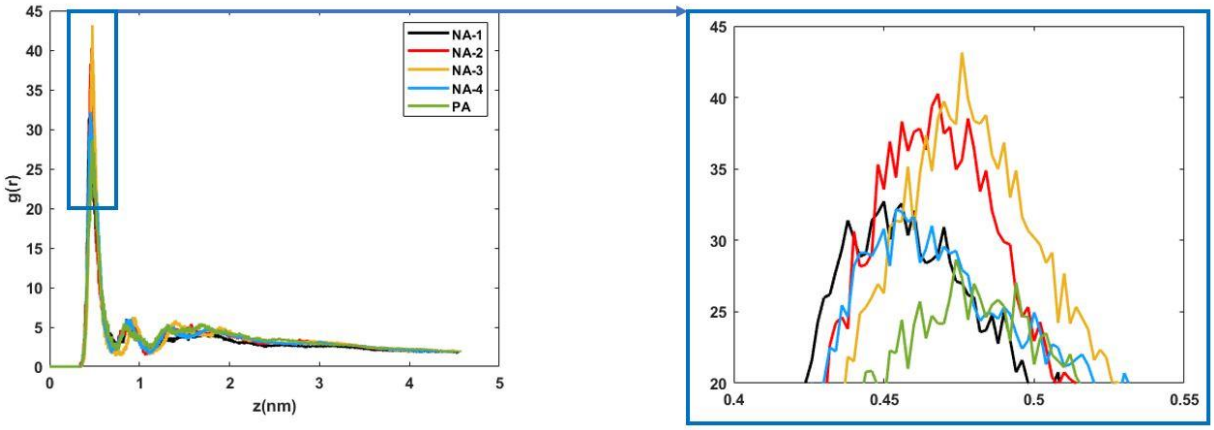

Figure 3.6 Radial distribution function $g(r)$ between PA cores in heptane/water systems

3.3.2 Orientation of PA Molecules at The Heptane/Water Interface

In this section, we will investigate the orientation of PA molecules at the heptane/water interface in exposure to NA molecules containing different cyclic and aliphatic substituents. Figure 3.7 shows the angle distribution and asphaltene orientation at the interface, over the last 5ns of the simulation time. From Figure 3.7, it is evident that VO79 orientation at the heptane/water interface is mostly non-parallel. Compared to HEP with no NAs, NA-2 and NA-3 molecules show the highest effect on the orientation of asphaltenes at the heptane/water interface, followed by NA-1. Again, NA-4 is the least effective NA among the 4 types of NA molecules investigated. This might be caused by the delicate balance among the interactions between NA and water molecules, NA/PA interactions, and NA/NA interactions. In return, they cause less crowded PA aggregation at the interface, and lead to more organized stacking and forming more perpendicular orientations at the interface.

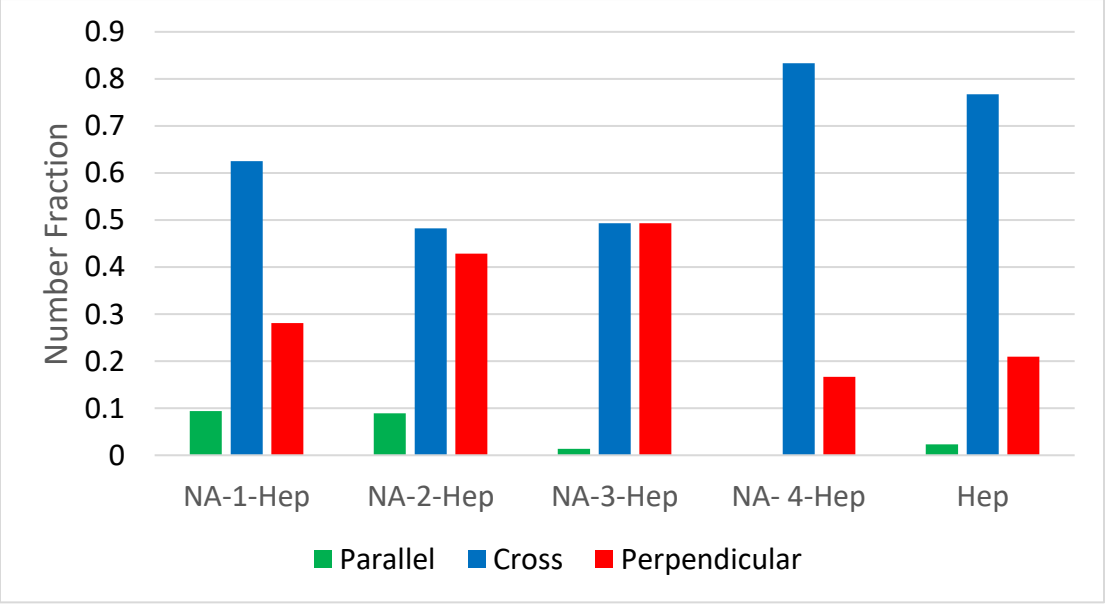

Figure 3.7 Orientations of PA molecules at the heptane/water interface in the systems with and without NA molecules

To understand this, we calculated the H-Bond formed between NA and PA and that between NA and water. These results are summarized in Table 3.2. From Table 3.2A, NA-1 has the largest number of H-bonds formed with PA, which demonstrates its effects on dragging PAs into bulk form the interface. NA-1 also has the least number of H-Bonds with water, consistent, again, with the fact that NA-1 mainly acts to drag PAs away from the interface. Contrarily, moving to NA-2 and NA-3, they formed a decreased number of H-Bonds with PA but an increased number of H-Bonds with water. This indicates that NA-2 and NA-3 migrates to the interface and competes with PAs to form H-Bonds with water. This competition will reduce the contact areas between PAs and water, leading to that PAs are more stacked at the interface and prefer more perpendicular orientations with respect to the interface. In addition, NA-3 molecules are very flexible at the interface, and their ability to fold may further increase its ability to form H-Bonds with water and reduce the contact area between PA and water, leading to that PAs are more stacked and prefer to be perpendicular to the interface. NA-4 forms the largest H-Bonds with water, corresponding to the fact that NA-4 migrates to the interface without PAs. This can be attributed to that both NA-4 and PA has core structures, which would make it more difficult for NA-4 to diffuse through the PA layers and compete with PAs. As a result, NA-4 has no significant effects on the accumulation and orientation of PAs.

Table 3.2 The number of H-bonds between NA/PA molecules (a), and NA/Water molecules (b)

a		b	
No. of NA/PA H-bonds		**No. of NA/Water H-bonds**	
Systems	**No.**	**Systems**	**No.**
NA-1-Hep	37.5	NA-1	128.5
NA-2-Hep	13.3	NA-2	152.2
NA-3-Hep	9.6	NA-3	172.3
NA-4-Hep	17.8	NA-4	198.3

3.3.3 Accumulation of PA Molecules at The Toluene/Water Interface

The final snapshots and density distribution profiles for toluene systems are shown in Figure 3.8. Examining the snapshot in Figure 3.8 reveals that the monomers and nanoaggregates of PA molecules coexist in the bulk toluene phase. Due to the solubility of toluene, PA molecules tend to go to the bulk phase, which can be further evidenced by the increased blue curves of PAs in the density profiles. While PA molecules were initially packed at the right interface, these nanoaggregates gradually migrate to the left interface, confirmed by the accumulation of PAs on the left interface as well as the peaks that appeared in the blue curves at ~0 nm. In the meanwhile, NAs, due to their interaction with water molecules, tend to go to the interface and replace or compete with PAs at the interface, leading to reduction in interfacial tension of these systems, as seen in the literature.[59]

Comparing the systems containing NA molecules with system Tol, the relevant snapshots exhibit more crowded PAs in the bulk (left panel in Figure 3.8), and the corresponding density profiles show that NA molecules introduce a more favoring

environment for PA molecules to aggregate in the bulk (right panel in Figure 3.8). Among systems containing NA molecules, NA-1 and NA-4 seem to depict a better environment in migrating PA molecules to the left interface, evidenced by the higher peaks of PA molecules at ~0 nm (density profiles in Figure 3.8). On the other hand, NA-2 has the smallest accumulation of PA molecules at the left interface (smaller peak of PA at ~ 0 nm, Figure 3.8b).

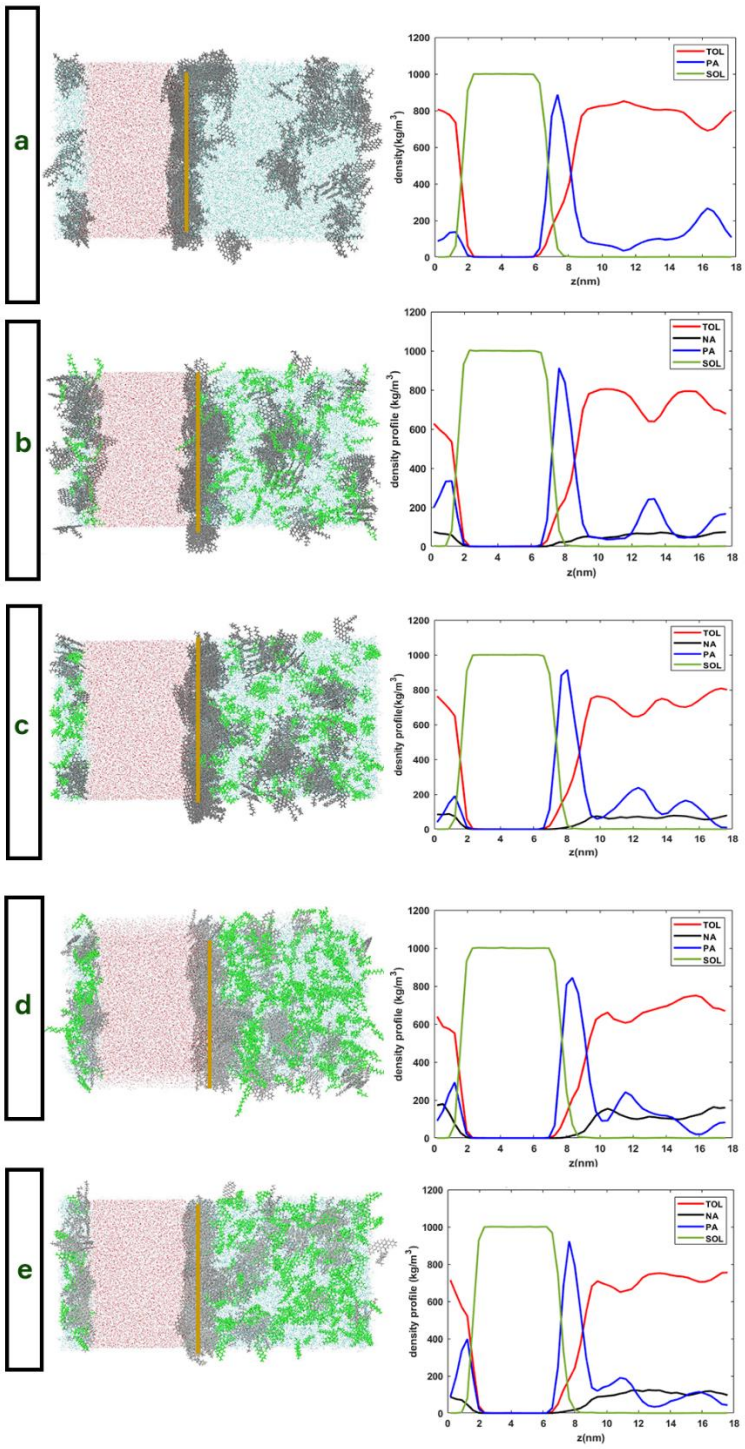

Figure 3.8 Snapshots and density profiles of a) Tol b) NA-1-Tol c) NA-2-Tol d) NA-3-Tol e) NA-4-Tol systems. The main interface, where PAs were initially packed, has been highlighted by a yellow line in each system.

To confirm the accumulation of PAs at the left interface, Figure 3.9 shows the number of PA molecules to each stacking present at the toluene/water interface. In this figure, each number shown in the grid depicts the number of PAs that are contributing to PA nano-aggregation. For instance, 11 in Figure 3.9a suggests there are 11 molecules in this nano-aggregation. These numbers are summarized in the caption of Figure 3.9, which shows the total number of PAs at the left interface. These numbers are consistent with the snapshots and density profiles shown in Figure 3.8.

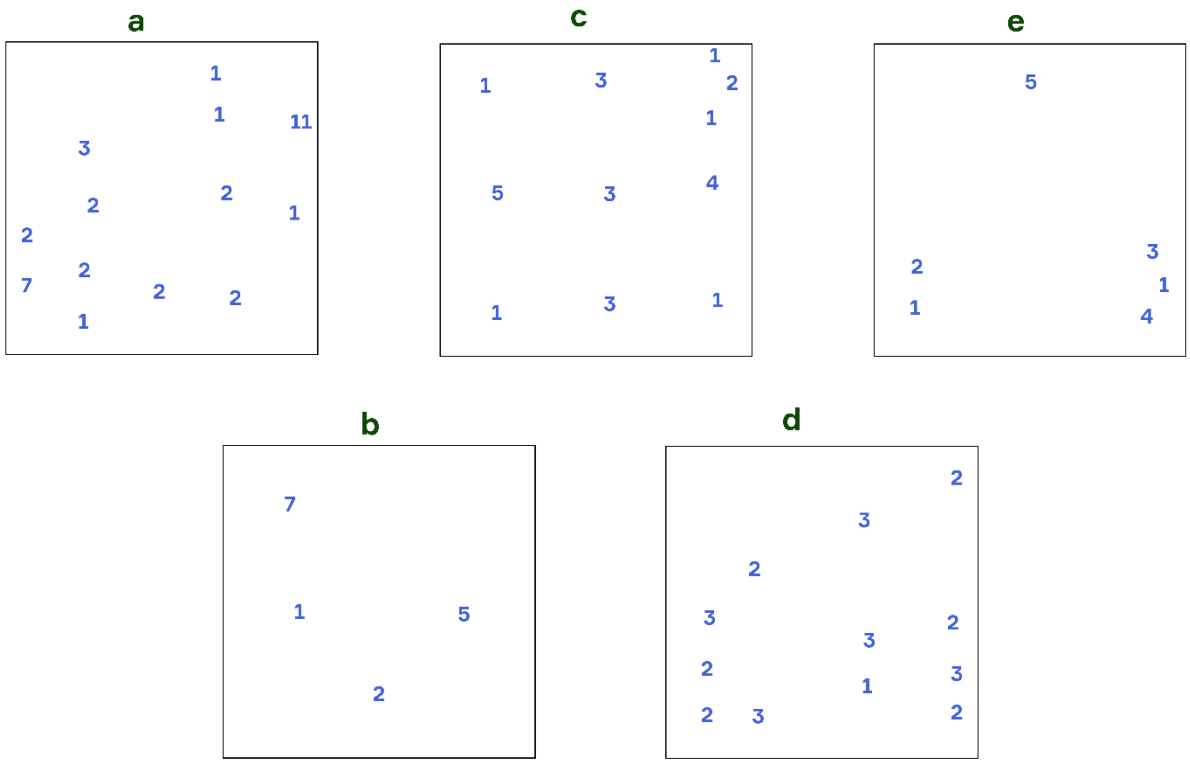

Figure 3.9 Monomers and nanoaggregates and the number of the PA molecules at the left interface: a) NA-1-Tol (total PA: 28) b) NA-2-Tol (total PA: 16) c) NA-3-Tol (total PA: 25) d) NA-4-Tol (total PA: 28), and e) Tol (total PA: 18) systems

3.3.4 Orientation of PA Molecules at The Toluene/Water Interface

To examine the effects of NAs on the orientation of PA molecules at the right interface where PAs were initially packed, Figure 3.10 plots the distributions for the orientations of PA molecules using a similar approach described earlier. As can be seen, the interaction between NA/water and NA/PA leads to change in the orientation of PA molecules at the interface, while at the same time, they compete or interact with PA molecules, leading to the decrease in interfacial tension at the oil/water interface.[59] Compared to system Tol, the system containing NA-4 shows negligible changes, while for the systems containing NA-1 or NA-2, we observe the largest effects on the PA orientation. Specifically, comparing system NA-1-Tol to system Tol, NA-1 increases the perpendicular orientation and decreases the cross (oblique) orientation. On the other hand, comparing system NA-2-Tol to system Tol, NA-2 decreases the perpendicular orientation at the interface and increases the cross orientation. Further examination of Figure 3.10 shows that NA-3 slightly increases the cross-orientation and meanwhile decreases the perpendicular orientation. The numbers of PA molecules bounded to the interface for NA-1-Tol, NA-2-Tol, NA-3-Tol, NA-4-Tol, and Tol systems are 68, 29, 53, 59, and 59, respectively. Considering Figure 3.10 and the aforementioned numbers, there is a straight correlation between PA orientation and the number of PAs bounded to the interface. For instance, system NA-1-Tol has the most PA molecules at the interface, where PAs prefer the perpendicular orientation the most; system NA-2-Tol has the fewest PA molecules at the interface, where cross orientation is mostly preferred by PA molecules. These effects of NAs seem to be drastically different from those obtained in heptane. To understand the underlying reasons, below, we will take a detailed look at the interactions present in each

system.

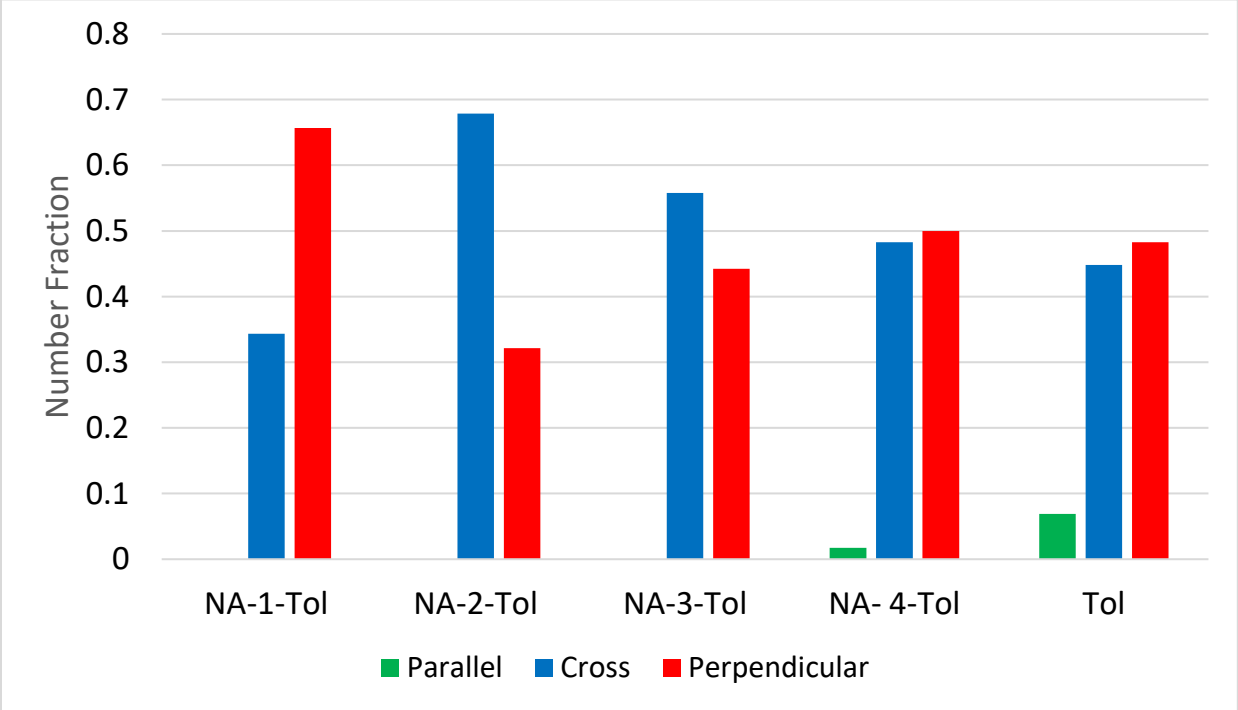

Figure 3.10 PA molecules orientation at the heptane/water interface in the systems with and without NA molecules

In Tables 3.6, we summarized H-Bonds formed between PA and NA, and among NA, and between NA and water, respectively. NA-1 molecules formed the largest number of H-Bonds with PA and water molecules, and meanwhile have the smallest number of H-Bonds among themselves. This is, NA-1 prefers to interact with water and PA molecules. The interaction between NA-1 and water would reduce the contact area between PA and water, and thus promotes the perpendicular orientation of PA at the interface. This is, oxygen atoms on the PA cores can form H-Bonds with water molecules. Meanwhile, the

H-Bonds formed between NA-1 and PA helps to saturate the oxygen atoms on the PA chains. NA-2, on the other hand, formed the smallest number of H-Bonds with PA and among themselves, and the number of H-Bonds formed between NA-2 and water molecules is only slightly higher than that between NA-4 and water molecules. This corresponds to the similarities in the chemical structures of NA-2 and toluene, which tends to solvate as many PA molecules as possible. Indeed, as shown in Tables 3.4 and 3.5, the accumulations of PA molecules at the interface are the smallest in system NA-2-Tol. Therefore, there is sufficient contact area for PA molecules to form cross orientation to have both core and chain oxygen atoms interacting with water molecules. Compared to NA-1 and NA-2, the number of H-Bonds formed by NA-3 are intermediate, leading to the intermediate effects of NA-3 on orientations. It is also noted that NA-3 has both chains and cyclic cores, making it possible to fold. This feature may explain the intermediate effects of NA-3. Regarding NA-4 molecules, they formed the smallest number of H-Bonds between NA-4 and water molecules, and the numbers of H-Bonds formed between NA-4 and PA and among NA-4 are very similar to those of NA-2, all of which are on the insignificant end. Since NA-4 has a large core in its molecular structure, these observations seem to suggest NA-4 tends to aggregate through cores and thus has negligible effects on PA accumulation.

Table 3.3 Number of H-bonds between a) PA and NA molecules b) NA molecules c) NA and water molecules

	a	B	c
System	**No. of PA/NA H-bond**	**No. of NA/NA H-bond**	**No. of NA/wat H-bond**
NA-1-Tol	31	4	42
NA-2-Tol	16	10	23.5
NA-3-Tol	17	12	31
NA-4-Tol	18	10.5	17

To further demonstrate the above points, we plotted, in Figure 3.11, the normalized density profiles by dividing the density profile generated for mass distributions with respect to the molecular weight of NA molecules. Detailed examination reveals that NA-1 can accumulate both at the interface and in the bulk, corresponding to NA-1 formed a large amount of H-Bond with water and PA molecules. On the other hand, NA-2 molecules are more or less dispersed in the bulk, due to its similar structure to toluene molecules. Moreover, NA-3 molecules show the highest fraction at the interface, while forming an intermediate number of H-Bonds (see Table 3.3). This is consistent with the special molecular structure of NA-3, which can form H-Bonds with water molecules but also makes them fold. Finally, NA-4 molecules are dominantly present and aggregate in the bulk, leading to insignificant interactions with PA and water molecules. All these confirm that the functioning of NA molecules highly depends on their molecular structures and the specific interactions that they can form with PA and water.

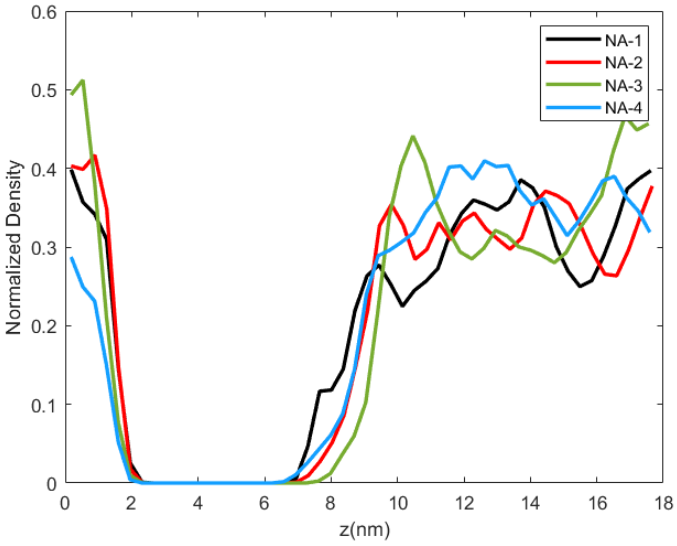

Figure 3.11 Normalized density profile of different NA molecules

3.4 Conclusion

MD-aided techniques were adopted in this study to investigate the behaviors of PA molecules (VO79) with the presence of NAs in different biphasic systems at molecular levels. The effects of solvents (oil phases) were first revealed. VO79 tends to stay at the water/heptane interface, while for toluene, they tend to go to the bulk. In addition, PA molecules form more perpendicular orientations at the water/toluene interface, while more oblique orientations were observed for PA molecules at the water/heptane interface. These different observations can be attributed to the different solvation powers between toluene and heptane. Due to the structural characteristics, VO79 is soluble in toluene, but insoluble in heptane.

A series of MD simulations further revealed the effect of NA molecular structures on the PA behaviors. In total, 4 different NA molecules have been adopted in this work, each of which are abundant in crude oil and have the same polar head with different nonpolar

tails varying from aliphatic to cycloaliphatic.

For the systems in which heptane is the oil phase, the presence of NAs promote stacking, but the extend of this enhancement is different. Moreover, NA molecules can affect PA accumulations and orientations at the interface. NA-1 of aliphatic tails acts as a solvent and drags PA molecules from the water/heptane interface to the bulk heptane, due to the structural similarities of NA-1 tail part and the heptane phase. In addition, due to the weak interaction between NA-1 and water, NA-1 has limited effects on the PA orientation. In NA-2-Hep, NA-2 has a cycloaliphatic tail, and thus possesses strong tendencies to interact with water molecules. Meanwhile, NA-2 has relatively less interactions with PA and insignificantly promote the migration of PAs into the bulk. As such, PA molecules tend to stay near the water/heptane interface and compete with NA-2 to form H-Bonds with water molecules. The competition between PA and NA-2 reduces the contact area between PA and water, leading to more perpendicular orientations at the interface. For NA-3, its molecular structure contains a combined aliphatic and cycloaliphatic tail, making NA-3 molecules foldable and enhancing interactions between NA-3 and water. Therefore, in system NA-3-Hep, it was observed that NA-3 enhances the stacking and perpendicular orientation of PAs at the interface. On the other hand, in system NA-4-Hep, the NA molecules (NA-4) are of a large cycloaliphatic core, leading to strong tendency to self-associate and the least effects on PA behaviors.

In systems where toluene represents the oil phase, it was observed that PA molecules tend to migrate from the water/toluene interface where they were initially introduced to the bulk as well as the other interface. In addition, different NA molecular structures exhibited different effects on the PA behaviors.

NA-1 of aliphatic tails has great tendencies to form H-bond with water, as well as with PA molecules. As a result, with the presence of NA-1, PA molecules prefer perpendicular orientation at the interface. In contrast, NA-2 with cycloaliphatic tails tend to drag and solvate PA molecules in the bulk, due to the structural similarities between the tail of NA-2 and toluene molecules. Therefore, PA molecules are less crowded at the interface and prefer oblique orientations to maximize H-bond formation between PA cores and water molecules, as well as between water molecules and the tails in PA molecules. Compared to NA-1 and NA-2, NA-3, due to the combined nature of aliphatic and cycloaliphatic tails, has an intermediate effect on the PA accumulation and orientation at the interface. Lastly, NA-4 containing large cycloaliphatic tails shows the least effects on the PA orientation at the interface due to its strong self-association. These results help to fundamentally understand the effects of NAs on the behaviors of surface-active materials (PA, asphaltene) during industrial oil productions.

Chapter 4. Molecular Insights into Soap Functioning and Its Wastewater Treatment

4.1 Introduction

Soaps are widely used nowadays. During an average day, for instance, a consumer will make use of numerous soaps from hand soap and shampoo to liquid dishwashing detergent and powdered laundry detergent. In fact, they are so commonly used that one often overlooks the functioning and impact of these substances.

The introduction of soaps for hygienic use created a positive impact on society in many ways; however, their environmental impact has not always been positive. The first evidence of using soap goes back to 2800 BC, which was found in a pot filled with boiled fat and ash during the Babylon civilization.[73] The process of using soap did not change until after World War || Due to the economic crisis, most people could not afford to buy traditional soap, so scientists used synthetic ingredients and revolutionized soapmaking, making it more affordable. Throughout history, hygienic purposes are the primary factor for the use of soaps, which improves the overall health of individuals and decreases infectious disease and the spread of disease. Unfortunately, the chemical compounds now found in soaps, like the ones used in handwashers, dishwashers, or laundry soaps, have been proven harmful from a health and environmental standpoint, due to the presence of cancer-prone ingredients in soaps.[74] The continued widespread use and waste of soap and its byproducts have created negative factors, such as increasing cancer rates, producing ecotoxicological risks in the environment, as well as affecting marine life and toxicity to aquatic life caused by pouring wastewater into rivers.[75] However, when new products are revealed, only the advantages of these products are examined while the harmful repercussions are ignored.

Soap varieties today extend from pure milk soaps, which contain no additives, to heavy-duty and all-purpose soaps, which contain synthetic materials that have been proven to be harmful to our health if they go into our daily food and drinking diet.[74,76] Heavy-duty soaps have alkaline substances added to intensify the cleansing power. Saponification and hydrolysis are the two main soapmaking processes that nowadays are been utilized to produce soap. Saponification involves heating fats and oils to be reacted with a liquid alkali. Overall, for soap production, we need 4 main ingredients, lye, water, oil base materials, and scent, and through saponification, the first three ingredients break down and form fatty acids acting as surfactants.[76] On the other hand, hydrolysis involves the neutralization of fatty acids (surfactants) with alkali fats and oils to extract fatty acids and glycerin.[77] The main component responsible for soap functioning is surfactant, which will be examined in detail in this chapter.

Surfactant typically has a polar head and a hydrophobic tail, and by forming a buffer between oil/water phase, it leads to reducing the interfacial tension of the aforementioned interfaces, weakening the oil/water film at the interface, promoting the oil/water miscibility, and enabling water to clean oily and greasy surfaces. Beyond soap, surfactants are used in a broad range of applications in pharmaceutical industries and biological studies, including solubilizing membrane proteins, and in crystallography studies.[78–80]

Concerning the surfactant application in soap, the polar head is connected to a string or tail of nonpolar fatty acids. The soap molecule can therefore act like a double agent. The polar end is attracted to water, while the fatty tail is attracted to the dirt or oil. When mixing soap with dirt/oil and water, the soap molecules break up the dirt by forming circles around dirt/oil droplets. The fatty chains go in the middle facing the dirt, while the polar

ends form the outside of the circle facing the surrounding water.[81] Surrounded by soap, grease/oil molecules become suspended and distributed in the water rather than stubbornly clinging to skin, clothing, surfaces, or towels.[81] This allows dirt and germs on skin, clothing, surfaces, or towels to be rinsed away with water. As such, surfactants in domestic wastewater can range from 1 to 10 mg/L.[82] The existence of surfactants in water above a certain concentration reduces the water quality, induces unpleasant taste and odor, and causes short and long-term changes in the ecosystem. Sewage treatment plants can reduce the concentration of surfactants to 1–3 mg/L from raw sewage but leave appreciable amounts of surfactants in the sludge which create environmental problems.[74] As such, the growing use of surfactants in different applications and the environmental hazards associated with surfactants have motivated the development of residential wastewater treatment technologies.

Generally, wastewater treatment has three main stages, namely primary wastewater treatment, secondary wastewater treatment, and tertiary wastewater treatment.[83] During primary treatment, wastewater is temporarily held in a settling tank, where heavier solids sink to the bottom while lighter solids float to the surface. Once settled, these materials are held back, while the remaining liquid is discharged or moved through to the more rigorous secondary phase of wastewater treatment.[83] Secondary treatment of wastewater works on a deeper level than primary and is designed to substantially degrade the biological content of the waste through aerobic biological processes.[83] Completing secondary wastewater treatment allows for safer release into the local environment, reducing common biodegradable contaminants down to safe levels. The aim of tertiary wastewater treatment is to raise the quality of the water to domestic and industrial

standards, or to meet specific requirements around the safe discharge of water.[83] In the case of water treated by municipalities, tertiary treatment also involves the removal of pathogens, which ensures that water is safe for drinking purposes.[84,85]

Tertiary treatment technologies can be the extensions of conventional secondary biological treatment to further stabilize oxygen-demanding substances in the wastewater or to remove nitrogen and phosphorus.[83,84] Tertiary treatment may also involve physical-chemical separation techniques such as carbon adsorption, flocculation/precipitation, membranes for advanced filtration, ion exchange, dichlorination, and reverse osmosis.[83,84] Selecting the most appropriate technique for the treatment of wastewater depends on many factors such as influent quality, effluent quality, environmental footprint, treatment cost, and energy consumption. Adsorption is suggested to be the most appropriate technique for the removal of surfactants from wastewater, due to it being highly efficient, easy to operate, environmentally friendly, and cost-effective.[86] Adsorption is a method for separating substances at the interface of two phases, such as liquid-liquid, gas-liquid, gas-solid, and liquid-solid. It can be classified into two classes: physisorption and chemisorption depending on the adsorbate–adsorbent interactions.[87]

In this chapter, we aim to investigate the liquid-liquid absorption and examine the possibility of using an economical extracting liquid. In the study done by Gallego et al.,[88] they revealed the feasibility of absorption of surfactants in wastewater by flow injection of continuous liquid-liquid extraction, and the efficiency of such a method was reported to be 79-95% that was correlated to chloride ions present in the procedure. Some of the conventional absorbents used in wastewater treatment are Granular activated carbon (GAC) and Organic polymer resin with the commercial name of Hydraffin CC 8*30,

Lewatit VPOC 1064 MD PH respectively.[86] However, using these materials is not only limited by their cost but also restricted by the fact that these materials are hardly available in a reasonable amount.[89] To achieve the highest efficiency, based on the work done by Singh et al., [50] some of the surfactants migrate across the oil/water interface and go to the oil bulk phase. Based on the study done by Lu et al.,[90] the migration of surfactants strongly depends on the solvent type, and solvents with benzenic structures can lead to less aggregation of surfactant. Chiang et al.[91] reported that the extraction efficiency of chlorobenzene from wastewater is close to 99%, and meanwhile, it does not have the toxicity of other similar benzenic liquids. Furthermore, chlorobenzene has chlorine elements in its molecular structure, making it of interest to be investigated.[92–94]

Utilizing chlorobenzene, the process that we investigated here to extract harmful surfactants from soap-containing wastewater can be categorized under the third stage in wastewater treatment. Specifically, the method used in our study is based on carbon adsorption by liquid-liquid continuous phase, as extractions polar components are one of the concerns in this process since wastewater from soapmaking processes can contain a high concentration of surface-active agents.[83,92] To further understand the extraction of surfactants existing in the water phase, this chapter aims to provide insights into their molecular-level behavior during the wastewater treatment process. Below, we first investigated the effect of surfactants as cleaners in the water phase. Then, we designed an environmentally friendly and high-efficiency water treatment process to extract these harmful surfactants from wastewater. [82]

4.3 Methods

4.3.1 Molecular Models and Simulation Systems

The surfactant chosen for this study is Lauryl Glucoside ($C_{18}H_{36}O_6$, Figure 4.1a), based on its wide applicability and use in health and skin care.[93] Commercial production of Lauryl Glucoside starts by mixing palm, corn, or coconut alcohol with sugar, glucose, or glucose polymer under acidic conditions.[94] While Lauryl Glucoside is listed in the safe cosmetics database at small concentrations for external use, any content in food, drinking, and smoking substances is strictly not allowed. Nonadecane (Figure 4.1b) was chosen as a model nonpolar component as a representator of grease, given that the nature of the grease is nonpolar. This is due to the following reasons. Short chain alkanes do not represent the viscosity and dynamic behavior of a complex nonpolar component (such as grease) accurately, whereas large chain alkane leads to large computational expense. As a compromise, nonadecane was adopted. Chlorobenzene (Figure 4.1c) was chosen to represent the phase for extracting polar and nonpolar components from water phase. The molecular structures for the aforementioned chemicals were generated in Avogadro[64] and the optimization were done in Gaussian.[65]

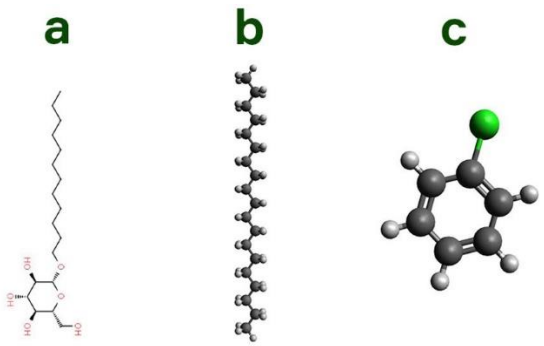

Figure 4.1 Molecular structures of a) Lauryl Glucoside, b) nonadecane, and c) chlorobenzene.

To investigate how surfactant functioning when using soap, we built two different systems, one with nonpolar component and water (system WO_S in Table 4.1), and the other, in addition to nonpolar components and water, having Lauryl Glucoside introduced as surfactant (system W_S in Table 4.1). Both systems have an initial box dimension of $5.4 * 5.4 * 5.4$ nm. During generating the initial configurations, for system WO_S, we first introduced nonpolar component, and then randomly inserted water molecules into our system. For system W_S, we followed the same procedure, but introduced surfactant molecules before inserting water molecules.

Table 4.1 System compositions

System	No. dodecane	No. Water	No. surfactant	No. chlorobenzene	dimension
WO_S	18	4695	0	0	5.4*5.4*5.4
W_S	18	3890	40	0	5.4*5.4*5.4
W_S_CH	18	3890	40	747	5.4*5.4*10.8

To investigate the extraction of surfactants from the water phase, we designed the second set of simulation (system W_S_CH in Table 4.1). For this system, an extra phase was introduced, in which surfactants and nonpolar components are expected to be miscible. The miscible phase should satisfy some criteria to be considered. Based on the study done by Lu et al.,[90] solvents that have benzene rings in their molecular structures have prominent inhibiting or disaggregation effect on surface-active materials, due to the polar similarity between the polar head of surfactants and benzene rings. However, benzene is of high risk for health and can cause illness like cancer in case of leaking to the surrounding environment. Thus, in this study, we adopted chlorobenzene as an alternative. During constructing initial configurations for system W_S_CH, we expanded system W_S in z direction, and then filled the extended part of the box with chlorobenzene molecules.

4.3.2 Simulation Details

The force field parameters for the molecules adopted in this study are taken from the GROningen Molecular Simulation 96 (GROMOS96) force field.[95] The topology for molecules used in this simulation were generated in Automated Topology Builder (ATB) and Repository.[96] The default topology obtained from ATB repository was then manually modified by adopting the partial charges obtained from Gaussian[65] geometry optimization to be compatible with the GROMOS force field. The water model used in this study is SPC/E water model.[33]

All simulations were performed using molecular dynamics package GROMACS.[70] After constructing the initial configuration, the first step is to optimize the static structure of the system by reducing the inter-atomic forces to be less than 100 KJ/(mol*nm). Steep

descent algorithm was used for this geometry optimization. Then, for systems WO_S and W_S, full dynamics simulations were conducted in NVT ensemble using Nose-Hoover thermostat[28] with the fixed temperature of 293.15 K. During this stage, the geometry of water molecules was maintained using LINCS algorithm[32] for bond constraints. A cut-off distance of 1.4 nm was applied for the Lennard-Jones (LJ) and short-range part of the coulombic interactions. The long-range electrostatic interactions were treated using the particle mesh Ewald method.[72]

In the next simulation (system W_S_CH in Table 4.1), where chlorobenzene was added to the final configuration of W_S system, the first step is, again, to optimize the static structure of the system based on steep descent algorithm. Then, full dynamics simulations were conducted in two stages. First, it was performed in NPT ensemble using Nose-Hoover thermostat[28] with the fixed temperature of 293.15 K and isotropic Berendsen barostat[30] with the fixed pressure of 1 bar. Afterwards, we extended the simulation with Parrinello-Rahman[31] as a more accurate barostat. During full dynamics simulations, all other parameters were the same with those described above for systems WO_S and W_S.

4.4 Result and Discussion

4.4.1 Surfactant Functioning in Aqueous Phase

The initial configuration for system WO_S was generated in a way that the nonpolar components were placed as far as possible from each other, and then the box was randomly filled with water molecules (left panel in Figure 4.2a). For system W_S, we added surfactant molecules, and placed them between the nonpolar components (left

panel in Figure 4.2b). For the system without surfactant (system WO_S), the nonpolar components tend to aggregate due to their hydrophobic nature (right panel in Figure 4.2a). By introducing surfactant (system W_S), the polar (Lauryl Glucoside) and nonpolar (nondecane) components still tend to aggregate, but this aggregation seems to be decreased (right panel in Figure 4.2b).

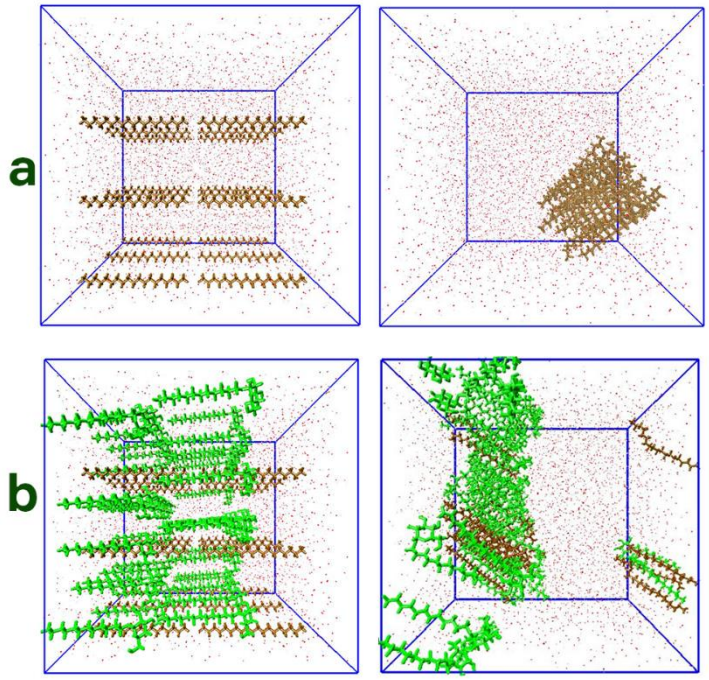

Figure 4.2 Initial (left) and final (right) configurations for a) system WO_S and b) system W_S. In both a) and b), water is red dotted, Lauryl Glucoside is in green, and nondecane is in ochre.

To examine the aggregation compactness, Figure 4.3 plots the radial distribution function $g(r)$ between the center of the mass of the nonpolar components (nondecane) existing in the water phase. It can be seen that with the presence of surfactant, the heights of all peaks are reduced, indicating that the presence of surfactants (Lauryl Glucoside) in

the system tends to decrease the aggregation of nonpolar components in the water phase, and thus increase the solubility of nondecane in water. Figure 4.2 and Figure 4.3 are consistent with each other, emphasizing the fact that the presence of surfactants can gravely affect the behaviors of nonpolar components in the water phase. To probe the underlying interactions, we calculated the interactions in each system and summarized in Table 4.2.

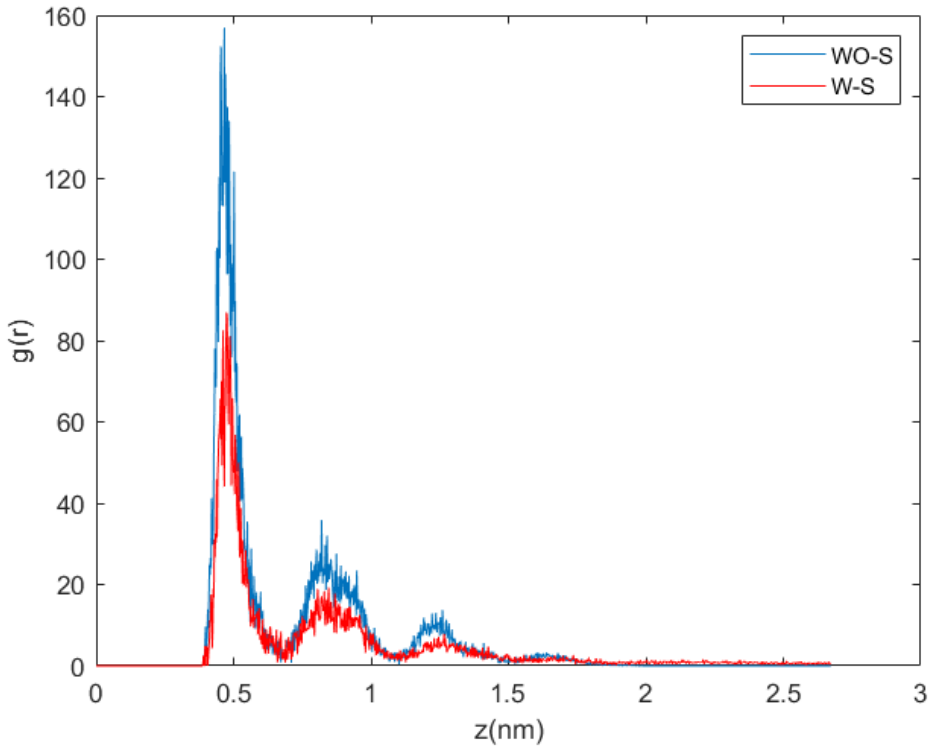

Figure 4.3 Radial distribution function $g(r)$ between the center of mass of nonpolar components

Based on Table 4.2, LJ interactions exhibit repulsive nature, while Coulombic interactions manifest attractive nature. Moreover, the overall negative values for total energies indicate that the superpositions of atomic non-bonded interactions lead to an

overall attractive energy. The larger the absolute value is in total energy, the stronger the attraction is among the molecules. As can be seen from Table 4.2, in the system containing surfactant (system W_S), the total energy is reduced in terms of absolute values, compared to the system without surfactant (system WO_S). This is, the introduced surfactant reduces the aggregation of the nonpolar components by weakening the non-bonded interactions. Together with Figures 4.2 and 4.3, it suggests that the disaggregating effect of surfactant was manifested through surrounding the nonpolar component and forming micelle.

Table 4.2 Energies calculated for systems WO_S and W_S

System	LJ (KJ/mol)	Coulomb (KJ/mol)	Total energy (KJ/mol)
WO_S	39086	-258866	-181111
W_S	25829	-216570	-139034

4.4.2 Surfactant Extraction from Wastewater

As mentioned earlier, a variety of techniques such as physical, chemical, biological, and membrane treatment are used for the removal of surfactants from wastewater. Robustness, chemicals free, and requirement of less operational input are the advantages of physical treatment techniques, while the high retention time, high capital cost (land/space requirement), and production of secondary waste are the major disadvantages.[97] Lower sludge generation and high pollutant removal efficiency are the advantages of chemical methods, while high operational and chemicals cost, and

production of secondary waste are some of the disadvantages.[98] Easy application and low cost are the advantages of biological methods and the generation of sludge during the treatment and high retention time are the major disadvantages.[99] Adsorption is suggested to be the most appropriate technique for the removal of surfactants from wastewater due to it being highly efficient, easy to operate, environmentally friendly and cost-effective.[86] In this section, we investigated liquid-liquid absorption and examined the possibility of using an economical extracting liquid.

To investigate the surfactant extraction in liquid-liquid wastewater treatment, the presence of surfactant and grease in water was mimicked, by introducing 18 dodecane and 40 Lauryl Glucoside molecules to the system, respectively, as nonpolar component and surfactant. Then, by importing chlorobenzene into our system, the presence of liquid was represented as the adsorption agent.

The initial and final configurations are shown in Figure 4.4. As can be seen, the organic polar and nonpolar components migrate to the bulk of the extraction phase (chlorobenzene) and form dimers and trimers that can be observed in Figure 4.4b, with complex aggregation being suppressed. In the study by Hosseinpour et al.,[100] the presence of surfactants at the interface can reduce the interfacial tension of the system leading to stable emulsions.[100] In our system, surfactant migrates to the bulk phase, which could further help to separate water, since it has been proposed that separations are facilitated by low emulsion stability during wastewater treatment.[101]

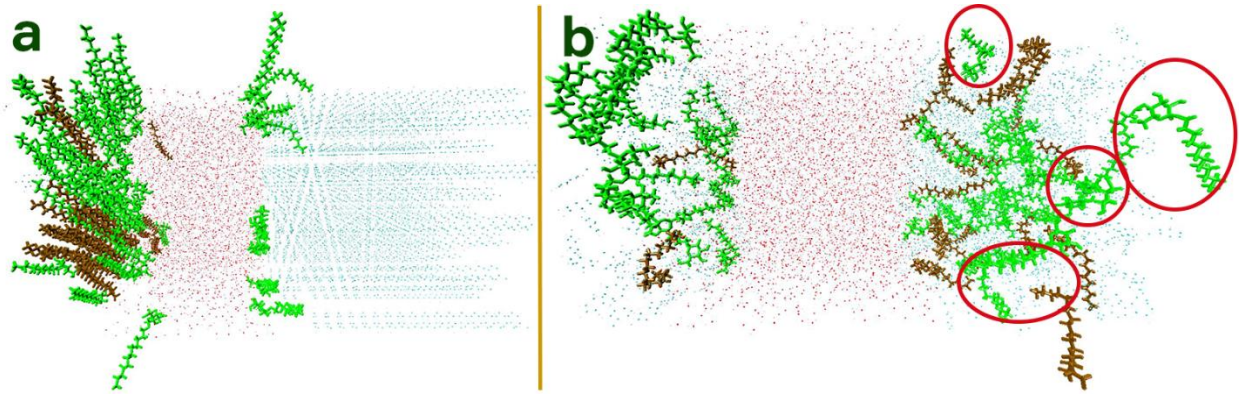

Figure 4.4 The initial (a) and final (b) configurations of system W_S_CH. In both figures, water is red dotted, Lauryl Glucoside is in green, nondecane is in ochre, and chlorobenzene is blue dotted. The dimmers and trimmers are highlighted by the red circles.

To quantitatively probe the distribution of surfactants (Lauryl Glucoside) and nonpolar (nonadecane) components during liquid-liquid extraction, we plotted the density profiles for system W_S_CH in Figure 4.5 and the radial distribution function $g(r)$ in Figure 4.6. As can be conceived from Figures 4.5 and 4.6, the surfactants (Lauryl Glucoside) are dispersed in oil phase. This is evidenced by the homogeneous density profile of Lauryl Glucoside observed in Figure 4.5 and the absence of broad peaks in the $g(r)$ shown in Figure 4.6. The behavior shown here is in alignment with the measured interaction energies in the system (LJ = 166.993 KJ/mol, coulomb = -220495 KJ/mol, and total energy = 135098 KJ/mol). Because of the benzenic structure of chlorobenzene, which makes chlorobenzene polar, there are sufficient interactions to promote the migration of surfactants to the bulk. While surfactant molecules can still form H-Bonds with water molecules, there are insufficient numbers of H-Bonds (7 in system W_S_CH compared to 59 in system W_S) to overcome the interactions between surfactants and

chlorobenzene.

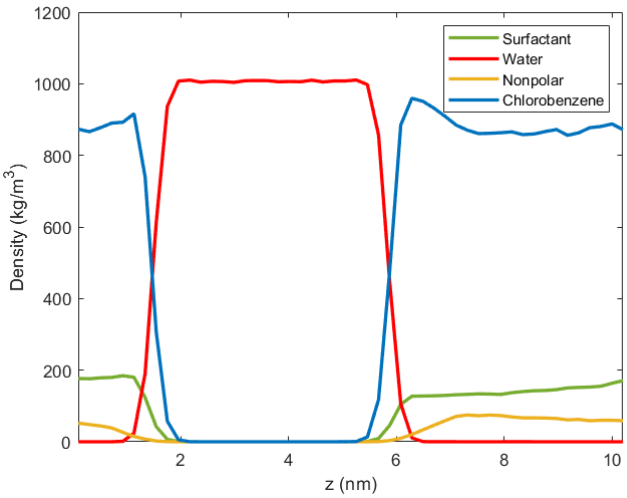

Figure 4.5 Density profile of the final configuration in system W_S_CH.

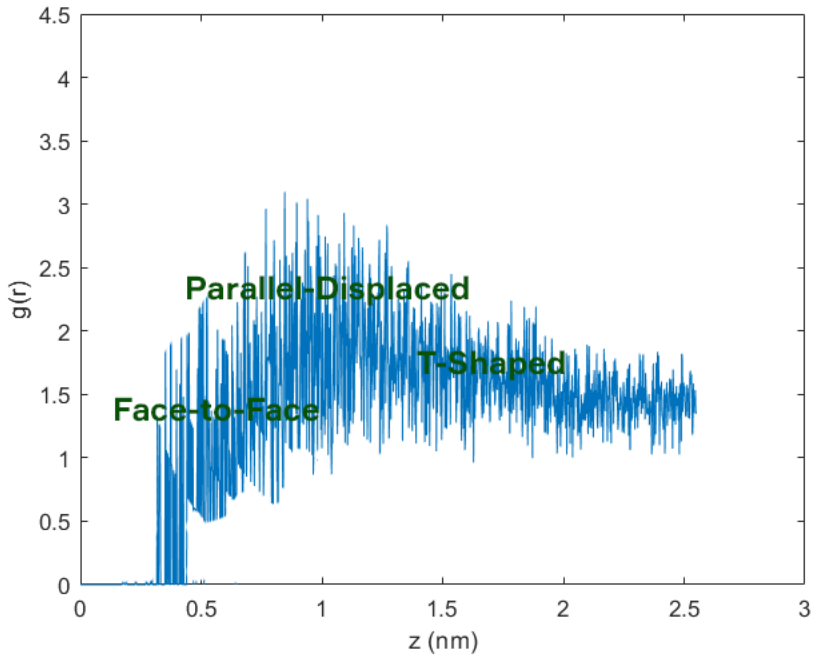

Figure 4.6 Radial distribution function $g(r)$ between the center of the mass of surfactant molecules over the last 2ns. A word of explanation is that due to averaging and fluctuations, the plot is noisy, corresponding to the reduced aggregation.

It is believed that intermolecular stacking of molecules with aromatic polar head structure may fall into face-to-face, T-shaped, and parallel-displaced geometries.[42] The minimum separation distance is typically observed when aromatic molecules are stacked face-to-face. In the case of parallel-displaced and T-shaped configuration, the spacing distance is assumed to be larger (up to around 1.00 nm), which depends on the size and structure of the aromatic molecule.[102] According to Chelli et al.,[103] in apolar environments, where residue-solvent dispersive interactions destabilize stacking, the possibility of forming H-Bond between the residues results in a stabilization of T-shaped structure, and this is evident by the snapshots and the radial distribution function plot. Physically speaking, the dimer in a sandwiched configuration is stabilized by London dispersion forces but destabilized by repulsive quadrupole/quadrupole interactions. By offsetting one of the rings, the parallel displaced configuration reduces these repulsive interactions and is stabilized.[104] The T-shaped configuration enjoys favorable quadrupole/quadrupole interactions, as the positive quadrupole of one ring interacts with the negative quadrupole of the other. The rings are furthest apart in this T-shaped configuration.[104,105] As can be seen in Figure 4.4b, and Figure 4.6, the number of T-shape staking is the predominant stacking between surfactant molecules, and has a higher probability compared to other forms of stacking e.g., face-to-face and parallel-displaced stacking. This can be attributed to the breakage of preferred interactions between polar heads, leading to multiple possible configurations during the liquid-liquid extraction.

Finally, we also comment on the toxicity of chlorobenzene. Based on previous studies,

very high concentration of chlorobenzene (5 g/Kg) can be harmful and lethal to our health.[106] However, for the method developed here, chlorobenzene is insoluble in water, and the remaining chlorobenzene, if any, evaporates into the air and can be gradually broken down by other chemicals and sunlight, and these byproducts are harmless to the environment.[107] Biodegradation in a wastewater inoculum was studied by Tabak et al.[108] Among 57 environmental pollutants tested, chlorobenzene at 5 mg/L (5 ppm) was among the more rapidly biodegraded substances, with 89% degradation in a week and 100% after adaptation. Biodegradation is therefore a major degradation process in oxygenated waters, whereas evaporation will play an additional role in surface waters.[93] From cost perspectives, on average, the operation expenditure, including operation and maintenance cost, is 58% of the total costs of tertiary wastewater treatment, and the average unit cost is $0.141 \pm 0.027\ \$/m^3$.[109,110] Methods like microfiltration-ultrafiltration and physicochemical-UV systems, are cheaper, being 0.12383 $\$/m^3$. and 0.081279 $\$/m^3$., respectively. But they are less efficient compared to surfactants absorption.[110] Common absorbents, like ion exchange resins, which are being used can cost up to 160 $\$/kg$,[111] increasing the capital and operational expenditure significantly. In this context, chlorobenzene (10-30 $\$/kg$) shows the potential as a cheaper material. With further materials design to enhance its biodegradation/evaporation, the studies presented here may provide an alternative strategy to the commonly used extraction absorbents/solvents.

4.5 Conclusion

MD-aided technique was adopted in this work to study the behavior of surfactant

(soap's main ingredient) in washing away the grease, and further investigate the extraction of surfactants from wastewater. In this first set of simulations, we had two different systems, one system containing only nonpolar component dispersed in water (WO_S), and in the second system, surfactant was introduced to the system (W_S). In this study, it was revealed that presence of surfactants can affect the aggregation of nonpolar substances like grease. Surfactants, because of their special molecular structure having a hydrophobic tail and a hydrophilic head, can form micelles that lead to dissolving nonpolar components in water. It was found the main interaction forces are of polar natures, i.e., Coulombic interactions.

In the second set of simulation, we introduced chlorobenzene to our system as the extracting liquid in liquid-liquid carbon adsorption, since the existence of surfactants in water above a certain concentration can induce unpleasant taste and odor, and is detrimental to human beings, aquatic life and vegetation.[75] It was shown that by introducing an extraction phase (chlorobenzene), surfactants and greases can migrate to the extraction phase from water. This is due to the strong attraction between surfactant and chlorobenzene, which breaks preferred interactions between polar heads and leads to multiple possible configurations during the liquid-liquid extraction. It is worth mentioning that this method is largely suitable for surfactant manufacturing industries, as the wastewater there contains a huge concentration of surfactant, making other methods, such as biological and mechanical methods, inefficient.

Chapter 5. Conclusion and Future Works

5.1 Conclusion

In this thesis, molecular dynamics (MD) techniques were adopted to probe the bulk and interfacial behavior of complex molecules in binary systems at atomistic levels. We first focused on crude oil processing, and then investigated soap functioning and extraction encountered in our daily life.

5.1.1 Effects of Naphthenic Acids on The Aggregation and Interfacial Behaviors of Asphaltenes

Two MD simulations were first performed to reveal the effects of solvent types on the asphaltene (PA compounds) accumulation and orientation at the interface. It was revealed that the VO79 molecules have the tendency to stay at the heptane/water interface, while they tend to migrate to the bulk when toluene was adopted. The underlying reason for such orientation difference is that toluene and heptane solvents have different solvation powers. The differences in solvation powers also leads to differences in the orientations of PA molecules at the interface. While at both heptane and toluene/water interfaces, non-parallel orientations of PA molecules are preferred, oblique orientations were largely observed at heptane/water interfaces, compared to that more perpendicular orientations of PA molecules were seen at toluene/water interfaces.

In the next stage, a series of MD simulations were performed to reveal the effect of molecular structures of NA molecules on the behaviors of PA molecules in the bulk and at the oil/water interface. Four NAs of different molecular structures were adopted, each of which has the same polar group (carboxylic head) but different tails varying from aliphatic nonpolar tail to cycloaliphatic nonpolar tail. For the systems containing heptane

as the solvent, while the presence of all types of NAs promote stacking, the extents of this enhancement are different. In addition, NAs have different effects on the accumulation and orientation of PAs at the interface. NA-1, which has an aliphatic tail, acts as a solvent, because of the similarity between its tail and the heptane solvent. As such, NA-1 drags PAs into the bulk, and has limited effects on the orientations of PA molecules at the interface. In NA-2-Hep system, where NA-2 has a small cycloaliphatic tail and prefers to interact with water molecules, PAs are more crowded at the interface due to the competition from NA-2 to form H-Bonds with water phase. This competition from NA-2 reduced the contact areas between PAs and water, leading to more perpendicular orientations of PAs at the heptane/water interface. Moreover, NA molecules composed of a combined aliphatic and cycloaliphatic tail (NA-3) are also found to enhance the perpendicular orientations of PA at the heptane/water interfaces. This again is due to the preferred interactions of NA-3 with water molecules, which reduce the contact areas between PA and water molecules. Contrarily, NA molecules with a large cycloaliphatic core (NA-4) has the least effect on the PA orientation, due to their self-association.

In systems containing toluene as solvent, the effects of NAs also depend on their molecular structures. While PAs were observed to migrate from the right interface (where PA molecules were initially packed) to bulk, as well as to the left interface (which originally has no PA molecules) in all toluene systems, NA-2 molecules, which have a cycloaliphatic tail, shows the least effects on this migration, and instead, they tend to solvate PA molecules in the bulk. This is due to the structural similarities between NA-2 and toluene. As such, PA molecules are less crowded at the toluene/water interface and prefer cross

(oblique) orientations to maximize the H-Bond formation between PA cores and water molecules, as well as between PA tails and water molecules. Contrarily, NA-1, which has an aliphatic tail, competes with PA to from H-Bonds with water molecules, leading to crowded PAs at the interface and more perpendicular orientations. NA-3, on the other hand, due to its combined aliphatic and cycloaliphatic tails, has an intermediate effect on PA accumulations and orientations at the toluene/water interfaces. Lastly, NA-4 composed of large cycloaliphatic tails shows the least effect on the PA orientation due to its strong tendency to self-interact within itself.

5.1.2 Molecular Insights into Soap Functioning and Its Wastewater Treatment

Following the above study for industrial applications, we adopted MD technique to study how surfactant in soap functions in dissolving grease, and how to extract these materials from wastewater as they are harmful and hazardous to health.

Two systems were first built to investigate the functioning of surfactants, with one system only containing nonpolar components (grease) dispersed in water (system WO_S), and the other one containing surfactant Lauryl Glucoside as well (system W_S). It was revealed that the presence of surfactant hinders the nano-aggregation of nonpolar components (grease), through forming micelles around grease molecules. This can be attributed to the special molecular structures of surfactants, which have hydrophobic tails to interact with grease and hydrophilic heads to interact with water. Analysis on structures and energies support the aforementioned observations. The existence of surfactants in water above a certain concentration can cause short and long-term changes in the ecosystem as they are detrimental to human beings, aquatic life and vegetation. We then investigated surfactant extraction from wastewater. There are different methods in

extracting surfactants from wastewater, e.g., chemical, mechanical, biological, membrane, and carbon absorption treatment. Due to the promising performances of carbon absorption, we focused on adsorption based on liquid-liquid extraction. To do so, chlorobenzene molecules were introduced to the simulation system, and it was shown that the nonpolar (grease)_and polar (surfactant) components dissolved in water migrate to the bulk of chlorobenzene. This is due to the polar similarity between the structure of surfactant and chlorobenzene, which helps to break the interactions between surfactant and water as well as among surfactant molecules.

5.2 Future Works

As can be seen from the above, molecular structures and interactions play decisive roles in modulating bulk and interface behaviors. These effects were investigated at a single concentration of NA, PA, grease, and Lauryl Glucoside. To gain a complete picture, it would be of interest to probe how the deterministic roles of molecular structures and interactions are affected by concentrations. In addition, the interaction mechanisms presented in this thesis focused on energy contributions. To quantitatively gain entropy contributions, it would be helpful to use advanced techniques such as umbrella sampling. These techniques would also allow us to obtain force-distance curves among different species that can be further linked to experimental measurements using atomic force microscopy and surface force apparatus.

Apart from using different concentrations and techniques, since experimental systems typically involve diverse compounds, it would also be of interest to adopt a range of mixed molecules to represent oil, PA, grease, and surfactant. We recognize the difficulties in extracting quantitative information from simulating molecular mixtures due to the high

dimensionality of MD simulations. In this regard, machine learning techniques would be helpful to enable dimension reductions and automated analysis. In addition, it is also noted MD relies on predefined force fields and simulating molecular mixtures may require the combination of different potentials. This combination would require careful calibrations to avoid artefacts introduced by the incompatibility of different potentials.

Finally, solid phases of fine particles are typically present in biphasic systems. As such, it would also be of interest to introduce solid interfaces into the simulation system. These solid interfaces would allow us to probe, for instance, the corrosive behaviors of NA molecules and depositions of PA molecules. For this kind of mixed liquid/solid systems, caution should, again, be taken when choosing force fields.

Chapter 6. Appendix

6.1 Input Script for NPT Run

This is .mdp file for the equilibration stage, showing 2ps timestep, 100ns duration, using Berendsen as barostat, studying the effect of naphthenic acids on the asphaltene behavior.

```
title                    = oplsaa  ;toluene/water NPT equilibration
; Run parameters
integrator               = md        ; leap-frog integrator
nsteps                   = 50000000     ; 2 * 50000000 = 100000 ps
dt                       = 0.002     ; 1 fs
; Output control
nstxout             = 0         ; suppress .trr output
nstvout             = 0         ; suppress .trr output
nstenergy           = 3000      ; save energies every 1.0 ps
nstlog              = 3000      ; update log file every 1.0 ps
nstxout-compressed  = 3000      ; write .xtc trajectory every 1.0 ps

; Bond parameters
continuation             = no       ; Restarting
constraint_algorithm     = lincs     ; holonomic constraints
constraints              = all-bonds   ; h bonds are constrained
;lincs_iter               = 2         ; accuracy of LINCS
;lincs_order              = 1         ; also related to accuracy

; Nonbonded settings
cutoff-scheme            = Verlet    ; Buffered neighbor searching
ns_type                  = grid      ; search neighboring grid cells
nstlist                  = 10        ; 20 fs, largely irrelevant with Verlet scheme
rcoulomb                 = 1.4       ; short-range electrostatic cutoff (in nm)
rvdw                     = 1.4       ; short-range van der Waals cutoff (in nm)
DispCorr                 = EnerPres  ; account for cut-off vdW scheme
; Electrostatics
coulombtype              = PME       ; Treatment of long range electrostatic interactions
pme_order                = 4         ; cubic interpolation
fourierspacing           = 0.16      ; grid spacing for FFT
; Temperature coupling is on
tcoupl                   = v-rescale             ; nose-hoover thermostat
tc-grps                  = UNL INP HEP        SOL             ; two coupling groups - more
accurate
tau_t                    = 0.1  0.1  0.1 0.1            ; time constant, in ps
ref_t                    = 300  300  300 300         ; reference temperature, one for each group,
in K
refcoord_scaling         = com
; Pressure  coupling is on
Pcoupl              = berendsen ;
Pcoupltype          = isotropic
tau_p               = 1.0
compressibility     = 1.44e-4       ; for heptane at 298 K the compressibility is 9.1e-5/bar
ref_p               = 1.0          ; reference pressure bar
; Periodic boundary conditions
pbc                      = xyz       ; 3-D PBC
; Velocity generation
gen_vel                  = yes        ; Velocity generation is off

```

6.2 Input Script for MD Run

This is .mdp file for the main MD stage, showing 2ps timestep, 200ns duration, using Parrinello-Rahman as barostat, studying the effect of naphthenic acids on the asphaltene behavior.

```
title          = gromos96 Lysozyme MD simulation
; Run parameters
integrator     = md               ; leap-frog integrator
nsteps                = 100000000     ; 2 * 100000000 = 200000 ps
dt                  = 0.002                  ; 2 fs
; Output control
nstxout             = 0         ; suppress .trr output
nstvout             = 0         ; suppress .trr output
nstenergy           = 10000      ; save energies every 1.0 ps
nstlog              = 10000      ; update log file every 1.0 ps
nstxout-compressed  = 10000      ; write .xtc trajectory every 1.0 ps
compressed-x-grps   = System    ; replaces xtc-grps
; Bond parameters
continuation               = yes             ; Restarting after NPT
constraint_algorithm    = lincs              ; holonomic constraints
constraints                 = all-bonds      ; all bonds (even heavy atom-H bonds) constrained
lincs_iter                  = 1                          ; accuracy of LINCS
lincs_order                 = 4                          ; also related to accuracy
; Neighborsearching
cutoff-scheme   = Verlet
ns_type                      = grid                              ; search neighboring grid cells
nstlist                      = 10                        ; 10 fs, largely irrelevant with
Verlet scheme
rlist         = 1.4
rcoulomb            = 1.4                               ; short-range electrostatic cutoff (in
nm)
rvdw                = 1.4                               ; short-range van der Waals cutoff (in
nm)
; Electrostatics
coulombtype         = PME                           ; Particle Mesh Ewald for long-range
electrostatics
pme-order           = 4                             ; cubic interpolation
fourierspacing  = 0.12                                ; grid spacing for FFT
; Temperature coupling is on
tcoupl                  = v-rescale             ; nose-hoover thermostat
tc-grps                 = UNL  INP  HEP      SOL             ; two coupling groups - more
accurate
tau_t                   = 0.1  0.1  0.1 0.1              ; time constant, in ps
ref_t                   = 300  300  300 300         ; reference temperature, one for each group,
in K

; Pressure coupling is on
pcoupl            = Parrinello-Rahman    ; Pressure coupling on in NPT
pcoupltype        = semiisotropic        ; uniform scaling of x-y box vectors, independent z
tau_p             = 7.0                  ; time constant, in ps
ref_p             = 1.0 1.0              ; reference pressure, x-y, z (in bar)
compressibility   = 0.0 1.44e-4        ; isothermal compressibility, bar^-1
refcoord_scaling        = com
; Periodic boundary conditions
pbc                      = xyz              ; 3-D PBC
; Dispersion correction
DispCorr                = EnerPres            ; account for cut-off vdW scheme
; Velocity generation
```

```
gen_vel                         = no                                    ; Velocity generation is off
```

6.3 Python Code for Calculating the Number of Asphaltene Molecules at Interface

This file reads the .gro file generated during the MD simulation and determines the polyaromatics bounded to the interface.

```
import numpy as np
from numpy.linalg import pinv
from numpy.random import seed
from numpy.random import rand
import sys
import time
import re
count=0
openfile= open('md.gro', 'r')
lst =[]
lst2 = []
mem=0
sum=0
max =0
cnt=0
writefile= open('frames.txt', 'w')
writefile2 = open ('file.txt', 'w')
for i in openfile:
    if i[5:8] == 'UNL':
        count= count +1
        sum =sum + float(i[38:44])
        if count == 102:
            count =0
            result=sum/102
            if result > 2:
                lst.append(result)
                lst2.append(i[2:5])
            sum=0
min_z= min(lst)
print (min_z)
writefile= open('frames.txt', 'a')
for j, res in enumerate(lst):
    if res < min_z+1:
        cnt+=1
        writefile2 = open ('file.txt', 'a')
        writefile2.write('atomname C10 C23 C34 and resnr '+ lst2[j]+';'+ '\n')
        #writefile.write(str(res)+ '      ' + lst2[j]+ '\n')
        writefile.write(lst2[j]+ ' ')
print(cnt)
openfile.close()
writefile.close()
writefile2.close()
```

6.4 Python Code for Determining Angle Distribution at Interface

This code determines the angle orientation of the polyaromatics bounded to the interface with respect to the oil/water interface.

```
import math
import numpy as np
import os
A= np.zeros((64, 501))
count = 0
lst=[]
writefile = open('angle.txt', 'w')
for i in range (0, 64):
        data = np.loadtxt('angle'+ str(i) + '.xvg', unpack= True, skiprows= 24)
        for j in range(251):
            big=0
            mid=0
            small=0
            x=math.cos((data [1][j])/57.3)
            count =+ 1
            y=+ abs(x)
        z= y/count
        writefile = open('angle.txt', 'a')
        writefile.write(str(z)+ '\n')
        lst.append(z)
print(len(lst))

count_max=0
count_mid=0
count_min= 0
for i in lst:
        if i >= 0.9:
                count_max = count_max +1
        elif 0.5 <= i < 0.9:
                count_mid = count_mid +1
        elif 0 <= i < 0.5:
                count_min = count_min +1
        else:
                continue
writefile = open('angle.txt', 'a')
writefile.write(str(count_max)+ '\n')
writefile.write(str(count_mid)+ '\n')
writefile.write(str(count_min)+ '\n')
print(count_max)
print(count_mid)
print(count_min)

```

6.5 VO79 Topology

The modified topology of the VO79, used throughout the MD simulation.

```
[ moleculetype ]
; Name            nrexcl
UNL             3

[ atoms ]
;   nr       type  resnr residue  atom   cgnr     charge       mass  typeB    chargeB
massB
     1  opls_145   1   UNL      C1     1   -0.088771     12.011
     2  opls_145   1   UNL      C2     2   -0.086481     12.011
     3  opls_145   1   UNL      C3     3   -0.136485    12.011
     4  opls_145   1   UNL      C4     4   0.064961     12.011
     5  opls_145   1   UNL      C5     5   0.021442     12.011
     6  opls_145   1   UNL      C6     6   -0.111411     12.011
     7  opls_145   1   UNL      C7     7   0.333144    12.011
     8  opls_145   1   UNL      C8     8   0.033827     12.011
     9  opls_145   1   UNL      C9     9   0.011605     12.011
    10  opls_145   1   UNL      C10    10   0.064578     12.011
    11  opls_146   1   UNL      H1     6   0.120272     1.008
    12  opls_146   1   UNL      H2     1   0.092259     1.008
    13  opls_146   1   UNL      H3     2   0.089224     1.008
    14  opls_146   1   UNL      H4     3   0.082092     1.008
    15  opls_179   1   UNL      O1     7   -0.506434     15.9994
    16  opls_145   1   UNL      C11    11   -0.130454     12.011
    17  opls_145   1   UNL      C12    12   -0.147030     12.011
    18  opls_145   1   UNL      C13    13   0.059976     12.011
    19  opls_145   1   UNL      C14    14   0.011551     12.011
    20  opls_146   1   UNL      H5    11   0.120708     1.008
    21  opls_146   1   UNL      H6    12   0.096255     1.008
    22  opls_145   1   UNL      C15    15   -0.188227     12.011
    23  opls_145   1   UNL      C16    16   0.026433     12.011
    24  opls_145   1   UNL      C17    17   0.306866     12.011
    25  opls_146   1   UNL      H7    15   0.091109     1.008
    26  opls_145   1   UNL      C18    18   0.060190     12.011
    27  opls_145   1   UNL      C19    19   0.016978     12.011
    28  opls_145   1   UNL      C20    20   0.020450     12.011
    29  opls_145   1   UNL      C21    21   -0.146826    12.011
    30  opls_145   1   UNL      C22    22   -0.130608    12.011
    31  opls_145   1   UNL      C23    23   0.034385    12.011
    32  opls_145   1   UNL      C24    24   0.011309     12.011
    33  opls_146   1   UNL      H8    21   0.096036    1.008
    34  opls_146   1   UNL      H9    22   0.120663    1.008
    35  opls_180   1   UNL      O2    17   -0.538560     15.9994
    36  opls_145   1   UNL      C25    25   0.315355     12.011
    37  opls_145   1   UNL      C26    26   0.065575     12.011
    38  opls_145   1   UNL      C27    27   -0.202735     12.011
    39  opls_146   1   UNL      H10    27   0.094731     1.008
    40  opls_180   1   UNL      O3    25   -0.530820     15.9994
    41  opls_145   1   UNL      C28    28   0.333122     12.011
    42  opls_145   1   UNL      C29    29   0.021495     12.011
    43  opls_145   1   UNL      C30    30   0.065730     12.011
    44  opls_179   1   UNL      O4    28   -0.506182     15.9994
    45  opls_145   1   UNL      C31    31   -0.111376     12.011
    46  opls_145   1   UNL      C32    32   -0.137390     12.011
    47  opls_145   1   UNL      C33    33   -0.086520     12.011
    48  opls_145   1   UNL      C34    34   -0.088746     12.011
    49  opls_146   1   UNL      H11    31   0.120127     1.008
    50  opls_146   1   UNL      H12    34   0.092265     1.008
    51  opls_146   1   UNL      H13    32   0.083663     1.008
    52  opls_146   1   UNL      H14    33   0.089703     1.008
```

```
 59.        53  opls_182   1   UNL      C35    35   0.066780     12.011
 60.        54  opls_136   1   UNL      C36    36   -0.213509     12.011
 61.        55  opls_140   1   UNL      H15    35   0.098304     1.008
 62.        56  opls_140   1   UNL      H16    35   0.103548     1.008
 63.        57  opls_136   1   UNL      C37    37   -0.185540     12.011
 64.        58  opls_140   1   UNL      H17    36   0.114063     1.008
 65.        59  opls_140   1   UNL      H18    36   0.112733     1.008
 66.        60  opls_136   1   UNL      C38    38   -0.170440     12.011
 67.        61  opls_140   1   UNL      H19    37   0.090296     1.008
 68.        62  opls_140   1   UNL      H20    37   0.094940     1.008
 69.        63  opls_136   1   UNL      C39    39   -0.179450     12.011
 70.        64  opls_140   1   UNL      H21    38   0.098125     1.008
 71.        65  opls_140   1   UNL      H22    38   0.088744     1.008
 72.        66  opls_136   1   UNL      C40    40   -0.169426     12.011
 73.        67  opls_140   1   UNL      H23    39   0.086235    1.008
 74.        68  opls_140   1   UNL      H24    39   0.089601     1.008
 75.        69  opls_136   1   UNL      C41    41   -0.172516     12.011
 76.        70  opls_140   1   UNL      H25    40   0.086517     1.008
 77.        71  opls_140   1   UNL      H26    40   0.088083     1.008
 78.        72  opls_135   1   UNL      C42    42   -0.317897     12.011
 79.        73  opls_140   1   UNL      H27    41  0.091743     1.008
 80.        74  opls_140   1   UNL      H28    41   0.095427     1.008
 81.        75  opls_140   1   UNL      H29    42   0.102567     1.008
 82.        76  opls_140   1   UNL      H30    42   0.101189     1.008
 83.        77  opls_140   1   UNL      H31    42   0.101920     1.008
 84.        78  opls_182   1   UNL      C43    43   0.049430     12.011
 85.        79  opls_136   1   UNL      C44    44   -0.201037     12.011
 86.        80  opls_140   1   UNL      H32    43   0.105072     1.008
 87.        81  opls_140   1   UNL      H33    43   0.112864     1.008
 88.        82  opls_136   1   UNL      C45    45   -0.185449     12.011
 89.        83  opls_140   1   UNL      H34    44   0.111731     1.008
 90.        84  opls_140   1   UNL      H35    44   0.102694     1.008
 91.        85  opls_136   1   UNL      C46    46   -0.174992     12.011
 92.        86  opls_140   1   UNL      H36    45   0.094434     1.008
 93.        87  opls_140   1   UNL      H37    45   0.095774     1.008
 94.        88  opls_136   1   UNL      C47    47   -0.175862    12.011
 95.        89  opls_140   1   UNL      H38    46   0.090695    1.008
 96.        90  opls_140   1   UNL      H39    46   0.091087     1.008
 97.        91  opls_136   1   UNL      C48    48   -0.166575     12.011
 98.        92  opls_140   1   UNL      H40    47   0.090233    1.008
 99.        93  opls_140   1   UNL      H41    47   0.090020     1.008
100.        94  opls_136   1   UNL      C49    49   -0.174493     12.011
101.        95  opls_140   1   UNL      H42    48   0.087950    1.008
102.        96  opls_140   1   UNL      H43    48   0.088336     1.008
103.        97  opls_135   1   UNL      C50    50   -0.317928    12.011
104.        98  opls_140   1   UNL      H44    49   0.092419     1.008
105.        99  opls_140   1   UNL      H45    49   0.092305    1.008
106.       100  opls_140   1   UNL      H46    50  0.102443     1.008
107.       101  opls_140   1   UNL      H47    50   0.101624     1.008
108.       102  opls_140   1   UNL      H48    50   0.102161     1.008
109.
110.
111.
112.
113. [ bonds ]
114. 1 2 1   0.139  392459.2
115. 1 6 1   0.139  392459.2
116. 1 12 1   0.108  307105.6
117. 2 3 1   0.140  392459.2
118. 2 13 1   0.108  307105.6
119. 3 4 1   0.142  392459.2
120. 3 14 1   0.108  307105.6
121. 4 5 1   0.141  392459.2
122. 4 10 1   0.152  392459.2
123. 5 6 1   0.141  392459.2
```

```
124. 5 7 1   0.147  392459.2
125. 6 11 1   0.108  307105.6
126. 7 8 1   0.148  392459.2
127. 7 15 1   0.122  376560.0
128. 8 9 1   0.142  392459.2
129. 8 16 1   0.138  392459.2
130. 9 10 1   0.141  392459.2
131. 9 19 1   0.145  392459.2
132. 10 22 1   0.138  392459.2
133. 16 17 1   0.137  392459.2
134. 16 20 1   0.108  307105.6
135. 17 18 1   0.142  392459.2
136. 17 21 1   0.107  307105.6
137. 18 19 1   0.142  392459.2
138. 18 26 1   0.142  392459.2
139. 19 23 1   0.145  392459.2
140. 22 24 1   0.140  392459.2
141. 22 25 1   0.106  307105.6
142. 23 24 1   0.145  392459.2
143. 23 28 1   0.148  392459.2
144. 24 35 1   0.135  376560.0
145. 26 27 1   0.143  392459.2
146. 26 29 1   0.142  392459.2
147. 27 28 1   0.145  392459.2
148. 27 32 1   0.145  392459.2
149. 28 36 1   0.146  392459.2
150. 29 30 1   0.137  392459.2
151. 29 33 1   0.107  307105.6
152. 30 31 1   0.138  392459.2
153. 30 34 1   0.108  307105.6
154. 31 32 1   0.142  392459.2
155. 31 41 1   0.148  392459.2
156. 32 37 1   0.141  392459.2
157. 35 78 1   0.139  267776.0
158. 36 38 1   0.141  392459.2
159. 36 40 1   0.136  376560.0
160. 37 38 1   0.138  392459.2
161. 37 43 1   0.152  392459.2
162. 38 39 1   0.106  307105.6
163. 40 53 1   0.140  267776.0
164. 41 42 1   0.147  392459.2
165. 41 44 1   0.122  376560.0
166. 42 43 1   0.141  392459.2
167. 42 45 1   0.141  392459.2
168. 43 46 1   0.142  392459.2
169. 45 48 1   0.139  392459.2
170. 45 49 1   0.108  307105.6
171. 46 47 1   0.140  392459.2
172. 46 51 1   0.108  307105.6
173. 47 48 1   0.139  392459.2
174. 47 52 1   0.108  307105.6
175. 48 50 1   0.108  307105.6
176. 53 54 1   0.152  224262.4
177. 53 55 1   0.111  284512.0
178. 53 56 1   0.111  284512.0
179. 54 57 1   0.153  224262.4
180. 54 58 1   0.111  284512.0
181. 54 59 1   0.110  284512.0
182. 57 60 1   0.154  224262.4
183. 57 61 1   0.111  284512.0
184. 57 62 1   0.111  284512.0
185. 60 63 1   0.153  224262.4
186. 60 64 1   0.111  284512.0
187. 60 65 1   0.111  284512.0
188. 63 66 1   0.154  224262.4
```

```
63 67 1   0.111  284512.0
63 68 1   0.111  284512.0
66 69 1   0.154  224262.4
66 70 1   0.111  284512.0
66 71 1   0.111  284512.0
69 72 1   0.153  224262.4
69 73 1   0.111  284512.0
69 74 1   0.111  284512.0
72 75 1   0.111  284512.0
72 76 1   0.111  284512.0
72 77 1   0.111  284512.0
78 79 1   0.154  224262.4
78 80 1   0.111  284512.0
78 81 1   0.111  284512.0
79 82 1   0.153  224262.4
79 83 1   0.110  284512.0
79 84 1   0.111  284512.0
82 85 1   0.153  224262.4
82 86 1   0.111  284512.0
82 87 1   0.111  284512.0
85 88 1   0.153  224262.4
85 89 1   0.111  284512.0
85 90 1   0.111  284512.0
88 91 1   0.153  224262.4
88 92 1   0.111  284512.0
88 93 1   0.111  284512.0
91 94 1   0.153  224262.4
91 95 1   0.111  284512.0
91 96 1   0.111  284512.0
94 97 1   0.153  224262.4
94 98 1   0.111  284512.0
94 99 1   0.111  284512.0
97 100 1   0.111  284512.0
97 101 1   0.111  284512.0
97 102 1   0.111  284512.0

[ angles ]
1 2 3 1  120.291  527.184
1 2 13 1  119.746  292.880
1 6 5 1  120.487  527.184
1 6 11 1  118.585  292.880
2 1 6 1  119.814  527.184
2 1 12 1  120.056  292.880
2 3 4 1  121.248  527.184
2 3 14 1  115.237  292.880
3 2 13 1  119.963  292.880
3 4 5 1  117.399  527.184
3 4 10 1  123.432  527.184
4 3 14 1  123.515  292.880
4 5 6 1  120.761  527.184
4 5 7 1  119.115  527.184
4 10 9 1  121.938  527.184
4 10 22 1  120.664  527.184
5 4 10 1  119.169  527.184
5 6 11 1  120.927  292.880
5 7 8 1  119.576  527.184
5 7 15 1  119.952  585.760
6 5 7 1  120.124  527.184
6 1 12 1  120.130  292.880
7 8 9 1  121.762  527.184
7 8 16 1  118.398  527.184
8 7 15 1  120.472  585.760
8 9 10 1  118.436  527.184
8 9 19 1  120.625  527.184
```

```
254. 8 16 17 1  120.589  527.184
255. 8 16 20 1  121.067  292.880
256. 9 8 16 1  119.839  527.184
257. 9 10 22 1  117.386  527.184
258. 9 19 18 1  117.812  527.184
259. 9 19 23 1  121.393  527.184
260. 10 9 19 1  120.939  527.184
261. 10 22 24 1  124.160  527.184
262. 10 22 25 1  118.381  292.880
263. 16 17 18 1  122.350  527.184
264. 16 17 21 1  112.571  292.880
265. 17 16 20 1  118.343  292.880
266. 17 18 19 1  118.774  527.184
267. 17 18 26 1  120.719  527.184
268. 18 17 21 1  125.078  292.880
269. 18 19 23 1  120.793  527.184
270. 18 26 27 1  120.619  527.184
271. 18 26 29 1  120.535  527.184
272. 19 18 26 1  120.505  527.184
273. 19 23 24 1  114.947  527.184
274. 19 23 28 1  118.832  527.184
275. 22 24 23 1  121.035  527.184
276. 22 24 35 1  115.473  585.760
277. 23 24 35 1  123.479  585.760
278. 23 28 27 1  118.241  527.184
279. 23 28 36 1  126.548  527.184
280. 24 23 28 1  126.195  527.184
281. 24 22 25 1  117.459  292.880
282. 24 35 78 1  127.136  627.600
283. 26 27 28 1  120.859  527.184
284. 26 27 32 1  117.743  527.184
285. 26 29 30 1  122.319  527.184
286. 26 29 33 1  125.170  292.880
287. 27 26 29 1  118.845  527.184
288. 27 28 36 1  115.202  527.184
289. 27 32 31 1  120.573  527.184
290. 27 32 37 1  120.994  527.184
291. 28 27 32 1  121.398  527.184
292. 28 36 38 1  120.359  527.184
293. 28 36 40 1  123.579  585.760
294. 29 30 31 1  120.563  527.184
295. 29 30 34 1  118.332  292.880
296. 30 29 33 1  112.510  292.880
297. 30 31 32 1  119.952  527.184
298. 30 31 41 1  118.266  527.184
299. 31 30 34 1  121.103  292.880
300. 31 32 37 1  118.432  527.184
301. 31 41 42 1  119.573  527.184
302. 31 41 44 1  120.437  585.760
303. 32 31 41 1  121.783  527.184
304. 32 37 38 1  117.440  527.184
305. 32 37 43 1  121.913  527.184
306. 35 78 79 1  111.125  418.400
307. 35 78 80 1  112.152  292.880
308. 35 78 81 1  107.672  292.880
309. 36 38 37 1  124.468  527.184
310. 36 38 39 1  118.244  292.880
311. 36 40 53 1  126.670  627.600
312. 37 38 39 1  117.283  292.880
313. 37 43 42 1  119.122  527.184
314. 37 43 46 1  123.539  527.184
315. 38 36 40 1  116.008  585.760
316. 38 37 43 1  120.633  527.184
317. 40 53 54 1  111.301  418.400
318. 40 53 55 1  109.860  292.880
```

```
319. 40 53 56 1  109.446  292.880
320. 41 42 43 1  119.174  527.184
321. 41 42 45 1  120.043  527.184
322. 42 41 44 1  119.990  585.760
323. 42 43 46 1  117.338  527.184
324. 42 45 48 1  120.500  527.184
325. 42 45 49 1  120.967  292.880
326. 43 42 45 1  120.783  527.184
327. 43 46 47 1  121.259  527.184
328. 43 46 51 1  123.605  292.880
329. 45 48 47 1  119.785  527.184
330. 45 48 50 1  120.139  292.880
331. 46 47 48 1  120.334  527.184
332. 46 47 52 1  119.963  292.880
333. 47 46 51 1  115.135  292.880
334. 47 48 50 1  120.076  292.880
335. 48 45 49 1  118.533  292.880
336. 48 47 52 1  119.703  292.880
337. 53 54 57 1  113.129  488.273
338. 53 54 58 1  108.252  313.800
339. 53 54 59 1  107.880  313.800
340. 54 53 55 1  108.174  313.800
341. 54 53 56 1  107.798  313.800
342. 54 57 60 1  109.688  488.273
343. 54 57 61 1  109.466  313.800
344. 54 57 62 1  109.674  313.800
345. 55 53 56 1  110.232  276.144
346. 57 54 58 1  108.732  313.800
347. 57 54 59 1  107.447  313.800
348. 57 60 63 1  111.693  488.273
349. 57 60 64 1  108.789  313.800
350. 57 60 65 1  108.774  313.800
351. 58 54 59 1  111.443  276.144
352. 60 57 61 1  109.081  313.800
353. 60 57 62 1  110.101  313.800
354. 60 63 66 1  112.928  488.273
355. 60 63 67 1  108.563  313.800
356. 60 63 68 1  109.795  313.800
357. 61 57 62 1  108.812  276.144
358. 63 60 64 1  109.925  313.800
359. 63 60 65 1  108.850  313.800
360. 63 66 69 1  113.656  488.273
361. 63 66 70 1  109.239  313.800
362. 63 66 71 1  107.625  313.800
363. 64 60 65 1  108.757  276.144
364. 66 63 67 1  107.273  313.800
365. 66 63 68 1  109.876  313.800
366. 66 69 72 1  110.941  488.273
367. 66 69 73 1  109.609  313.800
368. 66 69 74 1  110.416  313.800
369. 67 63 68 1  108.265  276.144
370. 69 66 70 1  109.529  313.800
371. 69 66 71 1  108.531  313.800
372. 69 72 75 1  110.362  313.800
373. 69 72 76 1  109.648  313.800
374. 69 72 77 1  110.347  313.800
375. 70 66 71 1  108.103  276.144
376. 72 69 73 1  108.927  313.800
377. 72 69 74 1  107.886  313.800
378. 73 69 74 1  109.013  276.144
379. 75 72 76 1  108.722  276.144
380. 75 72 77 1  109.097  276.144
381. 76 72 77 1  108.624  276.144
382. 78 79 82 1  111.554  488.273
383. 78 79 83 1  110.150  313.800
```

```
384. 78 79 84 1  110.512  313.800
385. 79 78 80 1  109.837  313.800
386. 79 78 81 1  110.999  313.800
387. 79 82 85 1  110.543  488.273
388. 79 82 86 1  109.897  313.800
389. 79 82 87 1  108.766  313.800
390. 80 78 81 1  104.874  276.144
391. 82 79 83 1  107.880  313.800
392. 82 79 84 1  109.913  313.800
393. 82 85 88 1  111.424  488.273
394. 82 85 89 1  108.970  313.800
395. 82 85 90 1  109.417  313.800
396. 83 79 84 1  106.681  276.144
397. 85 82 86 1  110.030  313.800
398. 85 82 87 1  108.712  313.800
399. 85 88 91 1  110.759  488.273
400. 85 88 92 1  109.042  313.800
401. 85 88 93 1  109.490  313.800
402. 86 82 87 1  108.852  276.144
403. 88 85 89 1  108.617  313.800
404. 88 85 90 1  109.676  313.800
405. 88 91 94 1  111.088  488.273
406. 88 91 95 1  109.238  313.800
407. 88 91 96 1  109.299  313.800
408. 89 85 90 1  108.685  276.144
409. 91 88 92 1  109.029  313.800
410. 91 88 93 1  109.641  313.800
411. 91 94 97 1  111.094  488.273
412. 91 94 98 1  109.677  313.800
413. 91 94 99 1  109.620  313.800
414. 92 88 93 1  108.847  276.144
415. 94 91 95 1  109.094  313.800
416. 94 91 96 1  109.384  313.800
417. 94 97 100 1  110.358  313.800
418. 94 97 101 1  109.588  313.800
419. 94 97 102 1  110.326  313.800
420. 95 91 96 1  108.699  276.144
421. 97 94 98 1  108.870  313.800
422. 97 94 99 1  108.750  313.800
423. 98 94 99 1  108.788  276.144
424. 100 97 101 1  108.718  276.144
425. 100 97 102 1  109.161  276.144
426. 101 97 102 1  108.649  276.144
427.
428.
429. [ dihedrals ]
430. 6 1 2 3 3
431. 12 1 2 3 3
432. 6 1 2 13 3
433. 12 1 2 13 3
434. 2 1 6 5 3
435. 12 1 6 5 3
436. 2 1 6 11 3
437. 12 1 6 11 3
438. 1 2 3 4 3
439. 13 2 3 4 3
440. 1 2 3 14 3
441. 13 2 3 14 3
442. 2 3 4 5 3
443. 14 3 4 5 3
444. 2 3 4 10 3
445. 14 3 4 10 3
446. 3 4 5 6 3
447. 10 4 5 6 3
448. 3 4 5 7 3
```

449. 10 4 5 7 3
450. 3 4 10 9 3
451. 5 4 10 9 3
452. 3 4 10 22 3
453. 5 4 10 22 3
454. 4 5 6 1 3
455. 7 5 6 1 3
456. 4 5 6 11 3
457. 7 5 6 11 3
458. 4 5 7 8 3
459. 6 5 7 8 3
460. 4 5 7 15 3
461. 6 5 7 15 3
462. 5 7 8 9 3
463. 15 7 8 9 3
464. 5 7 8 16 3
465. 15 7 8 16 3
466. 7 8 9 10 3
467. 16 8 9 10 3
468. 7 8 9 19 3
469. 16 8 9 19 3
470. 7 8 16 17 3
471. 9 8 16 17 3
472. 7 8 16 20 3
473. 9 8 16 20 3
474. 8 9 10 4 3
475. 19 9 10 4 3
476. 8 9 10 22 3
477. 19 9 10 22 3
478. 8 9 19 18 3
479. 10 9 19 18 3
480. 8 9 19 23 3
481. 10 9 19 23 3
482. 9 10 22 24 3
483. 4 10 22 24 3
484. 9 10 22 25 3
485. 4 10 22 25 3
486. 8 16 17 18 3
487. 20 16 17 18 3
488. 8 16 17 21 3
489. 20 16 17 21 3
490. 16 17 18 19 3
491. 21 17 18 19 3
492. 16 17 18 26 3
493. 21 17 18 26 3
494. 17 18 19 9 3
495. 26 18 19 9 3
496. 17 18 19 23 3
497. 26 18 19 23 3
498. 17 18 26 27 3
499. 19 18 26 27 3
500. 17 18 26 29 3
501. 19 18 26 29 3
502. 18 19 23 24 3
503. 9 19 23 24 3
504. 18 19 23 28 3
505. 9 19 23 28 3
506. 10 22 24 23 3
507. 25 22 24 23 3
508. 10 22 24 35 3
509. 25 22 24 35 3
510. 19 23 24 22 3
511. 28 23 24 22 3
512. 19 23 24 35 3
513. 28 23 24 35 3

514. 19 23 28 27 3
515. 24 23 28 27 3
516. 19 23 28 36 3
517. 24 23 28 36 3
518. 23 24 35 78 3
519. 22 24 35 78 3
520. 18 26 27 28 3
521. 29 26 27 28 3
522. 18 26 27 32 3
523. 29 26 27 32 3
524. 18 26 29 30 3
525. 27 26 29 30 3
526. 18 26 29 33 3
527. 27 26 29 33 3
528. 26 27 28 23 3
529. 32 27 28 23 3
530. 26 27 28 36 3
531. 32 27 28 36 3
532. 26 27 32 31 3
533. 28 27 32 31 3
534. 26 27 32 37 3
535. 28 27 32 37 3
536. 27 28 36 38 3
537. 23 28 36 38 3
538. 27 28 36 40 3
539. 23 28 36 40 3
540. 26 29 30 31 3
541. 33 29 30 31 3
542. 26 29 30 34 3
543. 33 29 30 34 3
544. 29 30 31 32 3
545. 34 30 31 32 3
546. 29 30 31 41 3
547. 34 30 31 41 3
548. 30 31 32 27 3
549. 41 31 32 27 3
550. 30 31 32 37 3
551. 41 31 32 37 3
552. 30 31 41 42 3
553. 32 31 41 42 3
554. 30 31 41 44 3
555. 32 31 41 44 3
556. 31 32 37 38 3
557. 27 32 37 38 3
558. 31 32 37 43 3
559. 27 32 37 43 3
560. 24 35 78 79 3
561. 24 35 78 80 3
562. 24 35 78 81 3
563. 28 36 38 37 3
564. 40 36 38 37 3
565. 28 36 38 39 3
566. 40 36 38 39 3
567. 28 36 40 53 3
568. 38 36 40 53 3
569. 32 37 38 36 3
570. 43 37 38 36 3
571. 32 37 38 39 3
572. 43 37 38 39 3
573. 32 37 43 42 3
574. 38 37 43 42 3
575. 32 37 43 46 3
576. 38 37 43 46 3
577. 36 40 53 54 3
578. 36 40 53 55 3

579. 36 40 53 56 3
580. 31 41 42 43 3
581. 44 41 42 43 3
582. 31 41 42 45 3
583. 44 41 42 45 3
584. 41 42 43 37 3
585. 45 42 43 37 3
586. 41 42 43 46 3
587. 45 42 43 46 3
588. 41 42 45 48 3
589. 43 42 45 48 3
590. 41 42 45 49 3
591. 43 42 45 49 3
592. 42 43 46 47 3
593. 37 43 46 47 3
594. 42 43 46 51 3
595. 37 43 46 51 3
596. 42 45 48 47 3
597. 49 45 48 47 3
598. 42 45 48 50 3
599. 49 45 48 50 3
600. 43 46 47 48 3
601. 51 46 47 48 3
602. 43 46 47 52 3
603. 51 46 47 52 3
604. 46 47 48 45 3
605. 52 47 48 45 3
606. 46 47 48 50 3
607. 52 47 48 50 3
608. 40 53 54 57 3
609. 55 53 54 57 3
610. 56 53 54 57 3
611. 40 53 54 58 3
612. 55 53 54 58 3
613. 56 53 54 58 3
614. 40 53 54 59 3
615. 55 53 54 59 3
616. 56 53 54 59 3
617. 53 54 57 60 3
618. 58 54 57 60 3
619. 59 54 57 60 3
620. 53 54 57 61 3
621. 58 54 57 61 3
622. 59 54 57 61 3
623. 53 54 57 62 3
624. 58 54 57 62 3
625. 59 54 57 62 3
626. 54 57 60 63 3
627. 61 57 60 63 3
628. 62 57 60 63 3
629. 54 57 60 64 3
630. 61 57 60 64 3
631. 62 57 60 64 3
632. 54 57 60 65 3
633. 61 57 60 65 3
634. 62 57 60 65 3
635. 57 60 63 66 3
636. 64 60 63 66 3
637. 65 60 63 66 3
638. 57 60 63 67 3
639. 64 60 63 67 3
640. 65 60 63 67 3
641. 57 60 63 68 3
642. 64 60 63 68 3
643. 65 60 63 68 3

644. 60 63 66 69 3
645. 67 63 66 69 3
646. 68 63 66 69 3
647. 60 63 66 70 3
648. 67 63 66 70 3
649. 68 63 66 70 3
650. 60 63 66 71 3
651. 67 63 66 71 3
652. 68 63 66 71 3
653. 63 66 69 72 3
654. 70 66 69 72 3
655. 71 66 69 72 3
656. 63 66 69 73 3
657. 70 66 69 73 3
658. 71 66 69 73 3
659. 63 66 69 74 3
660. 70 66 69 74 3
661. 71 66 69 74 3
662. 66 69 72 75 3
663. 73 69 72 75 3
664. 74 69 72 75 3
665. 66 69 72 76 3
666. 73 69 72 76 3
667. 74 69 72 76 3
668. 66 69 72 77 3
669. 73 69 72 77 3
670. 74 69 72 77 3
671. 35 78 79 82 3
672. 80 78 79 82 3
673. 81 78 79 82 3
674. 35 78 79 83 3
675. 80 78 79 83 3
676. 81 78 79 83 3
677. 35 78 79 84 3
678. 80 78 79 84 3
679. 81 78 79 84 3
680. 78 79 82 85 3
681. 83 79 82 85 3
682. 84 79 82 85 3
683. 78 79 82 86 3
684. 83 79 82 86 3
685. 84 79 82 86 3
686. 78 79 82 87 3
687. 83 79 82 87 3
688. 84 79 82 87 3
689. 79 82 85 88 3
690. 86 82 85 88 3
691. 87 82 85 88 3
692. 79 82 85 89 3
693. 86 82 85 89 3
694. 87 82 85 89 3
695. 79 82 85 90 3
696. 86 82 85 90 3
697. 87 82 85 90 3
698. 82 85 88 91 3
699. 89 85 88 91 3
700. 90 85 88 91 3
701. 82 85 88 92 3
702. 89 85 88 92 3
703. 90 85 88 92 3
704. 82 85 88 93 3
705. 89 85 88 93 3
706. 90 85 88 93 3
707. 85 88 91 94 3
708. 92 88 91 94 3

```
709. 93 88 91 94 3
710. 85 88 91 95 3
711. 92 88 91 95 3
712. 93 88 91 95 3
713. 85 88 91 96 3
714. 92 88 91 96 3
715. 93 88 91 96 3
716. 88 91 94 97 3
717. 95 91 94 97 3
718. 96 91 94 97 3
719. 88 91 94 98 3
720. 95 91 94 98 3
721. 96 91 94 98 3
722. 88 91 94 99 3
723. 95 91 94 99 3
724. 96 91 94 99 3
725. 91 94 97 100 3
726. 98 94 97 100 3
727. 99 94 97 100 3
728. 91 94 97 101 3
729. 98 94 97 101 3
730. 99 94 97 101 3
731. 91 94 97 102 3
732. 98 94 97 102 3
733. 99 94 97 102 3
734.
735.
736. [ dihedrals ]
737. 2 6 1 12 1   improper_Z_CA_X_Y
738. 1 3 2 13 1   improper_Z_CA_X_Y
739. 2 4 3 14 1   improper_Z_CA_X_Y
740. 3 5 4 10 1   improper_Z_CA_X_Y
741. 4 6 5 7 1   improper_Z_CA_X_Y
742. 5 1 6 11 1   improper_Z_CA_X_Y
743. 5 8 7 15 1   improper_Z_CA_X_Y
744. 7 9 8 16 1   improper_Z_CA_X_Y
745. 8 10 9 19 1   improper_Z_CA_X_Y
746. 9 4 10 22 1   improper_Z_CA_X_Y
747. 8 17 16 20 1   improper_Z_CA_X_Y
748. 16 18 17 21 1   improper_Z_CA_X_Y
749. 17 19 18 26 1   improper_Z_CA_X_Y
750. 18 9 19 23 1   improper_Z_CA_X_Y
751. 10 24 22 25 1   improper_Z_CA_X_Y
752. 19 24 23 28 1   improper_Z_CA_X_Y
753. 23 22 24 35 1   improper_Z_CA_X_Y
754. 18 27 26 29 1   improper_Z_CA_X_Y
755. 26 28 27 32 1   improper_Z_CA_X_Y
756. 27 23 28 36 1   improper_Z_CA_X_Y
757. 26 30 29 33 1   improper_Z_CA_X_Y
758. 29 31 30 34 1   improper_Z_CA_X_Y
759. 30 32 31 41 1   improper_Z_CA_X_Y
760. 31 27 32 37 1   improper_Z_CA_X_Y
761. 28 38 36 40 1   improper_Z_CA_X_Y
762. 32 38 37 43 1   improper_Z_CA_X_Y
763. 36 37 38 39 1   improper_Z_CA_X_Y
764. 31 42 41 44 1   improper_Z_CA_X_Y
765. 41 43 42 45 1   improper_Z_CA_X_Y
766. 42 37 43 46 1   improper_Z_CA_X_Y
767. 42 48 45 49 1   improper_Z_CA_X_Y
768. 43 47 46 51 1   improper_Z_CA_X_Y
769. 46 48 47 52 1   improper_Z_CA_X_Y
770. 45 47 48 50 1   improper_Z_CA_X_Y
771.
772.
773. [ pairs ]
```

774. 3 6 1
775. 3 12 1
776. 13 6 1
777. 13 12 1
778. 5 2 1
779. 5 12 1
780. 11 2 1
781. 11 12 1
782. 4 1 1
783. 4 13 1
784. 14 1 1
785. 14 13 1
786. 5 2 1
787. 5 14 1
788. 10 2 1
789. 10 14 1
790. 6 3 1
791. 6 10 1
792. 7 3 1
793. 7 10 1
794. 9 3 1
795. 9 5 1
796. 22 3 1
797. 22 5 1
798. 1 4 1
799. 1 7 1
800. 11 4 1
801. 11 7 1
802. 8 4 1
803. 8 6 1
804. 15 4 1
805. 15 6 1
806. 9 5 1
807. 9 15 1
808. 16 5 1
809. 16 15 1
810. 10 7 1
811. 10 16 1
812. 19 7 1
813. 19 16 1
814. 17 7 1
815. 17 9 1
816. 20 7 1
817. 20 9 1
818. 4 8 1
819. 4 19 1
820. 22 8 1
821. 22 19 1
822. 18 8 1
823. 18 10 1
824. 23 8 1
825. 23 10 1
826. 24 9 1
827. 24 4 1
828. 25 9 1
829. 25 4 1
830. 18 8 1
831. 18 20 1
832. 21 8 1
833. 21 20 1
834. 19 16 1
835. 19 21 1
836. 26 16 1
837. 26 21 1
838. 9 17 1

```
839. 9 26 1
840. 23 17 1
841. 23 26 1
842. 27 17 1
843. 27 19 1
844. 29 17 1
845. 29 19 1
846. 24 18 1
847. 24 9 1
848. 28 18 1
849. 28 9 1
850. 23 10 1
851. 23 25 1
852. 35 10 1
853. 35 25 1
854. 22 19 1
855. 22 28 1
856. 35 19 1
857. 35 28 1
858. 27 19 1
859. 27 24 1
860. 36 19 1
861. 36 24 1
862. 78 23 1
863. 78 22 1
864. 28 18 1
865. 28 29 1
866. 32 18 1
867. 32 29 1
868. 30 18 1
869. 30 27 1
870. 33 18 1
871. 33 27 1
872. 23 26 1
873. 23 32 1
874. 36 26 1
875. 36 32 1
876. 31 26 1
877. 31 28 1
878. 37 26 1
879. 37 28 1
880. 38 27 1
881. 38 23 1
882. 40 27 1
883. 40 23 1
884. 31 26 1
885. 31 33 1
886. 34 26 1
887. 34 33 1
888. 32 29 1
889. 32 34 1
890. 41 29 1
891. 41 34 1
892. 27 30 1
893. 27 41 1
894. 37 30 1
895. 37 41 1
896. 42 30 1
897. 42 32 1
898. 44 30 1
899. 44 32 1
900. 38 31 1
901. 38 27 1
902. 43 31 1
903. 43 27 1
```

```
904. 79 24 1
905. 80 24 1
906. 81 24 1
907. 37 28 1
908. 37 40 1
909. 39 28 1
910. 39 40 1
911. 53 28 1
912. 53 38 1
913. 36 32 1
914. 36 43 1
915. 39 32 1
916. 39 43 1
917. 42 32 1
918. 42 38 1
919. 46 32 1
920. 46 38 1
921. 54 36 1
922. 55 36 1
923. 56 36 1
924. 43 31 1
925. 43 44 1
926. 45 31 1
927. 45 44 1
928. 37 41 1
929. 37 45 1
930. 46 41 1
931. 46 45 1
932. 48 41 1
933. 48 43 1
934. 49 41 1
935. 49 43 1
936. 47 42 1
937. 47 37 1
938. 51 42 1
939. 51 37 1
940. 47 42 1
941. 47 49 1
942. 50 42 1
943. 50 49 1
944. 48 43 1
945. 48 51 1
946. 52 43 1
947. 52 51 1
948. 45 46 1
949. 45 52 1
950. 50 46 1
951. 50 52 1
952. 57 40 1
953. 57 55 1
954. 57 56 1
955. 58 40 1
956. 58 55 1
957. 58 56 1
958. 59 40 1
959. 59 55 1
960. 59 56 1
961. 60 53 1
962. 60 58 1
963. 60 59 1
964. 61 53 1
965. 61 58 1
966. 61 59 1
967. 62 53 1
968. 62 58 1
```

```
 969. 62 59 1
 970. 63 54 1
 971. 63 61 1
 972. 63 62 1
 973. 64 54 1
 974. 64 61 1
 975. 64 62 1
 976. 65 54 1
 977. 65 61 1
 978. 65 62 1
 979. 66 57 1
 980. 66 64 1
 981. 66 65 1
 982. 67 57 1
 983. 67 64 1
 984. 67 65 1
 985. 68 57 1
 986. 68 64 1
 987. 68 65 1
 988. 69 60 1
 989. 69 67 1
 990. 69 68 1
 991. 70 60 1
 992. 70 67 1
 993. 70 68 1
 994. 71 60 1
 995. 71 67 1
 996. 71 68 1
 997. 72 63 1
 998. 72 70 1
 999. 72 71 1
1000. 73 63 1
1001. 73 70 1
1002. 73 71 1
1003. 74 63 1
1004. 74 70 1
1005. 74 71 1
1006. 75 66 1
1007. 75 73 1
1008. 75 74 1
1009. 76 66 1
1010. 76 73 1
1011. 76 74 1
1012. 77 66 1
1013. 77 73 1
1014. 77 74 1
1015. 82 35 1
1016. 82 80 1
1017. 82 81 1
1018. 83 35 1
1019. 83 80 1
1020. 83 81 1
1021. 84 35 1
1022. 84 80 1
1023. 84 81 1
1024. 85 78 1
1025. 85 83 1
1026. 85 84 1
1027. 86 78 1
1028. 86 83 1
1029. 86 84 1
1030. 87 78 1
1031. 87 83 1
1032. 87 84 1
1033. 88 79 1
```

```
1034. 88 86 1
1035. 88 87 1
1036. 89 79 1
1037. 89 86 1
1038. 89 87 1
1039. 90 79 1
1040. 90 86 1
1041. 90 87 1
1042. 91 82 1
1043. 91 89 1
1044. 91 90 1
1045. 92 82 1
1046. 92 89 1
1047. 92 90 1
1048. 93 82 1
1049. 93 89 1
1050. 93 90 1
1051. 94 85 1
1052. 94 92 1
1053. 94 93 1
1054. 95 85 1
1055. 95 92 1
1056. 95 93 1
1057. 96 85 1
1058. 96 92 1
1059. 96 93 1
1060. 97 88 1
1061. 97 95 1
1062. 97 96 1
1063. 98 88 1
1064. 98 95 1
1065. 98 96 1
1066. 99 88 1
1067. 99 95 1
1068. 99 96 1
1069. 100 91 1
1070. 100 98 1
1071. 100 99 1
1072. 101 91 1
1073. 101 98 1
1074. 101 99 1
1075. 102 91 1
1076. 102 98 1
1077. 102 99 1
1078.
```

6.6 Permission of Reusing of Published Materials

ELSEVIER LICENSE

TERMS AND CONDITIONS

Dec 21, 2022

This Agreement between Mr. komeil jalali ("You") and Elsevier ("Elsevier") consists of your license details and the terms and conditions provided by Elsevier and Copyright Clearance Center.

License Number	5453710673476
License date	Dec 21, 2022
Licensed Content Publisher	Elsevier
Licensed Content Publication	Tribology International
Licensed Content Title	Modeling and simulation in tribology across scales: An overview
Licensed Content Author	A.I. Vakis,V.A. Yastrebov,J. Scheibert,L. Nicola,D. Dini,C. Minfray,A. Almqvist,M. Paggi,S. Lee,G. Limbert,J.F. Molinari,G. Anciaux,R. Aghababaei,S. Echeverri Restrepo,A. Papangelo,A. Cammarata,P. Nicolini,C. Putignano,G. Carbone,S. Stupkiewicz et al.
Licensed Content Date	Sep 1, 2018
Licensed Content Volume	125
Licensed Content Issue	n/a

6.7 Solvent Properties

As can be seen from the table below, our results obtained using OPLS-AA are very close to those from experimental measurements. The parameters used in these simulations (also see Chapter 2), as well as the OPLS-AA force field, were subsequently used in the studies described in Chapters 3 and 4.

Density ($^{kg}/_{m^3}$)

Force Field	Pentane	Toluene	Heptane	Water
OPLS-AA	622	862	684	998
Exp.[112]	616	865	682	999
GROMOS96	638	858	692	993

Self-Diffusion Coefficient $^{cm^2}/_{s}$

Force Field	Pentane	Heptane
OPLS-AA	4.2e-5	2.27e-5
GROMOS96	5.7e-5	3.1e-5
Exp.[113]	5.95e-5	3.25e-5

Chapter 7. References

(1) *Crude Oil Industry Overview*. https://www.nrcan.gc.ca/our-natural-resources/energy-sources-distribution/fossil-fuels/crude-oil/crude-oil-industry-overview/18078 (accessed 2022-09-08).

(2) Dusseault, M. B. *Comparing Venezuelan and Canadian Heavy Oil and Tar Sands*.

(3) *Asphaltenes, Heavy Oils, and Petroleomics*.

(4) Qian, K.; Robbins, W. K.; Hughey, C. A.; Cooper, H. J.; Rodgers, R. P.; Marshall, A. G. Resolution and Identification of Elemental Compositions for More than 3000 Crude Acids in Heavy Petroleum by Negative-Ion Microelectrospray High-Field Fourier Transform Ion Cyclotron Resonance Mass Spectrometry. *Energy and Fuels* **2001**, *15* (6), 1505–1511. https://doi.org/10.1021/ef010111z.

(5) Coletti, F.; Macchietto, S. A Dynamic, Distributed Model of Shell-and-Tube Heat Exchangers Undergoing Crude Oil Fouling. *Ind Eng Chem Res* **2011**, *50* (8), 4515–4533. https://doi.org/10.1021/ie901991g.

(6) Wu, X.; Jing, H.; Zheng, Y.; Yao, Z.; Ke, W. Erosion-Corrosion of Various Oil-Refining Materials in Naphthenic Acid. *Wear* **2004**, *256* (1–2), 133–144. https://doi.org/10.1016/S0043-1648(03)00370-3.

(7) Vakis, A. I.; Yastrebov, V. A.; Scheibert, J.; Nicola, L.; Dini, D.; Minfray, C.; Almqvist, A.; Paggi, M.; Lee, S.; Limbert, G.; Molinari, J. F.; Anciaux, G.; Aghababaei, R.; Echeverri Restrepo, S.; Papangelo, A.; Cammarata, A.; Nicolini, P.; Putignano, C.; Carbone, G.; Stupkiewicz, S.; Lengiewicz, J.; Costagliola, G.; Bosia, F.; Guarino, R.; Pugno, N. M.; Müser, M. H.; Ciavarella, M. Modeling and Simulation in Tribology across Scales: An Overview. *Tribol Int* **2018**, *125* (February), 169–199. https://doi.org/10.1016/j.triboint.2018.02.005.

(8) Feynman, R. P.; Leighton, R. B.; Sands, M.; Lindsay, R. B. The Feynman Lectures on Physics, Vol. 3: Quantum Mechanics . *Phys Today* **1966**, *19* (11), 80–83. https://doi.org/10.1063/1.3047826.

(9) Comby-Peyrot, I.; Bernard, F.; Bouchard, P. O.; Bay, F.; Garcia-Diaz, E. Development and Validation of a 3D Computational Tool to Describe Concrete Behaviour at Mesoscale. Application to the Alkali-Silica Reaction. *Comput Mater Sci* **2009**, *46* (4), 1163–1177. https://doi.org/10.1016/j.commatsci.2009.06.002.

(10) Fitzgerald, G.; Goldbeck-Wood, G.; Kung, P.; Petersen, M.; Subramanian, L.; Wescott, J. *Materials Modeling from Quantum Mechanics to The Mesoscale*; 2008; Vol. 24.

(11) Allen, M. P.; Tildesley, D. J. ©; Tildesley, D. J. *3 Molecular Dynamics 3.1 Equations of Motion for Atomic Systems*. https://academic.oup.com/book/27866/chapter/203861481.

(12) Swope, W. C.; Andersen, H. C.; Berens, P. H.; Wilson, K. R. A Computer Simulation Method for the Calculation of Equilibrium Constants for the Formation of Physical Clusters of Molecules: Application to Small Water Clusters. *J Chem Phys* **1982**, *76* (1), 637–649. https://doi.org/10.1063/1.442716.

(13) Mackerell, A. D.; Bashford, D.; Bellott, ⊥ M; Dunbrack, ⊥ R L; Evanseck, J. D.; Field, M. J.; Fischer, ⊥ S; Gao, ⊥ J; Guo, ⊥ H; Ha, ⊥ S; Joseph-Mccarthy, ⊥ D; Kuchnir, ǂ ⊥ L; Kuczera, ⊥ K; Lau, ⊥ F T K; Mattos, ⊥ C; Michnick, S.; Ngo, ⊥ T; Nguyen, ⊥ D T; Prodhom, ⊥ B; Reiher, ⊥ W E; Roux, ⊥ B; Schlenkrich, ⊥ M; Smith, J. C.; Stote, ⊥ R; Straub, ⊥ J; Watanabe, ⊥ M; Wiórkiewicz-Kuczera, ⊥ J; Yin, ⊥ D; Karplus, M. *All-Atom Empirical Potential for Molecular Modeling and Dynamics Studies of Proteins †*; 1998.

(14) Cornell, W. D.; Cieplak, P.; Bayly, C. I.; Gould, I. R.; Merz, K. M.; Ferguson, D. M.; Spellmeyer, D. C.; Fox, T.; Caldwell, J. W.; Kollman, P. A. *A Second Generation Force Field for the Simulation of Proteins, Nucleic Acids, and Organic Molecules*; 1995; Vol. 117.

(15) Oostenbrink, C.; Villa, A.; Mark, A. E.; van Gunsteren, W. F. A Biomolecular Force Field Based on the Free Enthalpy of Hydration and Solvation: The GROMOS Force-Field Parameter Sets 53A5 and 53A6. *J Comput Chem* **2004**, *25* (13), 1656–1676. https://doi.org/10.1002/jcc.20090.

(16) Jorgensen, W. L.; Maxwell, D. S.; Tirado-Rives, J. *Development and Testing of the OPLS All-Atom Force Field on Conformational Energetics and Properties of Organic Liquids*; 1996. https://pubs.acs.org/sharingguidelines.

(17) Pal, Snehanshu Ray, B. C. *Molecular Dynamics Simulation of Nanostructured Materials: An Understanding of Mechanical Behavior*; 2016; Vol. 1107.

(18) Buehler, M. J. *Atomistic Modeling of Materials Failure*; 2007.

(19) Jorgensen, W. L.; Madura, J. D.; Swenson, C. J. *Optimized Intermolecular Potential Functions for Liquid Hydrocarbons*; 1984; Vol. 106. https://pubs.acs.org/sharingguidelines.

(20) Jorgensen, W. L.; Maxwell, D. S.; Tirado-Rives, J. *Development and Testing of the OPLS All-Atom Force Field on Conformational Energetics and Properties of Organic Liquids*; 1996. https://pubs.acs.org/sharingguidelines.

(21) Ja00292a007.

(22) Caleman, C.; van Maaren, P. J.; Hong, M.; Hub, J. S.; Costa, L. T.; van der Spoel, D. Force Field Benchmark of Organic Liquids: Density, Enthalpy of Vaporization, Heat Capacities, Surface Tension, Isothermal Compressibility, Volumetric Expansion Coefficient, and Dielectric Constant. *J Chem Theory Comput* **2012**, *8* (1), 61–74. https://doi.org/10.1021/ct200731v.

(23) Udier-Blagović, M.; Morales De Tirado, P.; Pearlman, S. A.; Jorgensen, W. L. Accuracy of Free Energies of Hydration Using CM1 and CM3 Atomic Charges. *J Comput Chem* **2004**, *25* (11), 1322–1332. https://doi.org/10.1002/jcc.20059.

(24) Sweere, A. J. M.; Fraaije, J. G. E. M. Accuracy Test of the OPLS-AA Force Field for Calculating Free Energies of Mixing and Comparison with PAC-MAC. *J Chem Theory Comput* **2017**, *13* (5), 1911–1923. https://doi.org/10.1021/acs.jctc.6b01106.

(25) Jorgensen, W. L.; Tirado-rives, J. The OPLS [Optimized Potentials for Liquid Simulations] Potential Functions for Proteins, Energy Minimizations for Crystals of Cyclic Peptides and Crambin. **1988**, No. 4.

(26) Chen, X.; Hou, L.; Wei, X.; Bedrov, D. Transport Properties of Waxy Crude Oil: A Molecular Dynamics Simulation Study. *ACS Omega* **2020**, *5* (30), 18557–18564. https://doi.org/10.1021/acsomega.0c00070.

(27) Andersen, H. C. Molecular Dynamics Simulations at Constant Pressure and/or Temperature. *J Chem Phys* **1980**, *72* (4), 2384–2393. https://doi.org/10.1063/1.439486.

(28) Evans, D. J.; Holian, B. L. The Nose-Hoover Thermostat. *J Chem Phys* **1985**, *83* (8), 4069–4074. https://doi.org/10.1063/1.449071.

(29) Lippert, R. A.; Predescu, C.; Ierardi, D. J.; Mackenzie, K. M.; Eastwood, M. P.; Dror, R. O.; Shaw, D. E. Accurate and Efficient Integration for Molecular Dynamics Simulations at Constant Temperature and Pressure. *Journal of Chemical Physics* **2013**, *139* (16). https://doi.org/10.1063/1.4825247.

(30) Berendsen, H. J. C.; Postma, J. P. M.; van Gunsteren, W. F.; Dinola, A.; Haak, J. R. Molecular Dynamics with Coupling to an External Bath. *J Chem Phys* **1984**, *81* (8), 3684–3690. https://doi.org/10.1063/1.448118.

(31) Parrinello, M.; Rahman, A. Polymorphic Transitions in Single Crystals: A New Molecular Dynamics Method. *J Appl Phys* **1981**, *52* (12), 7182–7190. https://doi.org/10.1063/1.328693.

(32) Hess, B.; Bekker, H.; Berendsen, H. J. C.; Fraaije, J. G. E. M. LINCS: A Linear Constraint Solver for Molecular Simulations. *J Comput Chem* **1997**, *18* (12), 1463–1472. https://doi.org/10.1002/(SICI)1096-987X(199709)18:12<1463::AID-JCC4>3.0.CO;2-H.

(33) Berendsen, H. J. C.; Grigera, J. R.; Straatsma, T. P. The Missing Term in Effective Pair Potentials. *Journal of Physical Chemistry* **1987**, *91* (24), 6269–6271. https://doi.org/10.1021/j100308a038.

(34) Kukol, A. *Trying to Understand Waiting for Godot: An Adornian Analysis of Beckett's Signature Work*; Humana Press, 2016; Vol. 21. https://doi.org/10.1080/10848770.2016.1211417.

(35) *Molecular_dynamics_algorithm.png (1009×909)*. https://upload.wikimedia.org/wikipedia/commons/7/7b/Molecular_dynamics_algorithm.png (accessed 2022-09-08).

(36) Wang, S.; Civan, F. Preventing Asphaltene Deposition in Oil Reservoirs by Early Water Injection. *Society of Petroleum Engineers - SPE Production Operations Symposium 2005, POS 2005* **2005**. https://doi.org/10.2523/94268-ms.

(37) Hasanvand, M. Z.; Ahmadi, M. A.; Behbahani, R. M. Solving Asphaltene Precipitation Issue in Vertical Wells via Redesigning of Production Facilities. *Petroleum* **2015**, *1* (2), 139–145. https://doi.org/10.1016/j.petlm.2015.07.002.

(38) Jian, C.; Tang, T.; Bhattacharjee, S. Molecular Dynamics Investigation on the Aggregation of Violanthrone78-Based Model Asphaltenes in Toluene. *Energy and Fuels* **2014**, *28* (6), 3604–3613. https://doi.org/10.1021/ef402208f.

(39) Montanari, S. *Structures and Dynamics of Asphaltenes*; Oliver C. Mullins, E. Y. S., Ed.; Springer New York, NY, 1998.

(40) Kwan, C. L.; Yen, T. F. Electron Spin Resonance Study of Coal by Line Width and Line Shape Analysis. *Anal Chem* **1979**, *51* (8), 1225–1229. https://doi.org/10.1021/ac50044a028.

(41) Yen, T. F.; Gordon Erdman, J.; Pollack, S. S. Investigation of the Structure of Petroleum Asphaltenes by X-Ray Diffraction. *Preprints (Basel)* **1961**, *6* (1), 21–36.

(42) Pacheco-Sánchez, J. H.; Zaragoza, I. P.; Martínez-Magadán, J. M. Asphaltene Aggregation under Vacuum at Different Temperatures by Molecular Dynamics. *Energy and Fuels* **2003**, *17* (5), 1346–1355. https://doi.org/10.1021/ef020226i.

(43) Zhang, L.; Greenfield, M. L. Molecular Orientation in Model Asphalts Using Molecular Simulation. *Energy and Fuels* **2007**, *21* (2), 1102–1111. https://doi.org/10.1021/ef060449z.

(44) Sedghi, M.; Goual, L.; Welch, W.; Kubelka, J. E Ff Ect of Asphaltene Structure on Association and Aggregation Using Molecular Dynamics. **2013**.

(45) Gao, F.; Xu, Z.; Liu, G.; Yuan, S. Molecular Dynamics Simulation: The Behavior of Asphaltene in Crude Oil and at the Oil/Water Interface. *Energy and Fuels* **2014**, *28* (12), 7368–7376. https://doi.org/10.1021/ef5020428.

(46) Teklebrhan, R. B.; Ge, L.; Bhattacharjee, S.; Xu, Z.; Sjo, J.; Tg, A. Initial Partition and Aggregation of Uncharged Polyaromatic Molecules at the Oil − Water Interface : A Molecular Dynamics Simulation Study. **2014**.

(47) Jian, C.; Poopari, M. R.; Liu, Q.; Zerpa, N.; Zeng, H.; Tang, T. Reduction of Water/Oil Interfacial Tension by Model Asphaltenes: The Governing Role of Surface Concentration. *J Phys Chem B* **2016**, *120* (25), 5646–5654. https://doi.org/10.1021/acs.jpcb.6b03691.

(48) Mikami, Y.; Liang, Y.; Matsuoka, T.; Boek, E. S. Molecular Dynamics Simulations of Asphaltenes at the Oil–Water Interface: From Nanoaggregation to Thin-Film Formation. *Energy & Fuels* **2013**, *27* (4), 1838–1845.

(49) Yaseen, S.; Mansoori, G. A. Asphaltene Aggregation Due to Waterflooding (A Molecular Dynamics Study). *J Pet Sci Eng* **2018**, *170* (June), 177–183. https://doi.org/10.1016/j.petrol.2018.06.043.

(50) Singh, M. B.; Rampal, N.; Malani, A. Structural Behavior of Isolated Asphaltene Molecules at the Oil-Water Interface. *Energy and Fuels* **2018**, *32* (8), 8259–8267. https://doi.org/10.1021/acs.energyfuels.8b01648.

(51) Jalali, K.; Shahad, R.; Rashid, A. N.; Hawlader, S.; Jian, C. Solvent Nuances Modulate the Decreasing Effect of a Model Asphaltene on Interfacial Tension. *Energy and Fuels* **2020**, *34* (11), 13862–13870. https://doi.org/10.1021/acs.energyfuels.0c02639.

(52) Knudsen, K. D.; Simon, S.; Qassym, L.; Gao, B.; Sjöblom, J. Mixed Micelles of Tetrameric Acids and Naphthenic Acids in Water. *Energy and Fuels* **2014**, *28* (7), 4469–4479. https://doi.org/10.1021/ef500770z.

(53) Cunha, R. D.; Ferreira, L. J.; Orestes, E.; Coutinho-Neto, M. D.; de Almeida, J. M.; Carvalho, R. M.; Maciel, C. D.; Curutchet, C.; Homem-de-Mello, P. Naphthenic Acids Aggregation: The Role of Salinity. *Computation* **2022**, *10* (10), 170. https://doi.org/10.3390/computation10100170.

(54) Kiran, S. K.; Ng, S.; Acosta, E. J. Impact of Asphaltenes and Naphthenic Amphiphiles on the Phase Behavior of Solvent-Bitumen-Water Systems. *Energy and Fuels* **2011**, *25* (5), 2223–2231. https://doi.org/10.1021/ef1016285.

(55) Östlund, J. A.; Nydén, M.; Auflem, I. H.; Sjöblom, J. Interactions between Asphaltenes and Naphthenic Acids. *Energy and Fuels* **2003**, *17* (1), 113–119. https://doi.org/10.1021/ef020103y.

(56) Heaps, D. T.; Madasu, P. K.; Magers, D. H.; Buchanan, J. P. Investigation of the Precipitation Behavior of Asphaltenes in the Presence of Naphthenic Acids Using Light Scattering and Molecular Modeling Techniques. *Energy and Fuels* **2012**, *26* (3), 1862–1869. https://doi.org/10.1021/ef201719m.

(57) Teklebrhan, R. B.; Jian, C.; Choi, P.; Xu, Z.; Sjöblom, J. Role of Naphthenic Acids in Controlling Self-Aggregation of a Polyaromatic Compound in Toluene. *Journal of Physical Chemistry B* **2016**, *120* (14), 3516–3526. https://doi.org/10.1021/acs.jpcb.5b10082.

(58) Kiran, S. K.; Ng, S.; Acosta, E. J. Impact of Asphaltenes and Naphthenic Amphiphiles on the Phase Behavior of Solvent-Bitumen-Water Systems. *Energy and Fuels* **2011**, *25* (5), 2223–2231. https://doi.org/10.1021/ef1016285.

(59) Mokhtari, R.; Hosseini, A.; Fatemi, M.; Andersen, S. I.; Ayatollahi, S. Asphaltene Destabilization in the Presence of an Aqueous Phase: The Effects of Salinity, Ion Type, and Contact Time. *J Pet Sci Eng* **2022**, *208* (PE), 109757. https://doi.org/10.1016/j.petrol.2021.109757.

(60) Teklebrhan, R. B.; Jian, C.; Choi, P.; Xu, Z.; Sjöblom, J. Competitive Adsorption of Naphthenic Acids and Polyaromatic Molecules at a Toluene-Water Interface. *Journal of Physical Chemistry B* **2016**, *120* (50), 12901–12910. https://doi.org/10.1021/acs.jpcb.6b07938.

(61) Liu, L.; Sjöblom, J.; Xu, Z. Nanoaggregation of Polyaromatic Compounds Probed by Electrospray Ionization Mass Spectrometry. *Energy and Fuels* **2016**, *30* (5), 3742–3751. https://doi.org/10.1021/acs.energyfuels.5b02390.

(62) Pinto, F. E.; Barros, E. v.; Tose, L. v.; Souza, L. M.; Terra, L. A.; Poppi, R. J.; Vaz, B. G.; Vasconcelos, G.; Subramanian, S.; Simon, S.; Sjöblom, J.; Romão, W. Fractionation of Asphaltenes in N-Hexane

and on Adsorption onto CaCO3 and Characterization by ESI(+)FT-ICR MS: Part I. *Fuel* **2017**, *210* (March), 790–802. https://doi.org/10.1016/j.fuel.2017.09.028.

(63) Yarranton, H.; Baydak, E. N. Effect of Solvents on the Stability of Water-in-Bitumen Emulsions. *Energy and Fuels* **2022**, *36* (12), 6243–6260. https://doi.org/10.1021/acs.energyfuels.2c00996.

(64) López, R. Capillary Surfaces with Free Boundary in a Wedge. *Adv Math (N Y)* **2014**, *262*, 476–483. https://doi.org/10.1016/j.aim.2014.05.019.

(65) Frisch, M. J.; Trucks, G. W.; Schlegel, H. B.; Scuseria, G. E.; Robb, M. A.; Cheeseman, J. R.; Scalmani, G.; Barone, V.; Petersson, G. A.; Nakatsuji, H.; Li, X.; Caricato, M.; Marenich, A. v; Bloino, J.; Janesko, B. G.; Gomperts, R.; Mennucci, B.; Hratchian, H. P.; Ortiz, J. v; Izmaylov, A. F.; Sonnenberg, J. L.; Williams-Young, D.; Ding, F.; Lipparini, F.; Egidi, F.; Goings, J.; Peng, B.; Petrone, A.; Henderson, T.; Ranasinghe, D.; Zakrzewski, V. G.; Gao, J.; Rega, N.; Zheng, G.; Liang, W.; Hada, M.; Ehara, M.; Toyota, K.; Fukuda, R.; Hasegawa, J.; Ishida, M.; Nakajima, T.; Honda, Y.; Kitao, O.; Nakai, H.; Vreven, T.; Throssell, K.; Montgomery Jr., J. A.; Peralta, J. E.; Ogliaro, F.; Bearpark, M. J.; Heyd, J. J.; Brothers, E. N.; Kudin, K. N.; Staroverov, V. N.; Keith, T. A.; Kobayashi, R.; Normand, J.; Raghavachari, K.; Rendell, A. P.; Burant, J. C.; Iyengar, S. S.; Tomasi, J.; Cossi, M.; Millam, J. M.; Klene, M.; Adamo, C.; Cammi, R.; Ochterski, J. W.; Martin, R. L.; Morokuma, K.; Farkas, O.; Foresman, J. B.; Fox, D. J. Gaussian˜16 {R}evision {C}.01. 2016.

(66) Das, A.; Ali, S. M. Molecular Dynamics Simulation for the Test of Calibrated OPLS-AA Force Field for Binary Liquid Mixture of Tri-Iso-Amyl Phosphate and n -Dodecane. *Journal of Chemical Physics* **2018**, *148* (7). https://doi.org/10.1063/1.5009900.

(67) Sambasivarao, S. v.; Acevedo, O. Development of OPLS-AA Force Field Parameters for 68 Unique Ionic Liquids. *J Chem Theory Comput* **2009**, *5* (4), 1038–1050. https://doi.org/10.1021/ct900009a.

(68) Ribeiro, A. A. S. T.; Horta, B. A. C.; de Alencastro, R. B. MKTOP: A Program for Automatic Construction of Molecular Topologies. *J Braz Chem Soc* **2008**, *19* (7), 1433–1435. https://doi.org/10.1590/S0103-50532008000700031.

(69) Alejandre, J.; Tildesley, D. J.; Chapela, G. A. Molecular Dynamics Simulation of the Orthobaric Densities and Surface Tension of Water. *J Chem Phys* **1995**, *102* (11), 4574–4583. https://doi.org/10.1063/1.469505.

(70) Lindahl; Abraham; Hess; Spoel, van der. GROMACS Documentation. *GROMACS 2021.3 Manual* **2021**, 1–623.

(71) Rao, Ps.; Apparao, A.; Professor, A. *Energy Minimization and Conformation Analysis of Molecules Using Steepest Descent Method*. www.ijcsit.com.

(72) Darden, T.; York, D.; Pedersen, L. Particle Mesh Ewald: An N·log(N) Method for Ewald Sums in Large Systems. *J Chem Phys* **1993**, *98* (12), 10089–10092. https://doi.org/10.1063/1.464397.

(73) Levey, M. The Early History of Detergent Substances: A Chapter in Babylonian Chemistry. *J Chem Educ* **1954**, *31* (10), 521–524. https://doi.org/10.1021/ed031p521.

(74) Kumwenda, S. Challenges to Hygiene Improvement in Developing Countries. *The Relevance of Hygiene to Health in Developing Countries* **2019**, 1–18. https://doi.org/10.5772/intechopen.80355.

(75) Bautista-Toledo, M. I.; Méndez-Díaz, J. D.; Sánchez-Polo, M.; Rivera-Utrilla, J.; Ferro-García, M. A. Adsorption of Sodium Dodecylbenzenesulfonate on Activated Carbons: Effects of Solution Chemistry and Presence of Bacteria. *J Colloid Interface Sci* **2008**, *317* (1), 11–17. https://doi.org/10.1016/j.jcis.2007.09.039.

(76) Prieto Vidal, N.; Adeseun Adigun, O.; Huong Pham, T.; Mumtaz, A.; Manful, C.; Callahan, G.; Stewart, P.; Keough, D.; Horatio Thomas, R. The Effects of Cold Saponification on the Unsaponified Fatty Acid Composition and Sensory Perception of Commercial Natural Herbal Soaps. *Molecules* **2018**, *23* (9), 1–20. https://doi.org/10.3390/molecules23092356.

(77) Salimon, J.; Abdullah, B. M.; Salih, N. Hydrolysis Optimization and Characterization Study of Preparing Fatty Acids from Jatropha Curcas Seed Oil. *Chem Cent J* **2011**, *5* (1), 1–9. https://doi.org/10.1186/1752-153X-5-67.

(78) Privé, G. G. Detergents for the Stabilization and Crystallization of Membrane Proteins. *Methods* **2007**, *41* (4), 388–397. https://doi.org/10.1016/j.ymeth.2007.01.007.

(79) Tejaswi Naidu, K.; Prakash Prabhu, N. Protein-Surfactant Interaction: Sodium Dodecyl Sulfate-Induced Unfolding of Ribonuclease A. *Journal of Physical Chemistry B* **2011**, *115* (49), 14760–14767. https://doi.org/10.1021/jp2062496.

(80) van der Spoel, E.; Rozing, M. P.; Houwing-Duistermaat, J. J.; Eline Slagboom, P.; Beekman, M.; de Craen, A. J. M.; Westendorp, R. G. J.; van Heemst, D. *Heterologous Expression of MEmbrane Proteins*; 2015; Vol. 7.

(81) Stigter, D. Micelle Formation by Ionic Surfactants. II. Specificity of Head Groups, Micelle Structure. *Journal of Physical Chemistry* **1974**, *78* (24), 2480–2485. https://doi.org/10.1021/j100617a013.

(82) Jain, P.; Sharma, M.; Dureja, P.; Sarma, P. M.; Lal, B. Bioelectrochemical Approaches for Removal of Sulfate, Hydrocarbon and Salinity from Produced Water. *Chemosphere* **2017**, *166*, 96–108. https://doi.org/10.1016/j.chemosphere.2016.09.081.

(83) Mareddy, A. R. *Technology in EIA*; 2017. https://doi.org/10.1016/b978-0-12-811139-0.00012-8.

(84) Cabrera, M. N. Pulp Mill Wastewater: Characteristics and Treatment. *Biological Wastewater Treatment and Resource Recovery* **2017**. https://doi.org/10.5772/67537.

(85) States, U. Wastewater Treatment Works... The Basics. **1998**, No. May.

(86) Vergili, I.; Kaya, Y.; Gönder, Z. B.; Barlas, H. Column Studies for the Adsorption of Cationic Surfactant onto an Organic Polymer Resin and a Granular Activated Carbon. *Water Environment Research* **2010**, *82* (3), 209–215. https://doi.org/10.2175/106143009x12487095236351.

(87) Schmidt, M.; Masson, A.; Cheng, H. P.; Bréchignac, C. Physisorption and Chemisorption on Silver Clusters. *ChemPhysChem* **2015**, *16* (4), 855–865. https://doi.org/10.1002/cphc.201402726.

(88) Martinez-Jimenez, P.; Gallego, M.; Valcárcel, M. Indirect Atomic Absorption Determination of Aluminum by Flow Injection Analysis. *Microchemical Journal* **1986**, *34* (2), 190–195. https://doi.org/10.1016/0026-265X(86)90031-7.

(89) Cantone, S.; Ferrario, V.; Corici, L.; Ebert, C.; Fattor, D.; Spizzo, P.; Gardossi, L. Efficient Immobilisation of Industrial Biocatalysts: Criteria and Constraints for the Selection of Organic Polymeric Carriers and Immobilisation Methods. *Chem Soc Rev* **2013**, *42* (15), 6262–6276. https://doi.org/10.1039/c3cs35464d.

(90) LU, G. wu; LI, Y. feng; SONG, H.; YU, Y. hui; WANG, C. lei. Micromechanism of Petroleum Asphaltene Aggregation. *Petroleum Exploration and Development* **2008**, *35* (1), 67–72. https://doi.org/10.1016/S1876-3804(08)60010-5.

(91) Chiang, J. S.; Huang, S. da. Simultaneous Derivatization and Extraction of Anilines in Waste Water with Dispersive Liquid-Liquid Microextraction Followed by Gas Chromatography-Mass Spectrometric Detection. *Talanta* **2008**, *75* (1), 70–75. https://doi.org/10.1016/j.talanta.2007.10.036.

(92) Jacobsen, W. E. Environmental Impact. **1984**, 325–348. https://doi.org/10.1016/B978-0-12-814238-7.00015-5.

(93) Ab, A. C. O. H. U. D. Biophysical Characterization of Skin Damage and Recovery after Exposure to Different Surfactants. **1999**, 98–103.

(94) Heilig, M. L. United States Patent Office. *ACM SIGGRAPH Computer Graphics* **1994**, *28* (2), 131–134. https://doi.org/10.1145/178951.178972.

(95) van Gunsteren, W. F.; Berendsen, H. J. C. Groningen Molecular Simulation ({GROMOS}) Library Manual. *Biomos, Groningen* **1987**.

(96) Malde, A. K.; Zuo, L.; Breeze, M.; Stroet, M.; Poger, D.; Nair, P. C.; Oostenbrink, C.; Mark, A. E. An Automated Force Field Topology Builder (ATB) and Repository: Version 1.0. *J Chem Theory Comput* **2011**, *7* (12), 4026–4037. https://doi.org/10.1021/ct200196m.

(97) Fakhru'l-Razi, A.; Pendashteh, A.; Abdullah, L. C.; Biak, D. R. A.; Madaeni, S. S.; Abidin, Z. Z. Review of Technologies for Oil and Gas Produced Water Treatment. *J Hazard Mater* **2009**, *170* (2–3), 530–551. https://doi.org/10.1016/j.jhazmat.2009.05.044.

(98) Jain, P.; Sharma, M.; Dureja, P.; Sarma, P. M.; Lal, B. Bioelectrochemical Approaches for Removal of Sulfate, Hydrocarbon and Salinity from Produced Water. *Chemosphere* **2017**, *166*, 96–108. https://doi.org/10.1016/j.chemosphere.2016.09.081.

(99) Shannon, M. A.; Bohn, P. W.; Elimelech, M.; Georgiadis, J. G.; Marĩas, B. J.; Mayes, A. M. Science and Technology for Water Purification in the Coming Decades. *Nature* **2008**, *452* (7185), 301–310. https://doi.org/10.1038/nature06599.

(100) Hosseinpour, S.; Götz, V.; Peukert, W. Effect of Surfactants on the Molecular Structure of the Buried Oil/Water Interface. *Angewandte Chemie - International Edition* **2021**, *60* (47), 25143–25150. https://doi.org/10.1002/anie.202110091.

(101) Mohsin, M.; Meribout, M. Oil-Water de-Emulsification Using Ultrasonic Technology. *Ultrason Sonochem* **2015**, *22*, 573–579. https://doi.org/10.1016/j.ultsonch.2014.05.014.

(102) Headen, T. F.; Boek, E. S.; Skipper, N. T. Evidence for Asphaltene Nanoaggregation in Toluene and Heptane from Molecular Dynamics Simulations. *Energy and Fuels* **2009**, *23* (3), 1220–1229. https://doi.org/10.1021/ef800872g.

(103) Chelli, R.; Gervasio, F. L.; Procacci, P.; Schettino, V. Stacking and T-Shape Competition in Aromatic - Aromatic Amino Acid Interactions. **2002**, No. 13, 6133–6143.

(104) Battaglia, M. R.; Buckingham, A. D.; Williams, J. H. The Electric Quadrupole Moments of Benzene and Hexafluorobenzene. *Chem Phys Lett* **1981**, *78* (3), 421–423. https://doi.org/10.1016/0009-2614(81)85228-1.

(105) Riley, K. E.; Hobza, P. On the Importance and Origin of Aromatic Interactions in Chemistry and Biodisciplines. *Acc Chem Res* **2013**, *46* (4), 927–936. https://doi.org/10.1021/ar300083h.

(106) Of, J.; Toxicology, A.; Vapor, C. I.; Boi, H.; Chlorobenzene, C.; Permissible, C.; Limit, E.; State, S. O.; Osha, F.; State, T.; Code, C.; Title, R.; Changes, I.; War, F. W. Toxicology Update. **1990**, *10* (4), 307–310.

(107) States, U.; Contact, E. CHLOROBENZENE What Is CHLOROBENZENE ? **2013**, 9–10.

(108) Tabak, H. H.; Quave, S. A.; Mashni, C. I.; Barth, E. F. Biodegradability Studies With Organic Priority Pollutant Compounds. *Journal of the Water Pollution Control Federation* **1981**, *53* (10), 1503–1518.

(109) Ozgun, H.; Cicekalan, B.; Akdag, Y.; Koyuncu, I.; Ozturk, I. Comparative Evaluation of Cost for Preliminary and Tertiary Municipal Wastewater Treatment Plants in Istanbul. *Science of the Total Environment* **2021**, *778*, 146258. https://doi.org/10.1016/j.scitotenv.2021.146258.

(110) Gómez, M.; Plaza, F.; Garralón, G.; Pérez, J.; Gómez, M. A. A Comparative Study of Tertiary Wastewater Treatment by Physico-Chemical-UV Process and Macrofiltration-Ultrafiltration Technologies. *Desalination* **2007**, *202* (1–3), 369–376. https://doi.org/10.1016/j.desal.2005.12.076.

(111) Ahmed, M. B.; Zhou, J. L.; Ngo, H. H.; Guo, W. Adsorptive Removal of Antibiotics from Water and Wastewater: Progress and Challenges. *Science of the Total Environment* **2015**, *532*, 112–126. https://doi.org/10.1016/j.scitotenv.2015.05.130.

(112) Yaws, C. L. *Thermophysical Properties of Chemicals and Hydrocarbons*; William Andrew, 2008.

(113) Fishman, B. E.; Fishman, E. SELF-DIFFUSION IN LIQUID n-PENTANE AND Ra-HEPTANE1. **1955**, *381* (1), 2–5.